Multiethnic GWAS Reveals Polygenic Architecture of Earlobe Attachment

John R. Shaffer,[1,27] Jinxi Li,[2,27] Myoung Keun Lee,[3] Jasmien Roosenboom,[3] Ekaterina Orlova,[1] Kaustabh Adhikari,[4] 23andMe Research Team,[5] Carla Gallo,[6] Giovanni Poletti,[6] Lavinia Schuler-Faccini,[7] Maria-Cátira Bortolini,[7] Samuel Canizales-Quinteros,[8] Francisco Rothhammer,[9,10] Gabriel Bedoya,[11] Rolando González-José,[12] Paige E. Pfeffer,[13] Christopher A. Wollenschlaeger,[14] Jacqueline T. Hecht,[15] George L. Wehby,[16] Lina M. Moreno,[17] Anan Ding,[2] Li Jin,[2,18] Yajun Yang,[18] Jenna C. Carlson,[1,19] Elizabeth J. Leslie,[3] Eleanor Feingold,[1,19] Mary L. Marazita,[1,3,20,21] David A. Hinds,[5] Timothy C. Cox,[22,23,24] Sijia Wang,[2,18,*] Andrés Ruiz-Linares,[4,18,25] and Seth M. Weinberg[1,3,26,*]

The genetic basis of earlobe attachment has been a matter of debate since the early 20th century, such that geneticists argue both for and against polygenic inheritance. Recent genetic studies have identified a few loci associated with the trait, but large-scale analyses are still lacking. Here, we performed a genome-wide association study of lobe attachment in a multiethnic sample of 74,660 individuals from four cohorts (three with the trait scored by an expert rater and one with the trait self-reported). Meta-analysis of the three expert-rater-scored cohorts revealed six associated loci harboring numerous candidate genes, including *EDAR*, *SP5*, *MRPS22*, *ADGRG6* (*GPR126*), *KIAA1217*, and *PAX9*. The large self-reported 23andMe cohort recapitulated each of these six loci. Moreover, meta-analysis across all four cohorts revealed a total of 49 significant ($p < 5 \times 10^{-8}$) loci. Annotation and enrichment analyses of these 49 loci showed strong evidence of genes involved in ear development and syndromes with auricular phenotypes. RNA sequencing data from both human fetal ear and mouse second branchial arch tissue confirmed that genes located among associated loci showed evidence of expression. These results provide strong evidence for the polygenic nature of earlobe attachment and offer insights into the biological basis of normal and abnormal ear development.

Introduction

Earlobe attachment (MIM: 128900) is often presented as an example of a readily observable Mendelian phenotype in educational materials[1] and continues to be studied as a Mendelian phenotype in the contemporary primary literature (for example, see Ordu et al.[2]). Yet, as early as 1937, Wiener[3] pointed out that earlobe attachment is likely to be a polygenic trait exhibiting a continuous phenotypic distribution. Although earlobe attachment is a neutral morphological trait, understanding its genetic etiology is valuable in that it offers a glimpse into the biological basis of ear development, improving our understanding of genes potentially involved in developmental defects. Moreover, it serves as an instructive example of simple versus polygenic inheritance in an accessible trait.

Recent genome-wide association studies (GWASs) have investigated earlobe attachment[4,5] and reported significant associations with variants in *EDAR* (MIM: 604095) and *SP5* (MIM: 609391).[4] Although promising, these and other suggestive associations have yet to be replicated in independent samples. Of note, ethnic differences in the frequency of lobe attachment are well documented,[6] suggesting that genetic heterogeneity might underlie the trait

[1]Department of Human Genetics, Graduate School of Public Health, University of Pittsburgh, Pittsburgh, PA 15261, USA; [2]Chinese Academy of Sciences Key Laboratory of Computational Biology, Shanghai Institutes for Biological Sciences, University of Chinese Academy of Sciences, Chinese Academy of Sciences, Shanghai 200031, China; [3]Center for Craniofacial and Dental Genetics, Department of Oral Biology, University of Pittsburgh, Pittsburgh, PA 15219, USA; [4]Department of Genetics, Evolution and Environment, University College London, London, UK; [5]23andMe Inc., 899 West Evelyn Avenue, Mountain View, CA 94041, USA; [6]Laboratorios de Investigación y Desarrollo, Facultad de Ciencias y Filosofía, Universidad Peruana Cayetano Heredia, 430 Cercado de Lima, Peru; [7]Departamento de Genética, Universidade Federal do Rio Grande do Sul, Porto Alegre 90040-060, Brazil; [8]Unidad de Genómica de Poblaciones Aplicada a la Salud, Facultad de Química, Universidad Nacional Autónoma de México, Instituto Nacional de Medicina Genómica, Mexico City 4510, Mexico; [9]Instituto de Alta Investigación, Universidad de Tarapacá, Arica, Chile; [10]Facultad de Medicina, Universidad de Chile, Santiago 8320000, Chile; [11]Grupo Genética Molecular GENMOL, Universidad de Antioquia, Medellín 050003, Colombia; [12]Instituto Patagónico de Ciencias Sociales y Humanas, Centro Científico Tecnológico, Centro Nacional Patagónico, Consejo Nacional de Investigaciones Científicas y Técnicas, Puerto Madryn U9120, Argentina; [13]Center for Advanced Dental Education, Orthodontics Program, Saint Louis University, St. Louis, MO 63104, USA; [14]Department of Orthodontics, University of Pittsburgh, Pittsburgh, PA 15261, USA; [15]Department of Pediatrics, McGovern Medical School, University of Texas, Houston, TX 77030, USA; [16]Department of Health Management and Policy, University of Iowa, Iowa City, IA 52246, USA; [17]Department of Orthodontics, University of Iowa, Iowa City, IA 52242, USA; [18]Ministry of Education Key Laboratory of Contemporary Anthropology, Collaborative Innovation Center for Genetics and Development, School of Life Sciences, Fudan University, Shanghai 200433, China; [19]Department of Biostatistics, University of Pittsburgh, Pittsburgh, PA 15261, USA; [20]Clinical and Translational Science Institute, School of Medicine, University of Pittsburgh, Pittsburgh, PA 15261, USA; [21]Department of Psychiatry, School of Medicine, University of Pittsburgh, Pittsburgh, PA 15261, USA; [22]Center for Developmental Biology & Regenerative Medicine, Seattle Children's Research Institute, Seattle, WA 98101, USA; [23]Craniofacial Medicine, Department of Pediatrics, University of Washington, Seattle, WA 98195, USA; [24]Department of Anatomy & Developmental Biology, Monash University, Clayton, VIC 3800, Australia; [25]Laboratory of Biocultural Anthropology, Law, Ethics, and Health, Centre National de la Recherche Scientifique and Etablissement Français du Sang, UMR 7268, Aix-Marseille University, Marseille 13284, France; [26]Department of Anthropology, University of Pittsburgh, Pittsburgh, PA 15260, USA
[27]These authors contributed equally to this work
*Correspondence: wangsijia@picb.ac.cn (S.W.), smwst46@pitt.edu (S.M.W.)
https://doi.org/10.1016/j.ajhg.2017.10.001.

and that deciphering its genetic architecture might require trans-ethnic studies. This notion is supported by the fact that one of the two previously reported associations was with a missense *EDAR* variant that is common in Asian and American populations but absent or infrequent in European and African populations.

We propose that large-scale genetic studies of normal human morphological traits can provide insights into the genes and pathways involved in developmental malformations. For example, the external human ear exhibits a highly complex morphology that develops from the first and second branchial arches[7] and requires precise spatial and temporal coordination of tissue proliferation, fusion, and apoptosis. Disruption of these processes can cause birth defects, such as nonsyndromic microtia (congenital under-development of the external ear [MIM: 600674]), which is a fairly common developmental defect that differs in frequency across populations.[8] Moreover, because the jaw and associated masticatory musculature are also derived from the branchial arches, a number of craniofacial syndromes involving arch deficiencies, such as hemifacial macrosomia (MIM: 164210)[9] and Treacher Collins syndrome (MIM: 154500),[10] are characterized by external ear abnormalities. Understanding the genetic factors that contribute to normal structural variation in human ears could provide critical insights into ear morphogenesis, as well as morphogenetic processes in general. In this report, we focus on one aspect of external ear morphology: the lobe.

Specifically, we scanned the genome for variants associated with lobe attachment in 74,660 individuals from four independent and ethnically distinct samples. These included (1) European American (n = 1,791), Latin American (n = 5,062), and Chinese (n = 2,857) cohorts in which lobe attachment was scored as a tripartite (free, partially attached, or fully attached) phenotype by an objective expert rater and (2) a European-ancestry cohort (n = 64,950) comprising research participants who were customers of 23andMe, a personal genomics company, and self-reported lobe attachment as a binary (free or attached) phenotype. We performed two nested meta-analyses to combine results across the three expert-rater-scored cohorts and subsequently across all four cohorts. All participants were genotyped on an Illumina genome-wide array and imputed to the 1000 Genomes Project reference panel, and a GWAS was performed after adjustment for necessary covariates and principal components (PCs) of ancestry (see Table S1). Manhattan and quantile-quantile plots for the GWAS results in individual cohorts are shown in Figure S1.

Subjects and Methods

Study Design

We used a nested genome-wide meta-analysis approach to identify and replicate variants associated with ear attachment. A GWAS was performed separately in four independent cohorts representing populations with distinct ancestries. For three of these cohorts (European American, Latin American, and Chinese), lobe attachment was scored by objective raters as a tripartite phenotype. For the fourth cohort (European-ancestry individuals in the 23andMe sample), lobe attachment was self-reported as a dichotomous phenotype. Because of differences in phenotype definition (tripartite versus dichotomous) and collection method (rater-scored versus self-reported), we performed two genome-wide meta-analyses of (1) the three rater-scored cohorts and (2) all four cohorts.

Data Access

Summary statistics for the 10,000 most significant SNPs from the meta-analyses are provided in Table S2. The individual-level genetic data for the expert-rated European American cohort are available from dbGaP: phs000949.v1.p1. Full summary statistics for all SNPs in the European American, Latin American, and Chinese cohorts are available upon request. Summary statistics for the 23andMe cohort can be requested directly from 23andMe and will be made available to qualified researchers under the terms of a data-transfer agreement with 23andMe to protect the privacy of the participants. Please contact David Hinds for more information and to apply to access the data.

Recruitment and Phenotyping

The European American cohort consisted of 1,791 unrelated European-ancestry individuals aged 3–49 years and recruited from Pittsburgh, Seattle, Houston, and Iowa City as part of a 3D Facial Norms Project.[11,12] Participants were screened for conditions affecting craniofacial morphology, including a history of congenital malformations, trauma, and surgery. The Latin American cohort comprised 5,062 participants from the Consortium for the Analysis of the Diversity and Evolution of Latin America (CANDELA)[13] recruited from Brazil, Chile, Colombia, Mexico, and Peru. The Chinese cohort comprised 2,857 ethnic Han Chinese participants recruited from Taizhou in the Jiangsu Province of China as part of the Taizhou Longitudinal Study.[14] All participants provided informed consent, and all study protocols were approved by the institutional review boards of the pertinent research institutions.

In the European American, Latin American, and Chinese cohorts, earlobes were classified as free, partially attached, or attached. An individual was considered to possess attached earlobes if at least one ear was rated as attached. For the European American cohort, two independent observers examined the ears of participants from 3D craniofacial surface images captured by digital stereophotogrammetry. For the Latin American cohort, the same rater scored lobe attachment according to digital photography (Nikon) of the right side (45° angle) and front of the face. For the Chinese cohort, two independent observers scored lobe attachment from 2D digital photography (Canon EOS 600D) of both sides at a 45°angle.

An additional cohort, composed of research participants from the consumer base of 23andMe as previously described,[5,15] was included. For this study, the 23andMe sample comprised 64,950 unrelated individuals of European ancestry, and data on ear attachment were collected via self-reporting in online surveys using a dichotomous (attached or free) phenotype definition. Example imagery of attached and free earlobes was provided to participants for reference. 23andMe research participants provided informed consent and answered surveys online according

to a human subjects protocol approved by Ethical and Independent Review Services, an external institutional review board.

Genotyping, Quality Control, and Imputation

Genotyping was performed separately in the four cohorts. For the European American cohort, DNA was extracted from saliva samples and genotyped along with 72 HapMap control samples for 964,193 SNPs on the Illumina HumanOmniExpress+Exome v.1.2 array by the Center for Inherited Disease Research. Genetic data cleaning and quality control have been described in detail previously.[11] In brief, samples were interrogated for sex, chromosomal aberrations, relatedness, genotype call rate, and batch effects. SNPs were interrogated for call rate, discordance among 70 duplicate samples, Mendelian errors among HapMap controls (parent-offspring trios), deviations from Hardy-Weinberg equilibrium, and sex differences in allele frequencies and heterozygosity. For the Latin American cohort, DNA was extracted from blood samples obtained by a certified phlebotomist and genotyped for 730,525 SNPs on the Illumina HumanOmniExpress array. Quality filters included genotyping call rates per participant and per SNP and minor allele frequency (MAF). Because of admixture within the sample, filters for Hardy-Weinberg equilibrium were not implemented. For the Chinese cohort, DNA was extracted from peripheral-blood samples and genotyped for 887,270 SNPs on the Illumina HumanOmniZhonghua-8 array. SNP-level quality filters were applied for missing call rate, MAF, deviation of genotype frequencies from Hardy-Weinberg equilibrium, and technical filters (shown in Table S3).

For the 23andMe cohort, DNA extraction and genotyping were performed on saliva samples by Laboratory Corporation of America clinical laboratories certified by the Clinical Laboratory Improvement Amendments and accredited by the College of American Pathologists. Samples from this cohort were genotyped on one of four Illumina platforms: two versions of the HumanHap550 chip plus 25,000 custom SNPs, the HumanOmniExpress plus custom content to increase overlap with the HumanHap550 platforms, or a fully custom-designed array. Participants with samples that failed to reach 98.5% call rates were re-contacted for a replacement sample and were re-analyzed. Quality filters were applied for genotype call rate, MAF, Hardy-Weinberg equilibrium, and artifact effects by date.

For all studies, unobserved variants were imputed with haplotypes from the 1000 Genomes Project as the reference (phase 1 for the Latin American and 23andMe cohorts and phase 3 for the European American and Chinese cohorts). Pre-phasing (using SHAPEIT2[16] for the rater-scored cohorts and the company's own tool according to the Beagle[17] algorithm for the 23andMe cohort) was performed before imputation. Imputation was performed with IMPUTE2[18] for rater-scored cohorts and with Minimac2[19] for the 23andMe cohort. For the European and Latin American cohorts, masked variant analysis, in which genotyped SNPs were imputed for assessment of imputation quality, indicated high accuracy of imputation. Table S4 shows imputation quality filters.

Population Structure

To assess population structure, we performed principal-component analysis (PCA) within each cohort by using subsets of uncorrelated SNPs. Plots of the top PCs of ancestry for the European American, Chinese, and 23andMe cohorts are shown in Figure S5. The complex population structure in the Latin American sample was the focus of a previous investigation.[13] On the basis of scatterplots of the PCs and scree plots of the eigenvalues, we determined that adjustment for 4, 5, 0, and 5 PCs was necessary for the European American, Latin American, Chinese, and 23andMe cohorts, respectively. In the 23andMe cohort, we compared phased genomic segments with reference data across 31 populations to assign the mostly likely ancestry source of each segment.[20] We aggregated local-ancestry assignments to determine the overall proportions of ancestry of each individual. Of the 68,965 consenting 23andMe participants with available phenotypes, 64,950 individuals were determined to have >97.5% European ancestry and were included in this study. In general, genetically determined European ancestry closely matched the self-reported ancestry of the 23andMe participants.

Association Analyses

Earlobe attachment was analyzed as a semiquantitative phenotype (coded 0, 1, or 2 for free, partially attached, or attached earlobes, respectively) separately in the European American, Latin American, and Chinese cohorts. We tested genetic association while adjusting for necessary covariates (such as age, sex, height, and body mass index; see Table S1) and PCs of ancestry by using linear regression under the additive genetic model. For the analysis of the X chromosome, we coded genotypes as 0, 1, or 2 per the additive genetic model for females and as 0 or 2 for males in order to maintain the same scale between sexes. GWAS results for each study were combined via inverse-variance-weighted meta-analysis.

For the 23andMe cohort, earlobe attachment was analyzed as a binary phenotype (coded 0 for free or 1 for attached). We used logistic regression including adjustment for age, sex, genotyping platform, and the top five PCs to test for genetic association under the additive genetic model. Results across all four cohorts were combined via Stouffer's method[21] of inverse-weighted meta-analysis (based on p values, direction of effect, and sample size). This method of meta-analysis was chosen because it is robust to differences in the scale of the effect estimates among the expert-rater-scored cohorts and between the expert-rater-scored and self-reported 23andMe cohort as a result of differences in phenotype assessments. Compared with meta-analysis methods that use effect sizes and standard errors, Stouffer's method results in only a small loss of efficiency,[21] which is outweighed by its robustness to known and unknown phenotype differences across cohorts, and it does not require an assumption that effects are the same across cohorts. We used the binomial test (i.e., sign test) to model the consistency of direction of expert-rater-scored effects with the 23andMe cohort.

Functional Annotation

We used HaploReg[22] to query the lead SNP (i.e., the SNP with the smallest p value) at each associated locus in order to extract evidence of functional variation (promotor and enhancer histone marks, DNase hypersensitivity, expression quantitative trait locus [eQTL] information) for all SNPs in linkage disequilibrium (LD; $r^2 > 0.8$) with the lead SNP. 351 genes of interest were defined on the basis of a physical proximity of 500 kb to the lead SNP at each locus. These genes were queried in a number of online databases. We used Mouse Genome Informatics (MGI)[23] to annotate expression in relevant tissues and phenotypic consequences and used the VISTA Enhancer Browser[24] to annotate active enhancer elements in relevant tissues. We used OMIM, PubMed, DECIPHER,[25] and ClinVar[26] to annotate human phenotypic

information. We performed genomic enrichment analyses by using the Genomic Regions Enrichment of Annotations Tool (GREAT).[27]

Tissue Collection, RNA Isolation, and Sequencing

Branchial arch two tissue was dissected from wild-type embryonic day 10.5 mice, as well as equivalently staged homozygous *sbse* and *dmbo* embryos, and snap frozen on dry ice. RNA was isolated with the QIAGEN RNeasy Mini Kit (74104, QIAGEN), and its quality and concentration were assessed with an Agilent 2200 TapeStation system at the Genomics Core of the Fred Hutchinson Cancer Research Center. All samples had an RNA integrity number greater than 8. For each genotype, RNA was pooled from three male pups, and a total of 1 μg RNA of each genotype was sent to the Genomic Services Lab at the Hudson Alpha Institute for Biotechnology for preparation of indexed directional libraries and ribosomal reduction RNA sequencing (RNA-seq). Samples were paired-end sequenced with 250 million reads on an Illumina HiSeq v.4 PE100. The Cufflinks software suite was used for transcriptome assembly and differential expression analysis. We used the DESeq2 package to weight expression with count data and the Integrative Genomics Viewer to visualize sequences.[28,29]

For the analyses of human fetal RNA, ear tissue was obtained (after informed parental consent was provided) from material collected by the Birth Defects Research Laboratory (under approval by the institutional review board of the University of Washington). The gestational age of conceptuses, reported as the number of days after fertilization, was estimated from fetal foot length. The tissue was snap frozen, and RNA was processed as described above.

Results

Earlobe-Attachment Loci Observed in Trans-ethnic Meta-analysis

Rates of lobe attachment differed across the cohorts (Table S1), which was expected given the known differences across ethnic groups. Meta-analysis of the GWAS results from the three expert-rater-scored cohorts (see Figures 1A and 1B) yielded six loci that were significantly (i.e., $p < 5 \times 10^{-8}$) associated with earlobe attachment (Table 1; Figure 2): 2q13, 2q31.1, 3q23, 6q24.2, 10p12.2, and 14q13.1. These loci included the genes *EDAR* (2q13; lead SNP: rs3827760), *SP5* (2q31.1; lead SNP: rs6756973), *MRPS22* (MIM: 605810; 3q32; lead SNP: rs9866054), *ADGRG6* (*LOC153910* or *GPR126* [MIM: 612243]; 6q24.2; lead SNP: rs58122955), *KIAA1217* (MIM: 617367; 10p12.2; lead SNP: rs7096127), and *PAX9* (MIM: 167416; 14q13.1; lead SNP: rs1950357). One missense variant, rs3827760 in *EDAR*, was observed among the six lead SNPs and other variants in high LD ($r^2 > 0.8$) with the lead SNPs. The others were either intronic or intergenic, and as summarized by HaploReg,[22] several showed evidence of DNase hypersensitivity and histone marks indicative of enhancer or promoter regulatory elements in skin and other cell types. None of the lead SNPs or variants in high LD with the lead SNPs were known eQTLs.

Each of these six loci also showed significant evidence of association with earlobe attachment in the self-rated 23andMe cohort (Table 1). Moreover, in the meta-analysis across all four cohorts (Figures 1C and 1D), a total of 49 significant loci were observed (Figure S2; Table S5), which included the six loci observed in the meta-analysis of expert-rater-scored cohorts. Of the 49 loci, 15 showed significant associations (i.e., $p < 5 \times 10^{-8}$) in the 23andMe sample and replication-level p values of <0.001 in at least one additional cohort or in the meta-analysis across the three expert-rater-scored cohorts. Another 24 loci were driven primarily by significant associations observed in the 23andMe cohort; 14 of the 24 showed consistent directions of effects between 23andMe and all three expert-rater-scored cohorts (sign test $p = 1.29 \times 10^{-7}$), and 23 of 24 showed consistent directions of effects between 23andMe and at least two of the three expert-rater-scored cohorts (sign test $p = 1.49 \times 10^{-6}$). The remaining 4 of the 49 loci were significant only in the meta-analysis across all four cohorts but not in any individual cohort.

Functional Annotation

351 genes were located within 500 kb of the lead SNP across the 49 associated loci. Using public databases (see Subjects and Methods), we queried these 351 genes for documented expression and activity of enhancer elements in relevant tissues, as well as any known roles associated with ear phenotypes in human disorders or mouse models. Table S6 enumerates the genes at associated loci and the evidence substantiating their biological roles related to ear morphology. In total, 71 (20%) of the 351 genes were expressed in relevant tissues in mice (12 [3%] in the outer ear, 58 [17%] in the inner ear, and 39 [11%] in the branchial arches). Likewise, 21 (6%) of the genes were implicated in human syndromes manifesting with ear phenotypes, 22 (6%) were implicated in ear phenotypes in mouse models, and 16 (5%) were flanking active enhancer elements in relevant tissues. Overall, several plausible candidate genes were identified across the 49 associated loci identified via meta-analysis.

We performed genomic enrichment analysis by using GREAT[27] to determine whether the gene set comprising the two nearest genes across the 49 associated loci (indicated by the position of the lead SNP) was enriched with relevant annotations across several ontologies. Of most relevance, we observed significant enrichment of over 16-fold for the human phenotype annotations "microtia," "aplasia/hypoplasia of the external ear," and "aplasia/hypoplasia of the ear" (p values $< 1.5 \times 10^{-5}$ for all), as well as 5-fold enrichment for "low-set ears" and "abnormal location of ears" (p values < 0.0001 for both). Significant enrichment was also observed for several embryonic-development- and morphogenesis-related Gene Ontology biological processes, many mouse morphology (including ear) terms, and mouse expression in many relevant tissues (notably branchial arch and ear). Detailed enrichment results are shown in Figure S3.

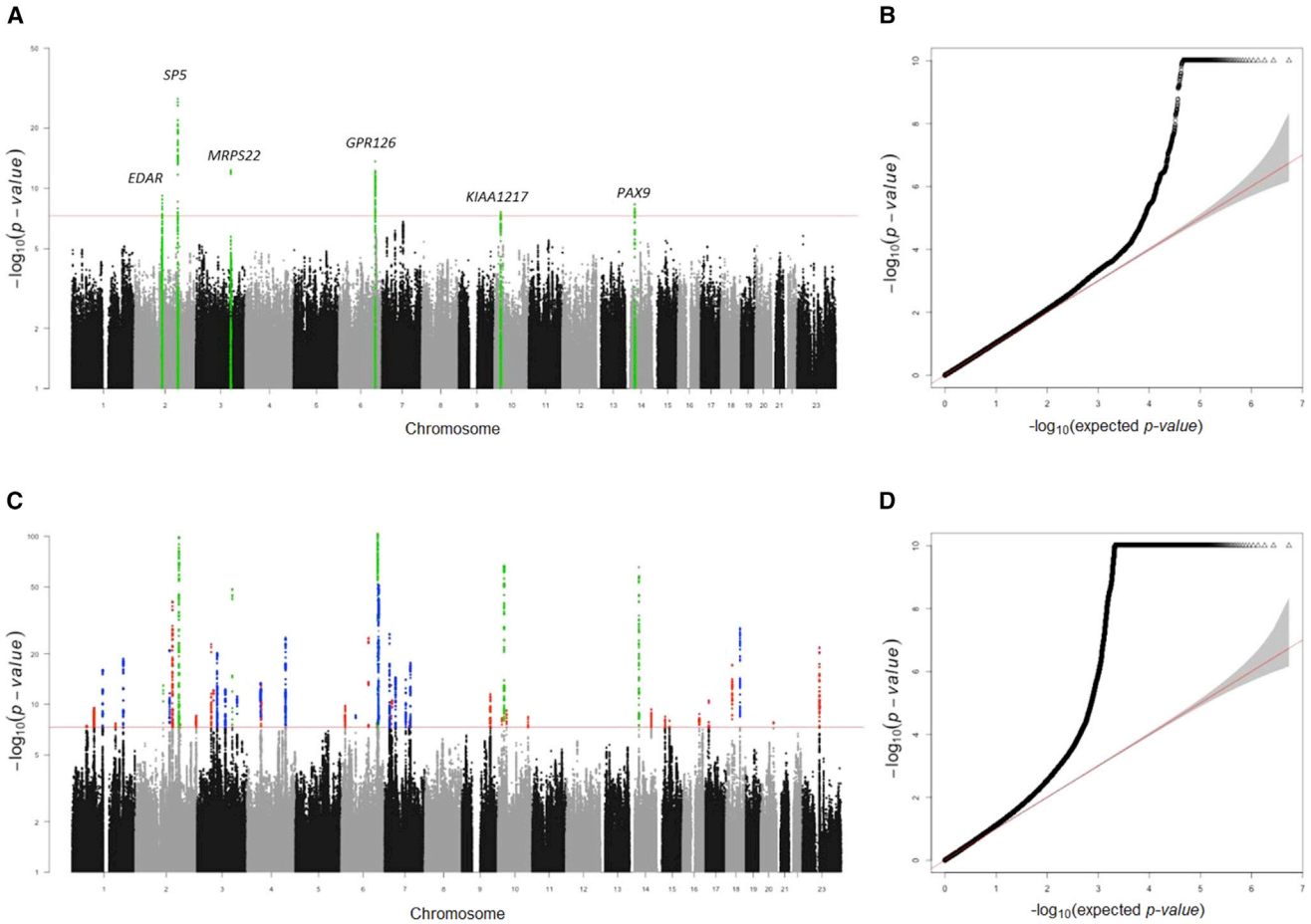

Figure 1. Genome-wide Scans

(Left) Manhattan plots showing the $-\log_{10}$-transformed p values (y axis) by physical genomic position (x axis) for each SNP in (A) the meta-analysis of the three rater-scored cohorts and (C) the meta-analysis of all four cohorts. The horizontal line represents the threshold for genome-wide significance ($p < 5 \times 10^{-8}$). (A) Six significant loci (green) were observed, and genes near the lead SNP in each locus are annotated. (C) 49 associated loci were observed: the same six loci in (A) are shown in green, and these reached genome-wide significance in more than one cohort; the 15 loci in blue showed genome-wide significance in one cohort and replication-level significance ($p < 0.001$) in at least one additional cohort or the meta-analysis of expert-rater-scored cohorts; and the 28 loci in red were observed via meta-analysis.

(Right) Quantile-quantile plots showing the observed distribution of $-\log_{10}$-transformed p values (y axis) against the expected distribution (x axis) under the null hypothesis of no association (diagonal line) for (B) the meta-analysis of the three rater-scored cohorts (genomic inflation factor = 1.066) and (D) the meta-analysis of all four cohorts (genomic inflation factor = 1.563). The presence of significantly associated loci is indicated by the deviation of observed p values from the tail of the null distribution, as shown by points above the diagonal in the upper right of the plots.

Expression Experiments

To confirm that genes located among associated loci are expressed in relevant tissues during development, we used RNA-seq to measure the expression of 174 genes located within 250 kb of one of the 49 lead SNPs. Gene expression was measured in two human fetal ears (at days 57 and 59 of development, when external ear structures are present but still developing[7]) and in mouse embryonic day 10.5 branchial arch tissue isolated from two mutants, *short body-short ear* (*sbse*) and dumbo (*dmbo*), and sex- and background-matched wild-type (C57BL/6) controls. These mutants present with microtia (*sbse*) or low-set ears with "lobe duplication" (*dmbo*).[30] For 4 of the 49 loci, no genes were located within 250 kb of the lead SNP. The majority of the remaining 45 loci had one or more genes that were robustly expressed in these relevant embryonic tissues (Figure S4). Human fetal ear tissue showed similar expression levels at days 57 and 59, and the greatest expression was observed on both days for *PRRX1* (MIM: 167420; 1q24.2), a homeobox gene with relevant biology (see Discussion). Some of the genes located at the six loci (especially 2q31.1 and 2q13; Figure 3) identified in the GWAS of rater-scored cohorts and recapitulated in the 23andMe cohort were among the top ranking genes (of the 174 genes tested) in terms of expression in humans or differential expression between mutant and wild-type mice. For example, mouse orthologs of both *SP5* (2q31.1) and *EDAR* (2q13) exhibited higher expression in *dmbo* mutant mice than in wild-type controls ($\log_2$ fold change > 0.5), and orthologs of *GAD1*

Table 1. Evidence of Association for the Lead SNP in Each Significant ($p < 5 \times 10^{-8}$) Locus Nominated in the Meta-analysis across the Rater-Scored Cohorts

	2q13	2q31.1	3q23	6q24.2	10p12.2	14q13.1
Gene candidate(s)	*EDAR*	*SP5*	*MRPS22*, *FOXL2*	*ADGRG6* (*GPR126*)	*KIAA1217*, *ARHGAP21*	*PAX9*, *NKX2-8*
Lead SNP	**rs3827760**	**rs6756973**	**rs9866054**	**rs58122955**	**rs7096127**	**rs1950357**
Base position	109,513,601	171,542,573	138,997,688	142,921,276	24,506,439	37,209,698
Functional position	missense	intronic	intergenic	intronic	intronic	intronic
Data source	genotyped	imputed	genotyped	imputed	imputed	imputed
Minor/major alleles	G/A	C/G	A/G	A/G	C/T	C/A
European American						
MAF	0.015	0.413	0.257	0.223	0.451	0.386
Beta	0.028	0.073	−0.041	0.119	−0.034	0.086
SE	0.081	0.020	0.022	0.023	0.019	0.020
p value	0.733	1.84×10^{-4}	0.059	2.78×10^{-7}	0.077	2.40×10^{-5}
Latin American						
MAF	0.404	0.661	0.550	0.185	0.490	0.359
Beta	0.062	0.088	−0.025	0.067	−0.043	0.027
SE	0.012	0.011	0.011	0.013	0.010	0.010
p value	7.67×10^{-8}	7.29×10^{-16}	0.019	2.34×10^{-7}	2.06×10^{-5}	9.41×10^{-3}
Chinese						
MAF	0.946	0.419	0.429	0.267	0.303	0.295
Beta	0.129	0.101	−0.128	0.051	−0.052	0.065
SE	0.032	0.015	0.015	0.017	0.016	0.016
p value	5.66×10^{-5}	9.84×10^{-12}	2.60×10^{-18}	0.002	0.001	8.04×10^{-5}
Meta-analysis for Rater-Scored Cohorts						
p value	6.65×10^{-10}	1.13×10^{-28}	5.27×10^{-13}	2.49×10^{-14}	2.44×10^{-8}	4.82×10^{-9}
23andMe						
MAF	0.007	0.410	0.249	0.238	0.451	0.389
OR	1.490	1.270	0.837	1.335	0.813	1.237
CI	(1.299, 1.709)	(1.238, 1.303)	(0.813, 0.862)	(1.296, 1.375)	(0.793, 0.834)	(1.206, 1.269)
p value	2.04×10^{-8}	4.90×10^{-76}	4.42×10^{-33}	3.31×10^{-87}	8.48×10^{-59}	8.26×10^{-59}
Meta-analysis for All Cohorts						
p value	1.16×10^{-13}	1.65×10^{-99}	4.78×10^{-43}	7.64×10^{-100}	1.56×10^{-65}	2.85×10^{-66}

Abbreviations are as follows: MAF, minor allele frequency; SE, standard error of the beta-coefficient; OR, odds ratio; and CI, 95% confidence interval of the odds ratio.

(MIM: 605363; 2q31.1), *MYO3B* (MIM: 610040; 2q31.1), and *SH3RF3* (2q13) showed reduced expression in the mutant mice ($\log_2$ fold change < -0.5). Thus, separate genes at the 2q13 and 2q31.1 loci were both up- and down-regulated (see Figures 2A and 2B for genetic association results for these loci). In a comparison of *sbse* mutants and wild-type mice, orthologs of *ERICH2* (2q31.1) and *NKX2-1* (2q13.1; MIM: 600635) were among the top over-expressed genes in *sbse* mutants among the 174 tested, and orthologs of *GAD1* (2q31.1) and *SH3RF3* (2q13) again exhibited reduced expression in the mutants (see Figures 2A, 2B, and 2F for genetic association results for these genes). Together, these results confirm the expression of genes located at associated loci in relevant human tissue and suggest that expression differs by ear phenotype for some genes at associated loci in a mouse model.

Discussion

We have performed the largest genome-wide study to date of earlobe attachment in 74,660 individuals from three

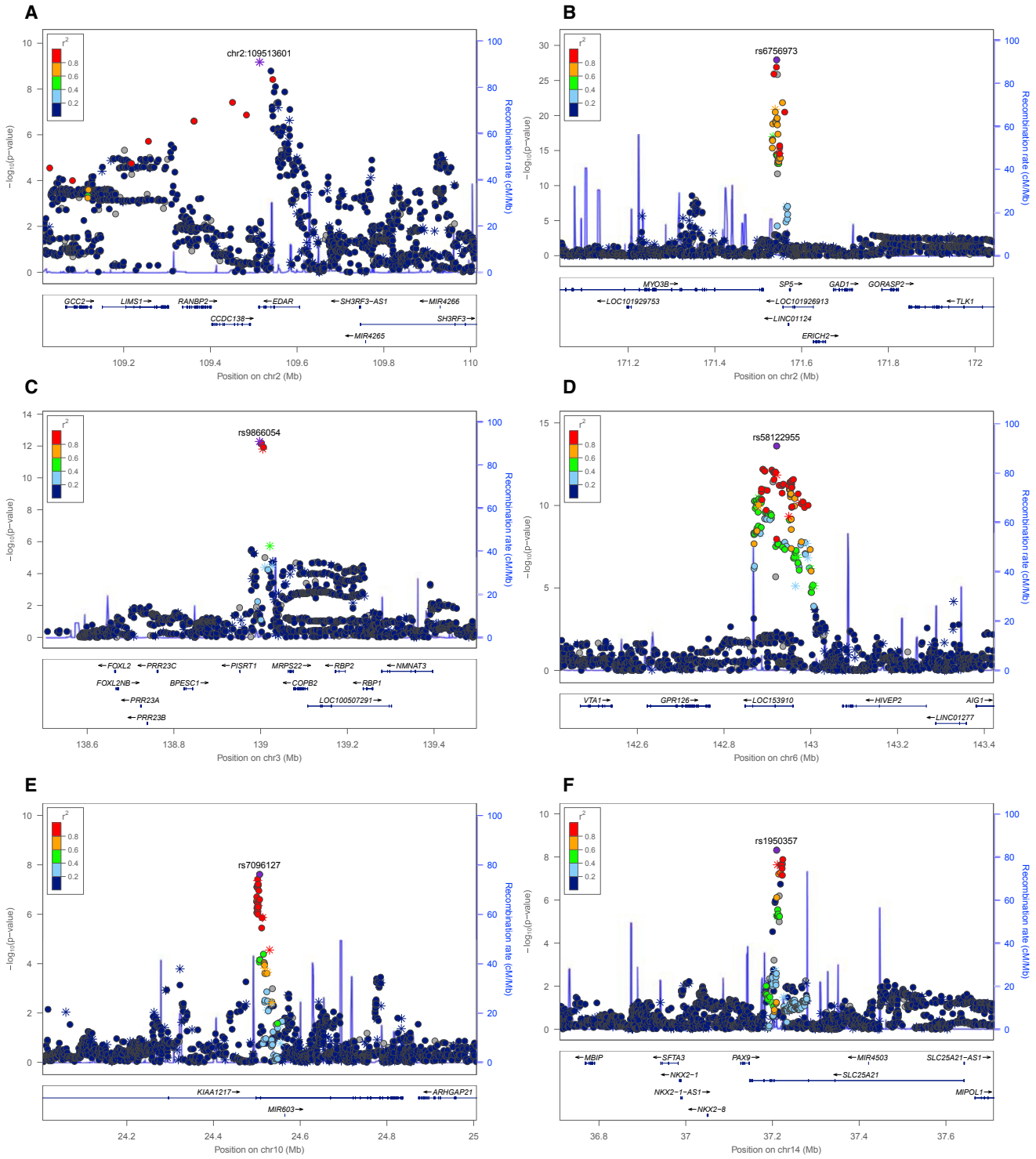

Figure 2. Regional Association Plots Showing Significant Associations Observed in the Meta-analysis of the Three Rater-Scored Cohorts

Regional plots near (A) *EDAR*, (B) *SP5*, (C) *MRPS22*, (D) *ADGRG6* (*GPR126*), (E) *KIAA1217*, and (F) *PAX9* show $-\log_{10}$-transformed p values (left y axis) by physical position (x axis). Shading denotes the LD (r^2) between each SNP and the lead SNP (purple). The blue overlay represents the recombination rate (right y axis). Gene positions are indicated under each plot.

ancestry groups. All six significant loci observed in the meta-analysis using the tripartite rater-scored phenotype were also significantly associated with earlobe attachment in the 23andMe cohort using the self-reported dichotomous phenotype. Furthermore, four of the six loci were the top ranking (by p value) associations observed in the 23andMe cohort (the other two loci ranked 7th and 42nd in the 23andMe GWAS). Thus, the GWAS of the 23andMe

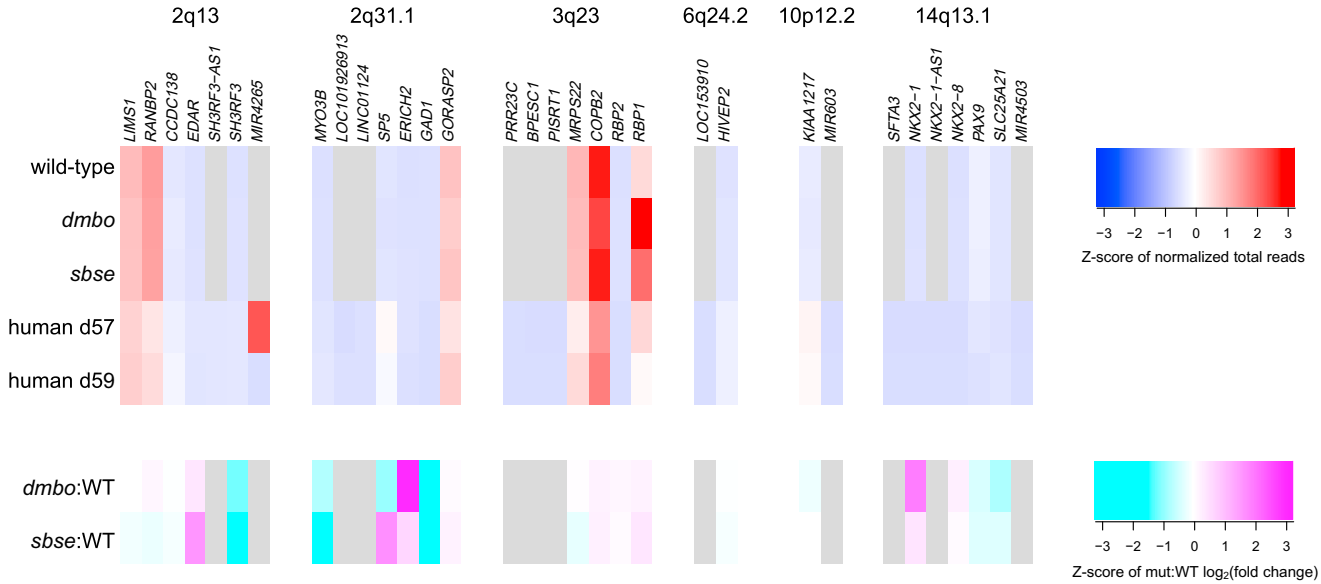

Figure 3. Heatmaps of Gene Expression
Heatmaps of gene expression in second branchial arch tissue from embryonic mice (wild-type mice and *dmbo* and *sbse* mutants) and fetal human pinna (at days 57 and 59) and for genes at the six loci observed in the meta-analysis of rater-scored cohorts; normalized total read counts are on the top, and fold changes between mutant mice and wild-type mice are on the bottom. The shading scale is shown for *Z* scores of expression and fold change. Genes for which expression data were not measured are shown in gray.

cohort recapitulated all of the major findings from the expert-rater-scored cohorts. Furthermore, four of the six loci contained genes showing notable expression (e.g., a high read count in humans and/or differential expression in mice) in relevant embryonic tissues.

Among the six associated loci from the rater-scored meta-analysis, two (2q13 at *EDAR* and 2q31.1 at *SP5*) have been previously identified in the Latin American cohort,[4] two (6q24.2 near *ADGRG6* [*GPR126*] and 10p12.2 at *KIAA1217*) have previously shown suggestive evidence of association,[4,5] and one (3q23 near *MRPS22*) has been previously implicated in earlobe size. In contrast, the association at 14q13.1 near *PAX9* did not show evidence of genetic association in previous studies.[4,5] These or nearby genes have known biological functions that indicate plausible roles in determining ear morphology. For example, *EDAR* encodes a cell-surface receptor important for the development of ectodermal tissues, including skin. The missense SNP rs3827760 (c.1109T>C [p.Val370Ala]) affects protein activity[31,32] and is associated with variation in tooth morphology, hair, sweat gland density, and facial morphology in Asians.[33–41] This variant was the top SNP in the *EDAR* region in the meta-analyses, and its frequency differs dramatically across populations (e.g., G allele frequency of <1% in Europeans, 39% in Latin Americans, and >90% in Han Chinese in the 1000 Genomes Project). Adhikari et al. have shown that *Edar* is expressed in the mouse pinna and that, compared with wild-type mice, mouse mutants with loss of *Edar* function exhibit reduced ear protrusion and length, as well as a different shape.[4]

SP5 encodes a transcription factor involved in the regulation of Wnt-mediated beta catenin signaling, which in turn is critical for multiple aspects of development, including that of the inner ear.[42] *ADGRG6* (*GPR126*) encodes a G-protein-coupled receptor whose disruption, via either mutation[43] or morpholino,[44] causes a swollen inner-ear phenotype in zebrafish. This locus was shown to be associated with earlobe size, a related phenotype, in the Latin American cohort.[4] *KIAA1217* is not known to be involved in ear development, but the associated variants are downstream of *ARHGAP21* (MIM: 609870), variants in which have been associated with mandibular prognathism,[45] a branchial arch defect.

The association at 3q23 occurs nearest *MRPS22*, which is implicated in a Cornelia de Lange-like phenotype including ear and skin dysmorphic features,[46] and is upstream of *FOXL2* (MIM: 605597), encoding a craniofacial transcription factor. This locus was previously implicated in earlobe size in the Latin American cohort.[4] The 14q13.3 association is near *PAX9*, encoding a transcription factor involved in mouth and tooth development, as well as *NKX2-8* (MIM: 603245), a homeobox candidate gene for microtia.[47]

In addition to the six loci identified via meta-analysis of rater-scored cohorts and recapitulated in 23andMe, meta-analysis across all four cohorts yielded 43 additional significant associations, driven primarily by the large 23andMe cohort. Among the more promising candidates were genes implicated in both human and mouse ear phenotypes: *TBX15* (MIM: 604127), *PRRX1*, and *ZEB2* (MIM: 605802). *TBX15* (the gene containing the lead SNP at this locus) is a transcription factor responsible for Cousin syndrome

(MIM: 260660), in which ears are low-set and posteriorly rotated.[48] In mouse, mutations in *TBX15* cause abnormal ear position and the "droopy ear" phenotype,[49] which resembles that seen in the *dmbo* mutants used in the expression analysis in this study. This locus was associated with ear phenotypes including antitragus size and folding of antihelix in the Latin American sample.[4] *PRRX1* (40 kb upstream of the lead SNP, which also showed the greatest expression in fetal human ear at day 57) is a homeobox gene implicated in Agnathia-otocephaly (characterized by severe malformations of the mouth, jaw, and ear; MIM: 202650),[50] and copy number variants affecting *PRRX1* have been observed in several patients with dysmorphic ear phenotypes. Moreover, *PRRX1* is expressed in the inner, middle, and outer ear and first and second branchial arches in mouse, and mutations cause lower ear position and abnormal Meckel's cartilage.[51] *ZEB2* (500kb downstream of lead SNP) is a homeobox gene implicated in Mowat-Wilson syndrome (MIM: 235730),[52] in which the ears are cupped and the earlobes are upturned with central depression. In mouse, *ZEB2* is expressed in the inner and middle ear, and first brachial arch, and knockouts lead to Mowat-Wilson-like features[53] or lack of first branchial arch during embryogenesis.[54] Other notable candidates include the growth factor *BMP5* (MIM: 112265), and homeobox transcription factors *DLX5* (MIM: 600028) and *DLX6* (MIM: 600030), which are all expressed in ear and related tissues and are all implicated in ear phenotypes in mice.[55,56]

The myriad associations overwhelmingly demonstrate the polygenic nature of earlobe attachment, standing in contrast to previous notions regarding its Mendelian nature, which have been perpetuated through the primary literature and educational materials for nearly a century. In fact, the large number of confidently identified loci is on par with many continuous anthropometric traits such as height and body composition. Moreover, earlobe attachment is correlated with other aspects of lobe morphology, including earlobe size, so the overlap in associated loci with the previous study of lobe size[4] is unsurprising. The effect sizes of variants observed in this study are fairly large for individual SNPs (resulting in a difference of up to 0.2 phenotype standard deviations per allele in the rater-scored cohorts and up to an odds ratio of 1.5 in the 23andMe cohort), although they are not large enough to cause Mendelian segregation. Moreover, differences in allele frequencies across ancestry groups were observed for some associated SNPs, which could explain part of the ethnic heterogeneity observed for earlobe attachment. Specifically, 16 of the lead SNPs of the 49 associated loci, notably the *EDAR* variant rs3827760 (which had a MAF difference of 0.93 between the European American and Chinese cohorts), showed MAF differences greater than 0.2 across the ancestry groups.

Consistent with a polygenic trait in a well-powered GWAS, we observed evidence of genomic inflation (e.g., genomic inflation factors greater than 1.0) separately in the meta-analyses and the 23andMe cohort. This occurs because the genomic inflation factor, although designed to be calculated from a set of independent null markers, is instead calculated in GWASs from the set of all of the SNPs tested, including truly associated SNPs in LD with causal variants. For polygenic traits (for which there are multiple truly associated loci) in well-powered studies (where small p values are obtained even for SNPs weakly correlated with true causal alleles), the lambda is expected to be greater than 1.[57] We argue that this inflation is not due to population stratification because association models were adjusted for genetic ancestry estimated from the genetic data in each cohort. Moreover, inflation was not observed in the individual expert-rater-scored cohorts or in a subset of 2,000 participants from the 23andMe cohort, as would be expected if population stratification had caused epidemiological confounding. Instead, the inflation observed for earlobe attachment, which is similar to that observed for highly polygenic traits such as height, is expected given the contributions of numerous associated loci each tagged by many correlated SNPs.

Strengths of this work include the high-quality phenotyping based on digital imagery in the rater-scored cohorts, the inclusion of cohorts from different ancestry groups, the large sample size, and the method of meta-analysis, which was chosen to be robust to phenotype differences across the cohorts. Although phenotype data were collected via self-report in the 23andMe cohort, the fact that associations observed in the rater-scored cohorts were also identified in the 23andMe cohort suggests that the large sample size of the 23andMe cohort counterbalances noise (if any) as a result of the method of data collection. Despite these strengths, and because of the differences in phenotype assessment across cohorts, this study was limited by the fact that, within our testing framework, we were not able to directly test the heterogeneity of effects among cohorts. In addition, the large sample size of the 23andMe cohort, which benefited the statistical power of study, most likely had an outsized effect on the meta-analysis across all four cohorts. For this reason, we also reported results for meta-analysis across the three expert-rater-scored cohorts.

In conclusion, we have identified 49 associations with earlobe attachment, including 21 loci meeting the standard of genome-wide discovery ($p < 5 \times 10^{-8}$) plus independent replication ($p < 0.001$) and 28 loci showing evidence of discovery only (i.e., without independent replication), via meta-analysis. These genes provide insight into the complex biology of ear development. The fact that we observed several associated genes in which pathogenic variants are known to cause human syndromes with ear phenotypes is consistent with our hypothesis that whereas deleterious variants in genes can cause congenital defects and Mendelian conditions, regulatory variants in the same genes can influence normal phenotypic variation. Ultimately, understanding

the genetics of normal human morphological traits can provide insights into the genes and pathways involved in developmental malformations.

Supplemental Data

Supplemental Data include four figures and six tables and can be found with this article online at https://doi.org/10.1016/j.ajhg.2017.10.001.

Consortia

Members of the 23andMe Research Team include Michelle Agee, Babak Alipanahi, Adam Auton, Robert K. Bell, Katarzyna Bryc, Sarah L. Elson, Pierre Fontanillas, Nicholas A. Furlotte, David A. Hinds, Bethann S. Hromatka, Karen E. Huber, Aaron Kleinman, Nadia K. Litterman, Matthew H. McIntyre, Joanna L. Mountain, Elizabeth S. Noblin, Carrie A.M. Northover, Steven J. Pitts, J. Fah Sathirapongsasuti, Olga V. Sazonova, Janie F. Shelton, Suyash Shringarpure, Chao Tian, Joyce Y. Tung, Vladimir Vacic, and Catherine H. Wilson.

Conflicts of Interest

D.H. is employed by and owns stock or stock options in 23andMe.

Acknowledgments

We thank the participants of the 3D Facial Norms Project, CANDELA, and the Taizhou Longitudinal Study for their contributions toward this effort. We thank the research participants and employees of 23andMe for making this work possible. We thank Daniela Luquetti, Esra Camci, and Jessica Rosin (Seattle Children's Research Institute [SCRI]) and Mei Deng and Ian Glass (Birth Defects Research Laboratory, University of Washington) for contributions to tissue collection and RNA preparation for sequencing and Andrew Timms (SCRI) for initial bioinformatics processing. This work was funded by the following grants and contracts: Chinese Academy of Sciences Strategic Priority Research Program grant XDB13041000 (S.W.); National Natural Science Foundation of China grant 91631307 (S.W.), National Institute of Dental and Craniofacial Research grants and contracts U01-DE020078 (S.M.W. and M.L.M.), U01-DE020057 (M.L.M. and Jeffery C. Murray), R01-DE016148 (M.L.M. and S.M.W.), R00-DE02560 (E.J.L.), R01-DE027023 (S.M.W. and J.R.S.), and HHSN268201200008I (Center for Inherited Disease Research, Johns Hopkins University); National Human Genome Research Institute grant X01-HG007821 (M.L.M., S.M.W., and E.F.); Centers for Disease Control grant R01-DD000295 (G.L.W.); Leverhulme Trust grant F/07 134/DF (A.R.-L.); Biotechnology and Biological Sciences Research Council grant BB/I021213/1 (A.R.-L.); and the Laurel Foundation Endowment for Craniofacial Research (T.C.C.).

Received: July 24, 2017
Accepted: October 4, 2017
Published: November 30, 2017

Web Resources

1000 Genomes Project, http://www.internationalgenome.org/
23andMe, https://www.23andme.com/
Beagle, http://faculty.washington.edu/browning/beagle/beagle.html
ClinVar, https://www.ncbi.nlm.nih.gov/clinvar/
dbGaP, https://www.ncbi.nlm.nih.gov/gap
DECIPHER, http://decipher.sanger.ac.uk/
GREAT, http://great.stanford.edu/public/html/
HaploReg, http://archive.broadinstitute.org/mammals/haploreg/
IMPUTE2, http://mathgen.stats.ox.ac.uk/impute/impute_v2.html
Integrative Genomics Viewer, http://software.broadinstitute.org/software/igv/
Minimac2, https://genome.sph.umich.edu/wiki/Minimac2
Mouse Genome Informatics, http://www.informatics.jax.org/
OMIM, http://www.omim.org/
PubMed, https://www.ncbi.nlm.nih.gov/pubmed/
SHAPEIT, http://mathgen.stats.ox.ac.uk/genetics_software/shapeit/shapeit.html
VISTA Enhancer Browser, https://enhancer.lbl.gov/

References

1. Barnes, P., and Mertens, T.R. (1976). A survey and evaluation of human genetic traits used in classroom laboratory studies. J. Hered. *67*, 347–352.
2. Ordu, K.S., Didia, B.C., and Egbunefu, N. (2014). Inheritance Pattern of Earlobe Attachment amongst Nigerians. Green. J. Hum. Phys. Anat. *2*, 1–7.
3. Wiener, A.S. (1937). Complications in ear genetics. J. Hered. *28*, 425–426.
4. Adhikari, K., Reales, G., Smith, A.J., Konka, E., Palmen, J., Quinto-Sanchez, M., Acuña-Alonzo, V., Jaramillo, C., Arias, W., Fuentes, M., et al. (2015). A genome-wide association study identifies multiple loci for variation in human ear morphology. Nat. Commun. *6*, 7500.
5. Eriksson, N., Macpherson, J.M., Tung, J.Y., Hon, L.S., Naughton, B., Saxonov, S., Avey, L., Wojcicki, A., Pe'er, I., and Mountain, J. (2010). Web-based, participant-driven studies yield novel genetic associations for common traits. PLoS Genet. *6*, e1000993.
6. Lai, L.Y., and Walsh, R.J. (1966). Observations on ear lobe types. Acta Genet. Stat. Med. *16*, 250–257.
7. Cox, T.C., Camci, E.D., Vora, S., Luquetti, D.V., and Turner, E.E. (2014). The genetics of auricular development and malformation: new findings in model systems driving future directions for microtia research. Eur. J. Med. Genet. *57*, 394–401.
8. Luquetti, D.V., Leoncini, E., and Mastroiacovo, P. (2011). Microtia-anotia: a global review of prevalence rates. Birth Defects Res. A Clin. Mol. Teratol. *91*, 813–822.
9. Beleza-Meireles, A., Clayton-Smith, J., Saraiva, J.M., and Tassabehji, M. (2014). Oculo-auriculo-vertebral spectrum: a review of the literature and genetic update. J. Med. Genet. *51*, 635–645.
10. Vincent, M., Geneviève, D., Ostertag, A., Marlin, S., Lacombe, D., Martin-Coignard, D., Coubes, C., David, A., Lyonnet, S., Vilain, C., et al. (2016). Treacher Collins syndrome: a clinical and molecular study based on a large series of patients. Genet. Med. *18*, 49–56.
11. Shaffer, J.R., Orlova, E., Lee, M.K., Leslie, E.J., Raffensperger, Z.D., Heike, C.L., Cunningham, M.L., Hecht, J.T., Kau, C.H., Nidey, N.L., et al. (2016). Genome-Wide Association Study Reveals Multiple Loci Influencing Normal Human Facial Morphology. PLoS Genet. *12*, e1006149.

12. Weinberg, S.M., Raffensperger, Z.D., Kesterke, M.J., Heike, C.L., Cunningham, M.L., Hecht, J.T., Kau, C.H., Murray, J.C., Wehby, G.L., Moreno, L.M., and Marazita, M.L. (2016). The 3D Facial Norms Database: Part 1. A Web-Based Craniofacial Anthropometric and Image Repository for the Clinical and Research Community. Cleft Palate Craniofac. J. *53*, e185–e197.
13. Ruiz-Linares, A., Adhikari, K., Acuña-Alonzo, V., Quinto-Sanchez, M., Jaramillo, C., Arias, W., Fuentes, M., Pizarro, M., Everardo, P., de Avila, F., et al. (2014). Admixture in Latin America: geographic structure, phenotypic diversity and self-perception of ancestry based on 7,342 individuals. PLoS Genet. *10*, e1004572.
14. Wang, X., Lu, M., Qian, J., Yang, Y., Li, S., Lu, D., Yu, S., Meng, W., Ye, W., and Jin, L. (2009). Rationales, design and recruitment of the Taizhou Longitudinal Study. BMC Public Health *9*, 223.
15. Tung, J.Y., Do, C.B., Hinds, D.A., Kiefer, A.K., Macpherson, J.M., Chowdry, A.B., Francke, U., Naughton, B.T., Mountain, J.L., Wojcicki, A., and Eriksson, N. (2011). Efficient replication of over 180 genetic associations with self-reported medical data. PLoS ONE *6*, e23473.
16. Delaneau, O., Zagury, J.F., and Marchini, J. (2013). Improved whole-chromosome phasing for disease and population genetic studies. Nat. Methods *10*, 5–6.
17. Browning, S.R., and Browning, B.L. (2007). Rapid and accurate haplotype phasing and missing-data inference for whole-genome association studies by use of localized haplotype clustering. Am. J. Hum. Genet. *81*, 1084–1097.
18. Howie, B.N., Donnelly, P., and Marchini, J. (2009). A flexible and accurate genotype imputation method for the next generation of genome-wide association studies. PLoS Genet. *5*, e1000529.
19. Fuchsberger, C., Abecasis, G.R., and Hinds, D.A. (2015). minimac2: faster genotype imputation. Bioinformatics *31*, 782–784.
20. Durand, E.Y., Do, C.B., Mountain, J.L., and Macpherson, J.M. (2014). Ancestry Composition: A Novel, Efficient Pipeline for Ancestry Deconvolution. bioRxiv. https://doi.org/10.1101/010512.
21. Willer, C.J., Li, Y., and Abecasis, G.R. (2010). METAL: fast and efficient meta-analysis of genomewide association scans. Bioinformatics *26*, 2190–2191.
22. Ward, L.D., and Kellis, M. (2012). HaploReg: a resource for exploring chromatin states, conservation, and regulatory motif alterations within sets of genetically linked variants. Nucleic Acids Res. *40*, D930–D934.
23. Eppig, J.T., Smith, C.L., Blake, J.A., Ringwald, M., Kadin, J.A., Richardson, J.E., and Bult, C.J. (2017). Mouse Genome Informatics (MGI): Resources for Mining Mouse Genetic, Genomic, and Biological Data in Support of Primary and Translational Research. Methods Mol. Biol. *1488*, 47–73.
24. Visel, A., Minovitsky, S., Dubchak, I., and Pennacchio, L.A. (2007). VISTA Enhancer Browser–a database of tissue-specific human enhancers. Nucleic Acids Res. *35*, D88–D92.
25. Firth, H.V., Richards, S.M., Bevan, A.P., Clayton, S., Corpas, M., Rajan, D., Van Vooren, S., Moreau, Y., Pettett, R.M., and Carter, N.P. (2009). DECIPHER: Database of Chromosomal Imbalance and Phenotype in Humans Using Ensembl Resources. Am. J. Hum. Genet. *84*, 524–533.
26. Landrum, M.J., Lee, J.M., Benson, M., Brown, G., Chao, C., Chitipiralla, S., Gu, B., Hart, J., Hoffman, D., Hoover, J., et al. (2016). ClinVar: public archive of interpretations of clinically relevant variants. Nucleic Acids Res. *44* (D1), D862–D868.
27. McLean, C.Y., Bristor, D., Hiller, M., Clarke, S.L., Schaar, B.T., Lowe, C.B., Wenger, A.M., and Bejerano, G. (2010). GREAT improves functional interpretation of cis-regulatory regions. Nat. Biotechnol. *28*, 495–501.
28. Trapnell, C., Williams, B.A., Pertea, G., Mortazavi, A., Kwan, G., van Baren, M.J., Salzberg, S.L., Wold, B.J., and Pachter, L. (2010). Transcript assembly and quantification by RNA-Seq reveals unannotated transcripts and isoform switching during cell differentiation. Nat. Biotechnol. *28*, 511–515.
29. Love, M.I., Huber, W., and Anders, S. (2014). Moderated estimation of fold change and dispersion for RNA-seq data with DESeq2. Genome Biol. *15*, 550.
30. Rosin, J.M., Li, W., Cox, L.L., Rolfe, S.M., Latorre, V., Akiyama, J.A., Visel, A., Kuramoto, T., Bobola, N., Turner, E.E., and Cox, T.C. (2016). A distal 594 bp ECR specifies Hmx1 expression in pinna and lateral facial morphogenesis and is regulated by the Hox-Pbx-Meis complex. Development *143*, 2582–2592.
31. Mou, C., Thomason, H.A., Willan, P.M., Clowes, C., Harris, W.E., Drew, C.F., Dixon, J., Dixon, M.J., and Headon, D.J. (2008). Enhanced ectodysplasin-A receptor (EDAR) signaling alters multiple fiber characteristics to produce the East Asian hair form. Hum. Mutat. *29*, 1405–1411.
32. Bryk, J., Hardouin, E., Pugach, I., Hughes, D., Strotmann, R., Stoneking, M., and Myles, S. (2008). Positive selection in East Asians for an EDAR allele that enhances NF-kappaB activation. PLoS ONE *3*, e2209.
33. Fujimoto, A., Ohashi, J., Nishida, N., Miyagawa, T., Morishita, Y., Tsunoda, T., Kimura, R., and Tokunaga, K. (2008). A replication study confirmed the EDAR gene to be a major contributor to population differentiation regarding head hair thickness in Asia. Hum. Genet. *124*, 179–185.
34. Fujimoto, A., Kimura, R., Ohashi, J., Omi, K., Yuliwulandari, R., Batubara, L., Mustofa, M.S., Samakkarn, U., Settheetham-Ishida, W., Ishida, T., et al. (2008). A scan for genetic determinants of human hair morphology: EDAR is associated with Asian hair thickness. Hum. Mol. Genet. *17*, 835–843.
35. Kimura, R., Yamaguchi, T., Takeda, M., Kondo, O., Toma, T., Haneji, K., Hanihara, T., Matsukusa, H., Kawamura, S., Maki, K., et al. (2009). A common variation in EDAR is a genetic determinant of shovel-shaped incisors. Am. J. Hum. Genet. *85*, 528–535.
36. Park, J.H., Yamaguchi, T., Watanabe, C., Kawaguchi, A., Haneji, K., Takeda, M., Kim, Y.I., Tomoyasu, Y., Watanabe, M., Oota, H., et al. (2012). Effects of an Asian-specific nonsynonymous EDAR variant on multiple dental traits. J. Hum. Genet. *57*, 508–514.
37. Kamberov, Y.G., Wang, S., Tan, J., Gerbault, P., Wark, A., Tan, L., Yang, Y., Li, S., Tang, K., Chen, H., et al. (2013). Modeling recent human evolution in mice by expression of a selected EDAR variant. Cell *152*, 691–702.
38. Tan, J., Yang, Y., Tang, K., Sabeti, P.C., Jin, L., and Wang, S. (2013). The adaptive variant EDARV370A is associated with straight hair in East Asians. Hum. Genet. *132*, 1187–1191.
39. Tan, J., Peng, Q., Li, J., Guan, Y., Zhang, L., Jiao, Y., Yang, Y., Wang, S., and Jin, L. (2014). Characteristics of dental morphology in the Xinjiang Uyghurs and correlation with the EDARV370A variant. Sci. China Life Sci. *57*, 510–518.
40. Peng, Q., Li, J., Tan, J., Yang, Y., Zhang, M., Wu, S., Liu, Y., Zhang, J., Qin, P., Guan, Y., et al. (2016). EDARV370A

associated facial characteristics in Uyghur population revealing further pleiotropic effects. Hum. Genet. *135*, 99–108.
41. Wu, S., Tan, J., Yang, Y., Peng, Q., Zhang, M., Li, J., Lu, D., Liu, Y., Lou, H., Feng, Q., et al. (2016). Genome-wide scans reveal variants at EDAR predominantly affecting hair straightness in Han Chinese and Uyghur populations. Hum. Genet. *135*, 1279–1286.
42. Jacques, B.E., Puligilla, C., Weichert, R.M., Ferrer-Vaquer, A., Hadjantonakis, A.K., Kelley, M.W., and Dabdoub, A. (2012). A dual function for canonical Wnt/β-catenin signaling in the developing mammalian cochlea. Development *139*, 4395–4404.
43. Geng, F.S., Abbas, L., Baxendale, S., Holdsworth, C.J., Swanson, A.G., Slanchev, K., Hammerschmidt, M., Topczewski, J., and Whitfield, T.T. (2013). Semicircular canal morphogenesis in the zebrafish inner ear requires the function of gpr126 (lauscher), an adhesion class G protein-coupled receptor gene. Development *140*, 4362–4374.
44. Patra, C., van Amerongen, M.J., Ghosh, S., Ricciardi, F., Sajjad, A., Novoyatleva, T., Mogha, A., Monk, K.R., Mühlfeld, C., and Engel, F.B. (2013). Organ-specific function of adhesion G protein-coupled receptor GPR126 is domain-dependent. Proc. Natl. Acad. Sci. USA *110*, 16898–16903.
45. Perillo, L., Monsurrò, A., Bonci, E., Torella, A., Mutarelli, M., and Nigro, V. (2015). Genetic association of ARHGAP21 gene variant with mandibular prognathism. J. Dent. Res. *94*, 569–576.
46. Smits, P., Saada, A., Wortmann, S.B., Heister, A.J., Brink, M., Pfundt, R., Miller, C., Haas, D., Hantschmann, R., Rodenburg, R.J., et al. (2011). Mutation in mitochondrial ribosomal protein MRPS22 leads to Cornelia de Lange-like phenotype, brain abnormalities and hypertrophic cardiomyopathy. Eur. J. Hum. Genet. *19*, 394–399.
47. Qiao, R., He, Y., Pan, B., Xiao, S., Zhang, X., Li, J., Zhang, Z., Hong, Y., Xing, Y., and Ren, J. (2015). Understanding the molecular mechanisms of human microtia via a pig model of HOXA1 syndrome. Dis. Model. Mech. *8*, 611–622.
48. Lausch, E., Hermanns, P., Farin, H.F., Alanay, Y., Unger, S., Nikkel, S., Steinwender, C., Scherer, G., Spranger, J., Zabel, B., et al. (2008). TBX15 mutations cause craniofacial dysmorphism, hypoplasia of scapula and pelvis, and short stature in Cousin syndrome. Am. J. Hum. Genet. *83*, 649–655.
49. Candille, S.I., Van Raamsdonk, C.D., Chen, C., Kuijper, S., Chen-Tsai, Y., Russ, A., Meijlink, F., and Barsh, G.S. (2004). Dorsoventral patterning of the mouse coat by Tbx15. PLoS Biol. *2*, E3.
50. Dasouki, M., Andrews, B., Parimi, P., and Kamnasaran, D. (2013). Recurrent agnathia-otocephaly caused by DNA replication slippage in PRRX1. Am. J. Med. Genet. A. *161A*, 803–808.
51. ten Berge, D., Brouwer, A., Korving, J., Martin, J.F., and Meijlink, F. (1998). Prx1 and Prx2 in skeletogenesis: roles in the craniofacial region, inner ear and limbs. Development *125*, 3831–3842.
52. Garavelli, L., and Mainardi, P.C. (2007). Mowat-Wilson syndrome. Orphanet J. Rare Dis. *2*, 42.
53. Van de Putte, T., Francis, A., Nelles, L., van Grunsven, L.A., and Huylebroeck, D. (2007). Neural crest-specific removal of Zfhx1b in mouse leads to a wide range of neurocristopathies reminiscent of Mowat-Wilson syndrome. Hum. Mol. Genet. *16*, 1423–1436.
54. Van de Putte, T., Maruhashi, M., Francis, A., Nelles, L., Kondoh, H., Huylebroeck, D., and Higashi, Y. (2003). Mice lacking ZFHX1B, the gene that codes for Smad-interacting protein-1, reveal a role for multiple neural crest cell defects in the etiology of Hirschsprung disease-mental retardation syndrome. Am. J. Hum. Genet. *72*, 465–470.
55. Hellingman, C.A., Verwiel, E.T., Slagt, I., Koevoet, W., Poublon, R.M., Nolst-Trenité, G.J., Baatenburg de Jong, R.J., Jahr, H., and van Osch, G.J. (2011). Differences in cartilage-forming capacity of expanded human chondrocytes from ear and nose and their gene expression profiles. Cell Transplant. *20*, 925–940.
56. Birnbaum, S., Reutter, H., Mende, M., de Assis, N.A., Diaz-Lacava, A., Herms, S., Scheer, M., Lauster, C., Braumann, B., Schmidt, G., et al. (2009). Further evidence for the involvement of MYH9 in the etiology of non-syndromic cleft lip with or without cleft palate. Eur. J. Oral Sci. *117*, 200–203.
57. Hinrichs, A.L., Larkin, E.K., and Suarez, B.K. (2009). Population stratification and patterns of linkage disequilibrium. Genet. Epidemiol. *33* (*Suppl 1*), S88–S92.

The American Journal of Human Genetics, Volume *101*

Supplemental Data

Multiethnic GWAS Reveals Polygenic Architecture of Earlobe Attachment

John R. Shaffer, Jinxi Li, Myoung Keun Lee, Jasmien Roosenboom, Ekaterina Orlova, Kaustabh Adhikari, 23andMe Research Team, Carla Gallo, Giovanni Poletti, Lavinia Schuler-Faccini, Maria-Cátira Bortolini, Samuel Canizales-Quinteros, Francisco Rothhammer, Gabriel Bedoya, Rolando González-José, Paige E. Pfeffer, Christopher A. Wollenschlaeger, Jacqueline T. Hecht, George L. Wehby, Lina M. Moreno, Anan Ding, Li Jin, Yajun Yang, Jenna C. Carlson, Elizabeth J. Leslie, Eleanor Feingold, Mary L. Marazita, David A. Hinds, Timothy C. Cox, Sijia Wang, Andrés Ruiz-Linares, and Seth M. Weinberg

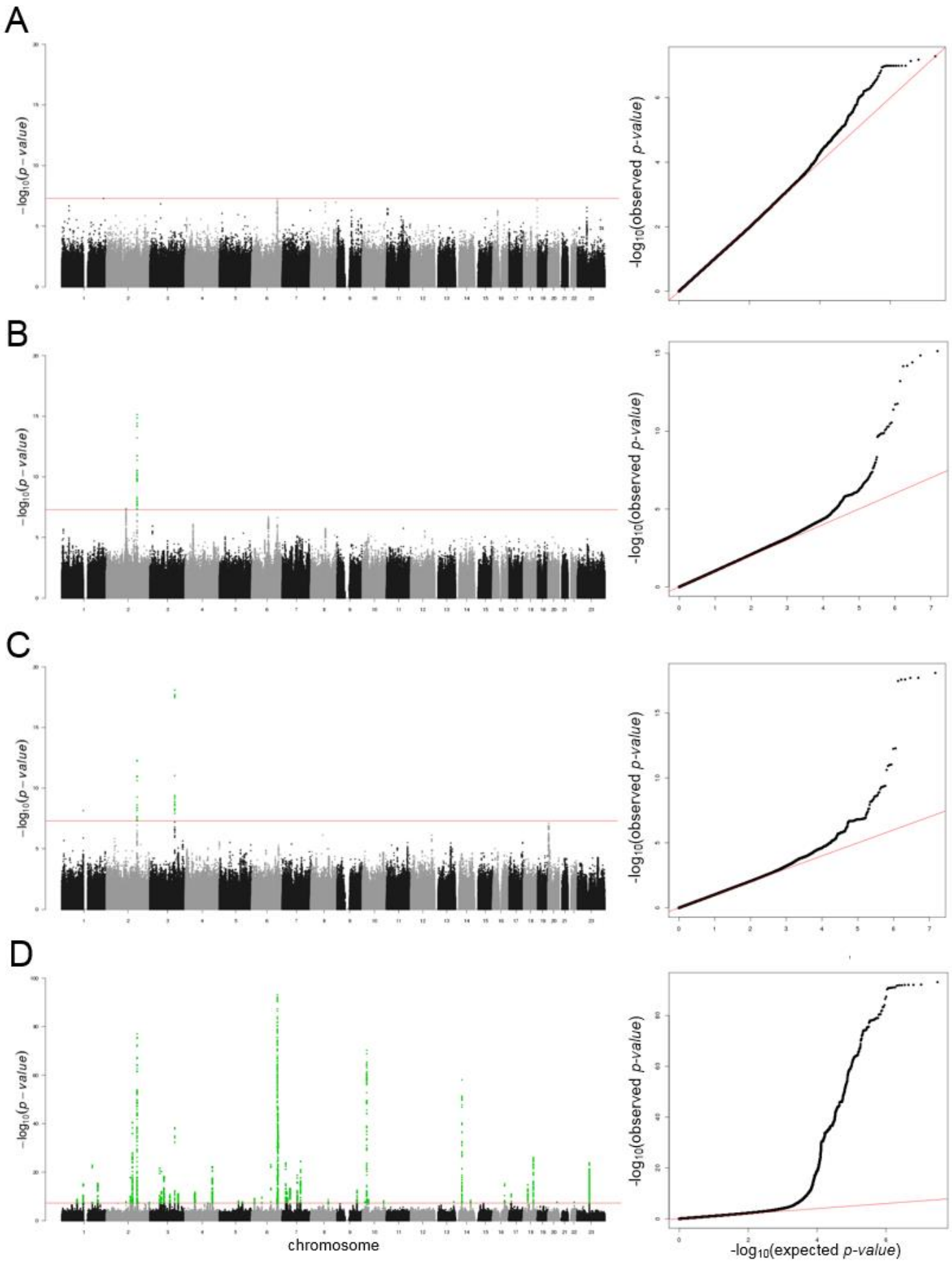

Figure S1: GWAS results shown as Manhattan (left) and quantile-quantile (right) plots for the (A) European American, (B) Latin American, (C) Chinese, and (D) 23andMe cohorts.

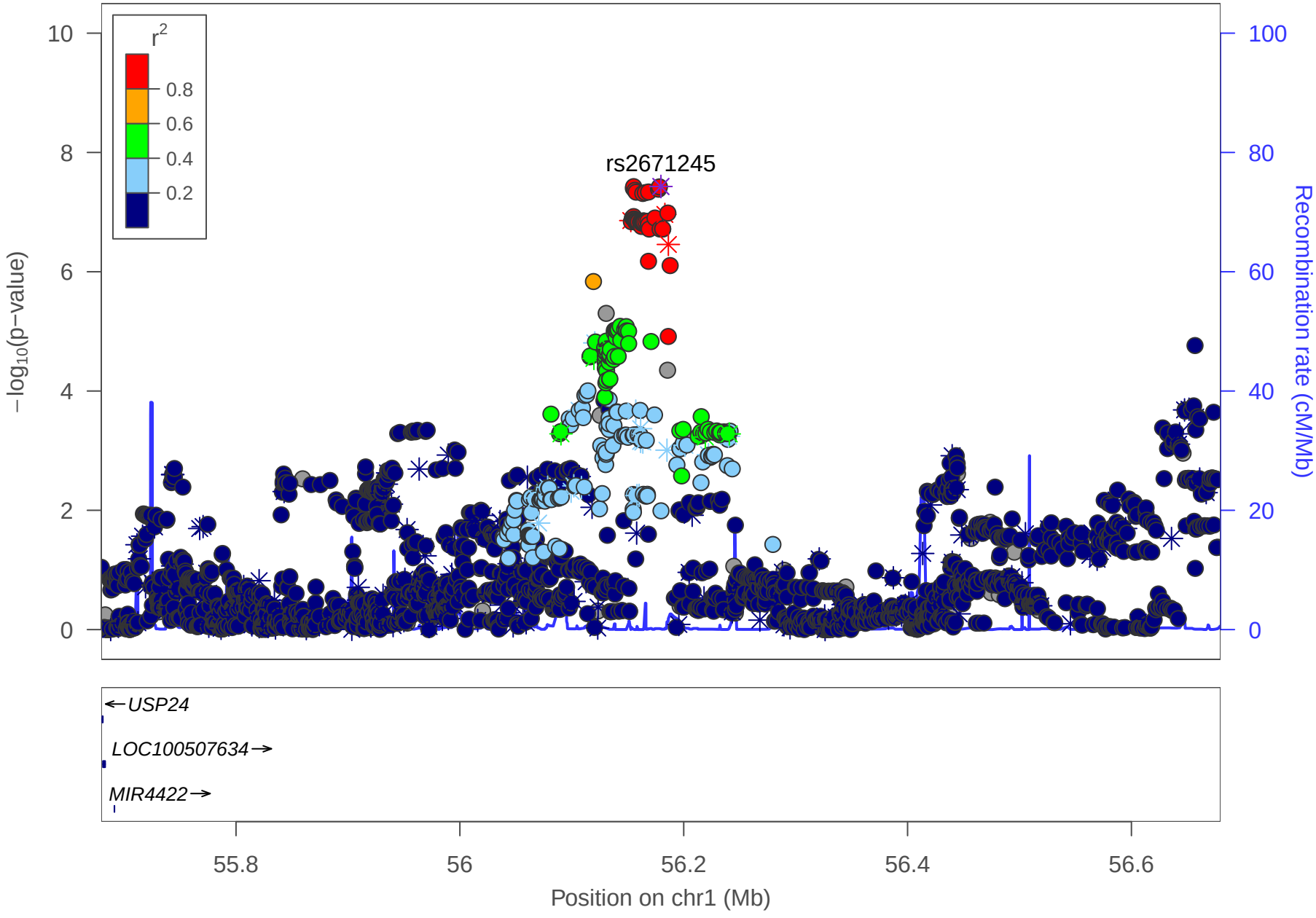
r2
0.8
0.6
0.4
0.2
rs2671245
10
8
6
4
2
0
100
80
60
40
20
0
−log10(p−value)
Recombination rate (cM/Mb)
←USP24
LOC100507634→
MIR4422→
55.8
56
56.2
56.4
56.6
Position on chr1 (Mb)

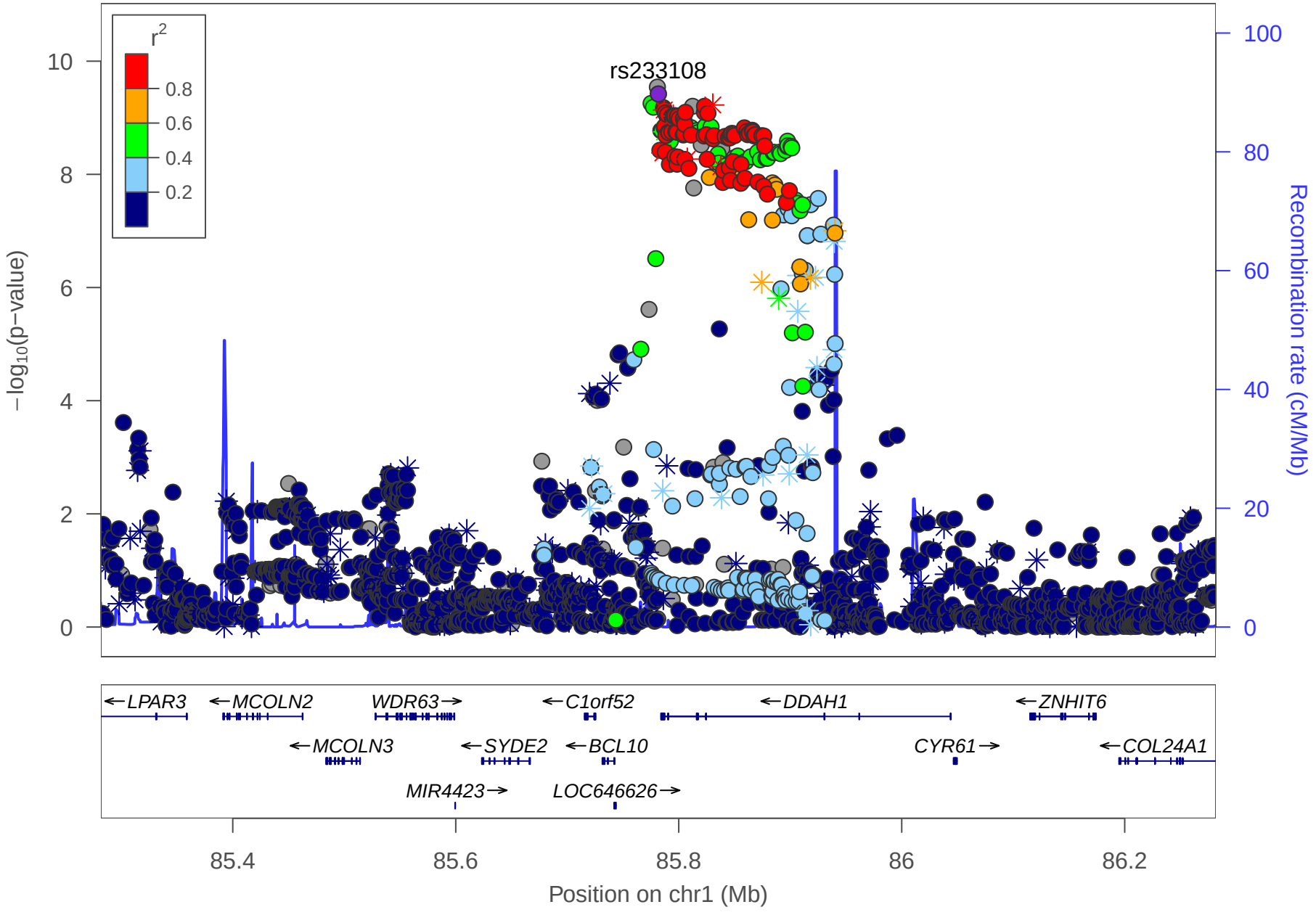
r2
0.8
0.6
0.4
0.2
rs233108
10
8
6
4
2
0
−log10(p−value)
100
80
60
40
20
0
Recombination rate (cM/Mb)
←LPAR3
←MCOLN2
WDR63→
←C1orf52
←DDAH1
←ZNHIT6
←MCOLN3
←SYDE2
←BCL10
CYR61→
←COL24A1
MIR4423→
LOC646626→
85.4
85.6
85.8
86
86.2
Position on chr1 (Mb)

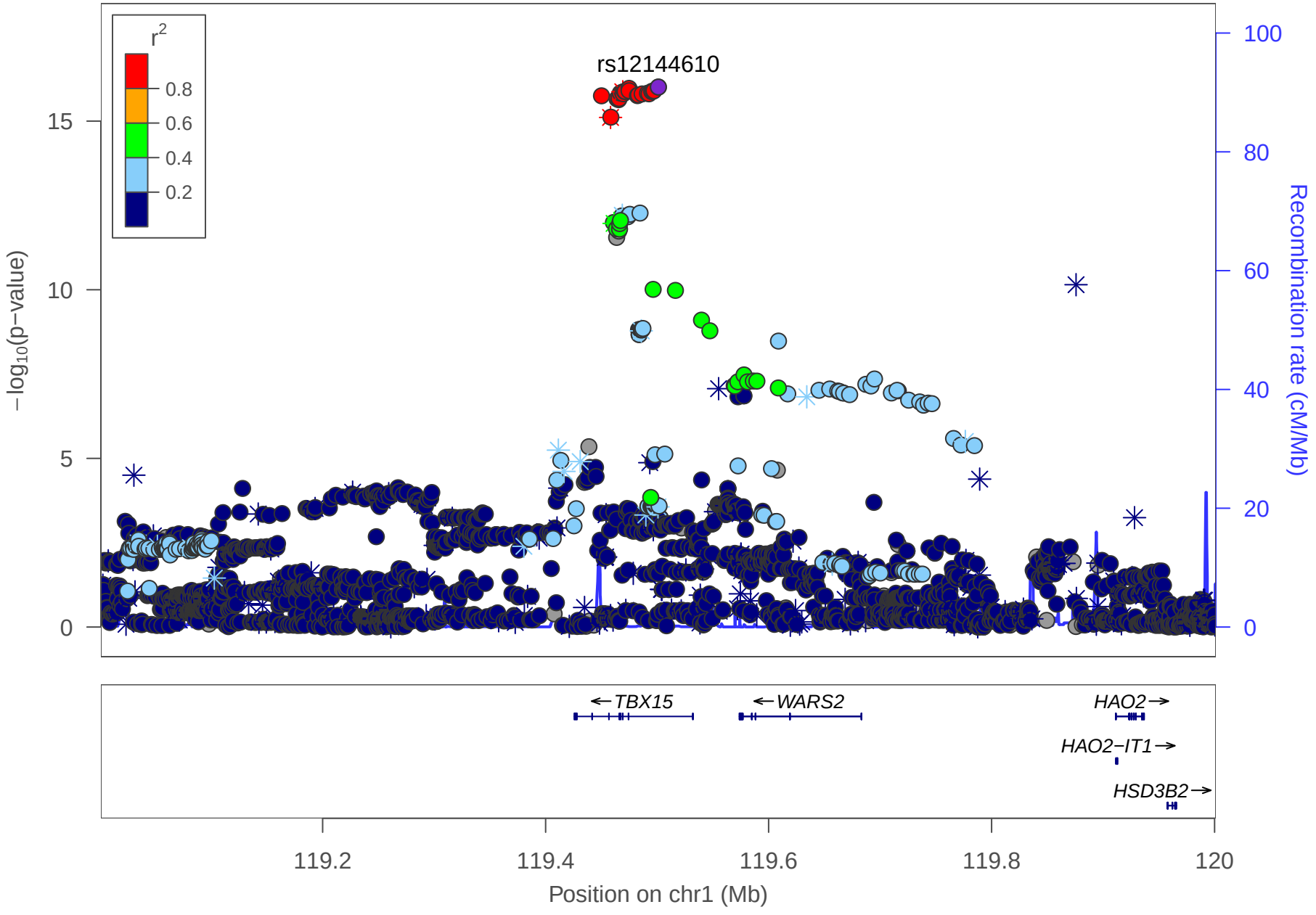
r2
0.8
0.6
0.4
0.2
rs12144610
15
10
5
0
−log10(p−value)
100
80
60
40
20
0
Recombination rate (cM/Mb)
←TBX15
←WARS2
HAO2→
HAO2−IT1→
HSD3B2→
119.2
119.4
119.6
119.8
120
Position on chr1 (Mb)

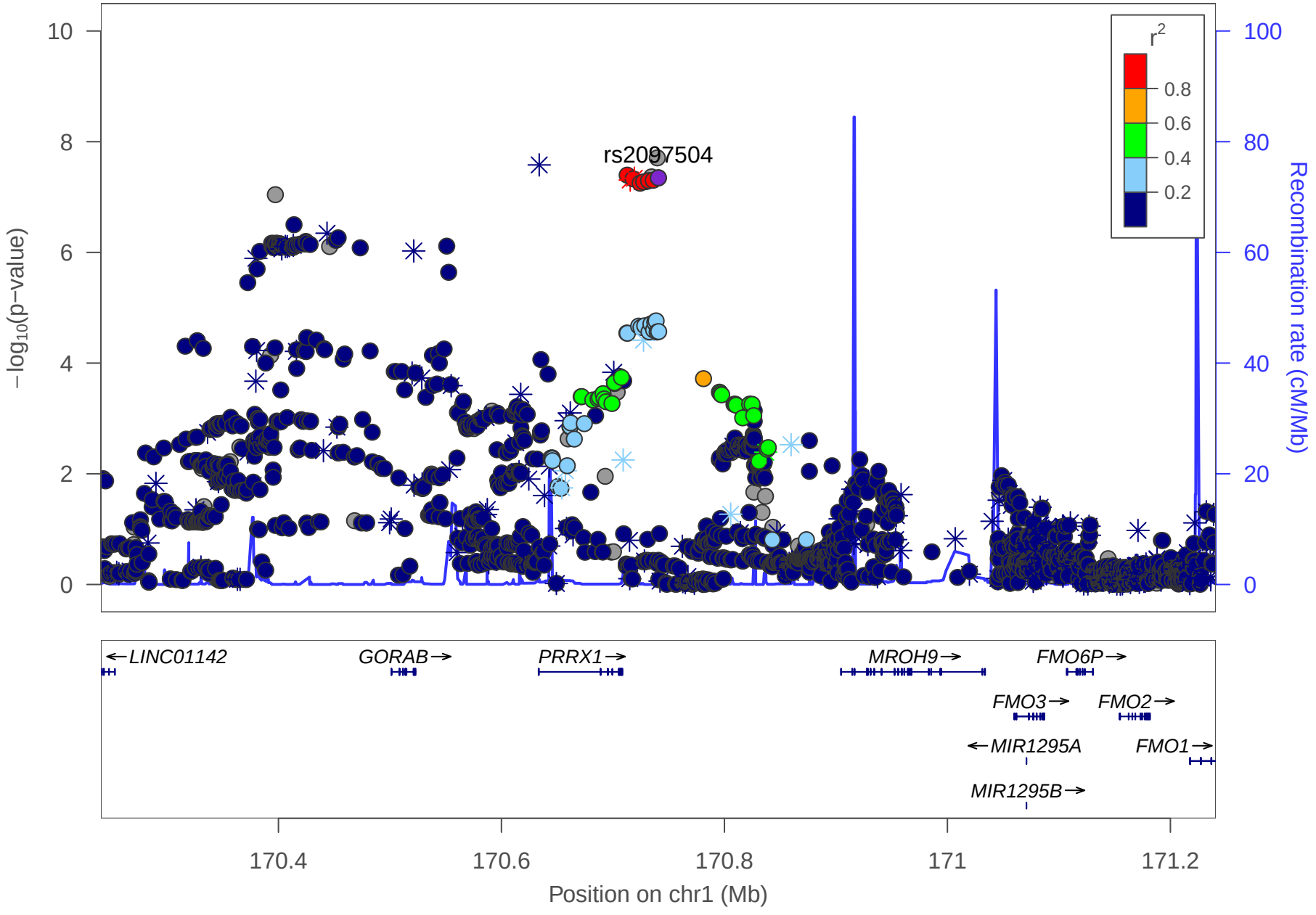
rs2097504
r2
0.8
0.6
0.4
0.2
−log10(p−value)
Recombination rate (cM/Mb)
10
8
6
4
2
0
100
80
60
40
20
0
LINC01142
GORAB
PRRX1
MROH9
FMO6P
FMO3
FMO2
MIR1295A
FMO1
MIR1295B
170.4
170.6
170.8
171
171.2
Position on chr1 (Mb)

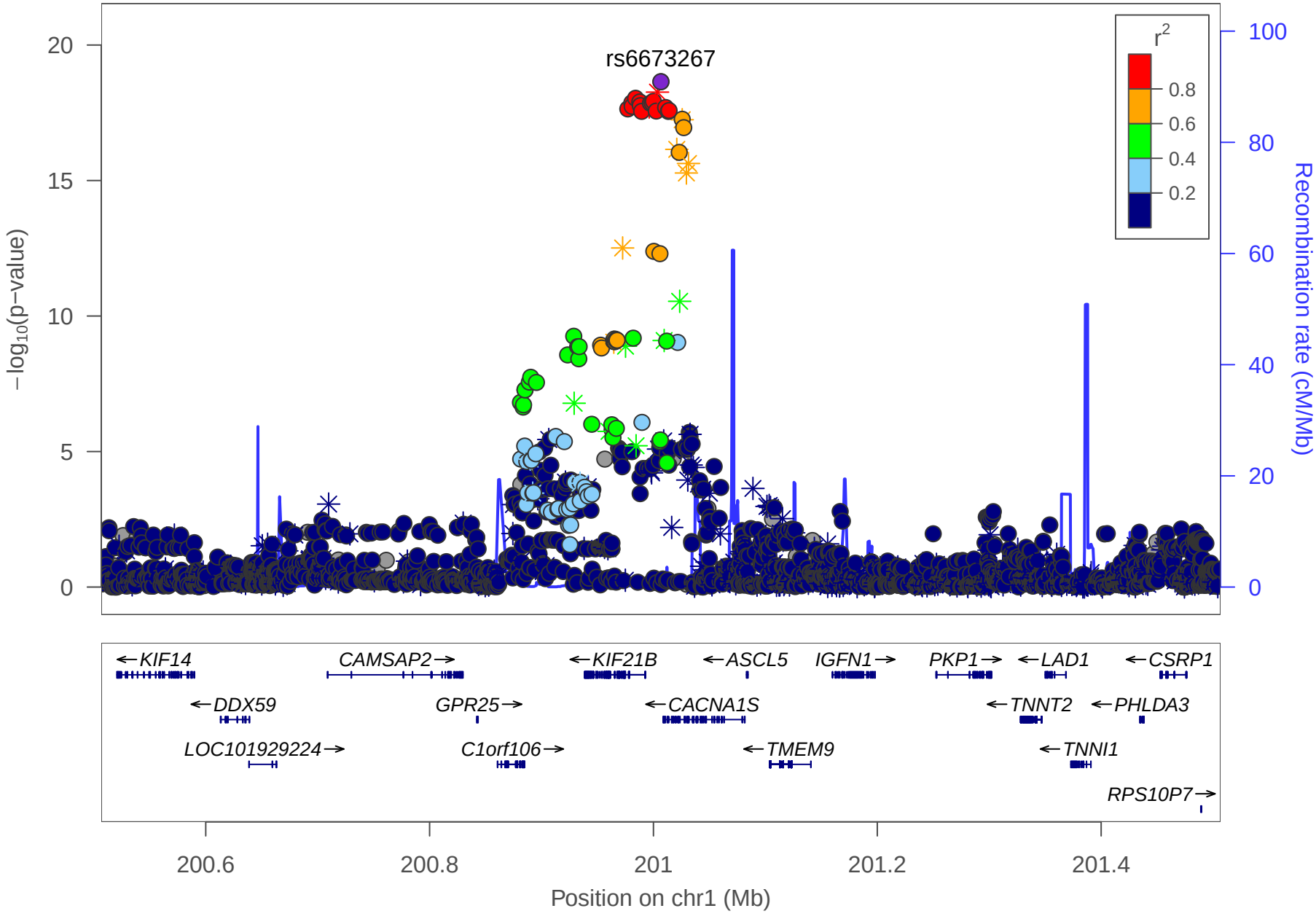
rs6673267
r2
0.8
0.6
0.4
0.2
−log10(p−value)
Recombination rate (cM/Mb)
20
15
10
5
0
100
80
60
40
20
0
←KIF14
CAMSAP2→
←KIF21B
←ASCL5
IGFN1→
PKP1→
←LAD1
←CSRP1
←DDX59
GPR25→
←CACNA1S
←TNNT2
←PHLDA3
LOC101929224→
C1orf106→
←TMEM9
←TNNI1
RPS10P7→
200.6
200.8
201
201.2
201.4
Position on chr1 (Mb)

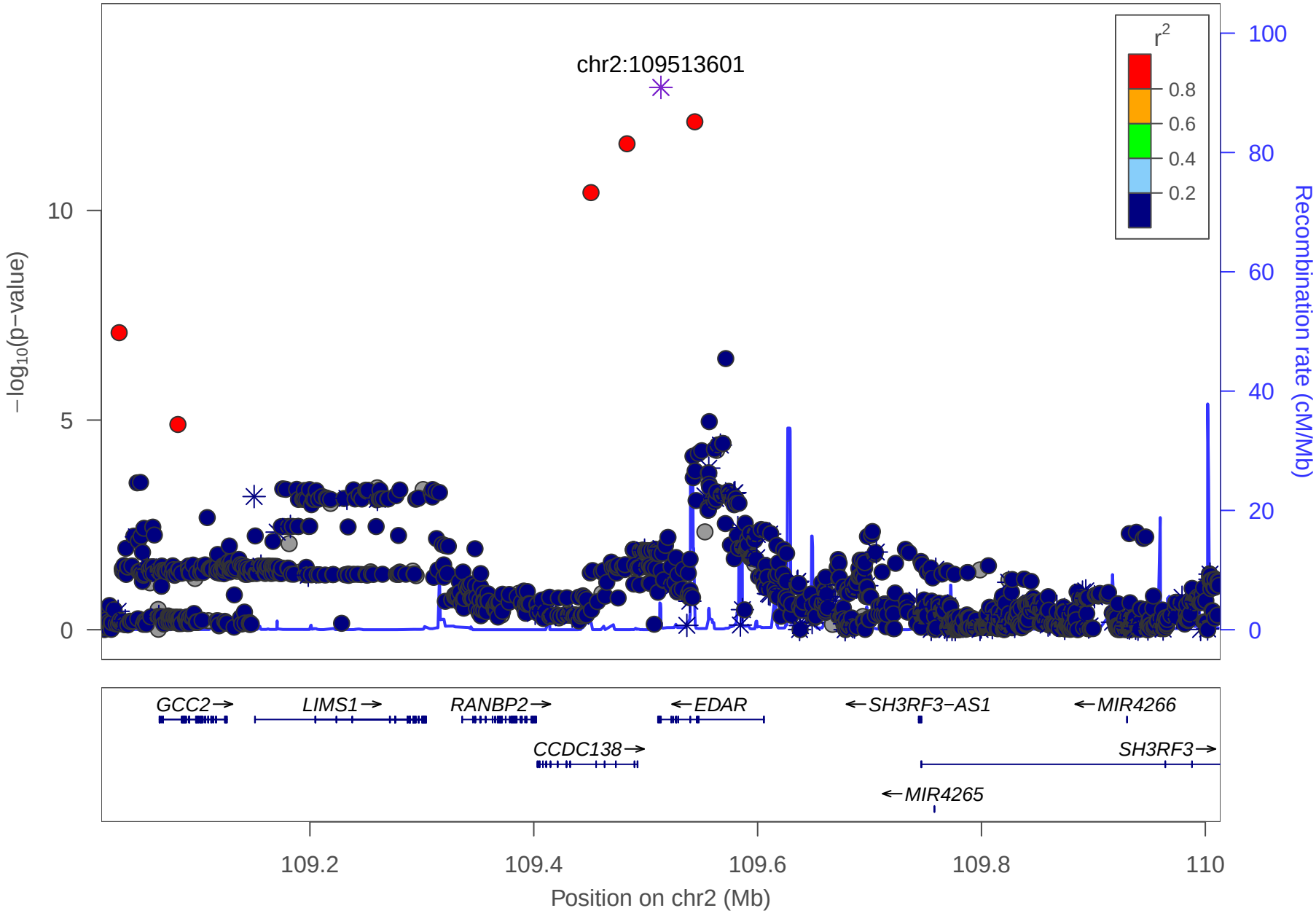
chr2:109513601
r2
0.8
0.6
0.4
0.2
−log10(p−value)
10
5
0
100
80
60
40
20
0
Recombination rate (cM/Mb)
GCC2→
LIMS1→
RANBP2→
←EDAR
←SH3RF3−AS1
←MIR4266
CCDC138→
SH3RF3→
←MIR4265
109.2
109.4
109.6
109.8
110
Position on chr2 (Mb)

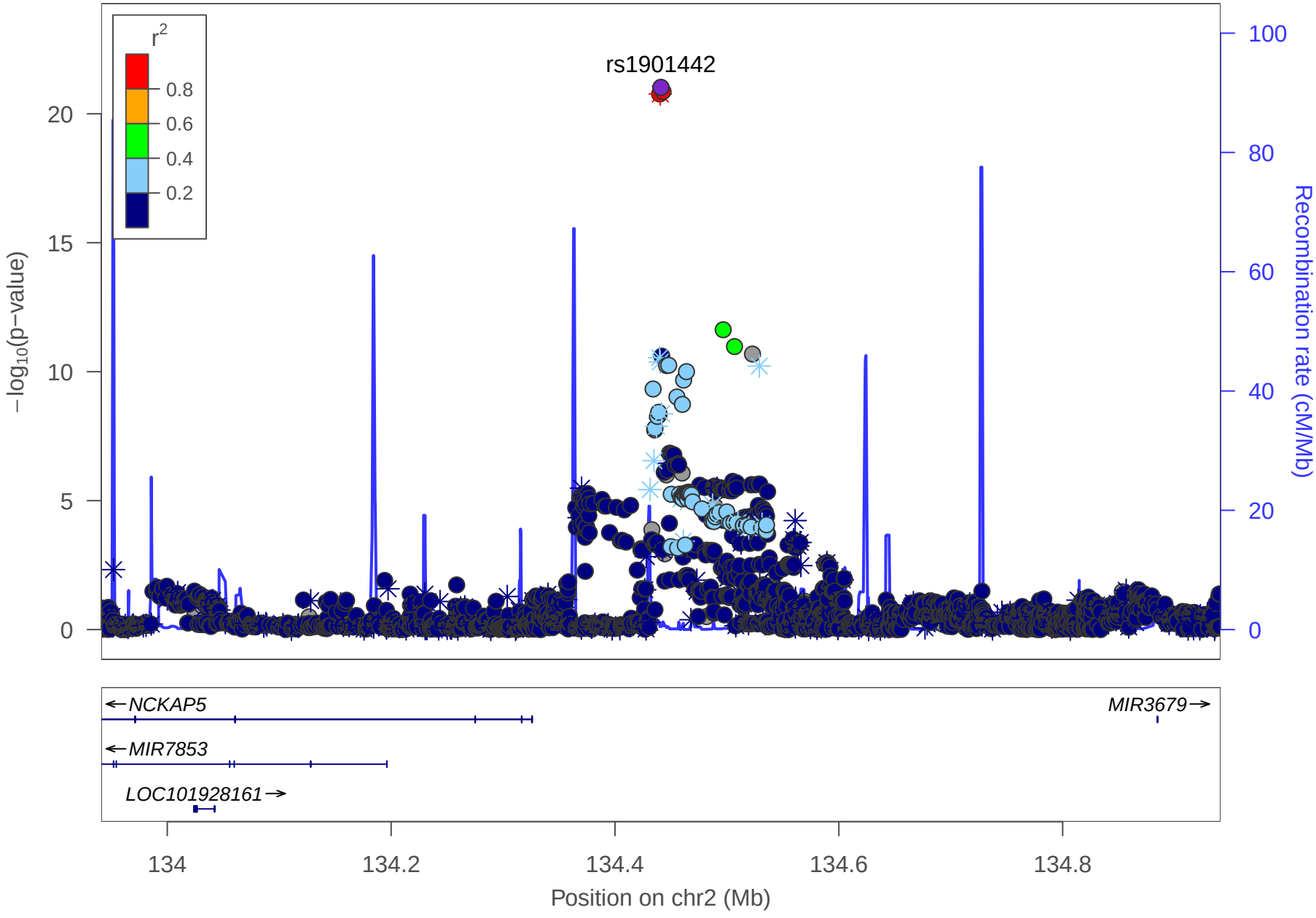
r2
0.8
0.6
0.4
0.2
rs1901442
20
15
10
5
0
−log10(p−value)
100
80
60
40
20
0
Recombination rate (cM/Mb)
←NCKAP5
MIR3679→
←MIR7853
LOC101928161→
134
134.2
134.4
134.6
134.8
Position on chr2 (Mb)

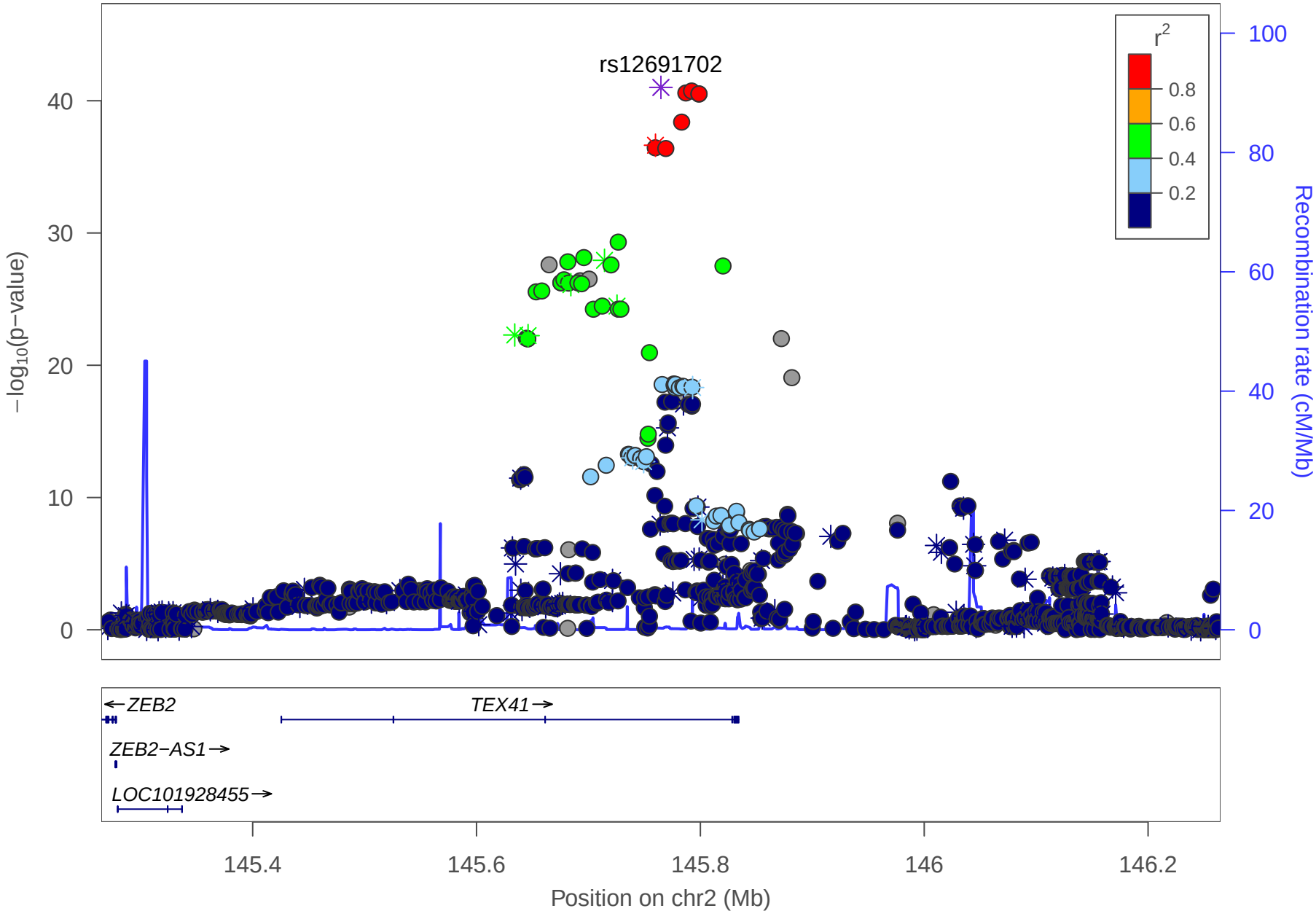
rs12691702
r2
0.8
0.6
0.4
0.2
−log10(p−value)
Recombination rate (cM/Mb)
0
10
20
30
40
0
20
40
60
80
100
ZEB2
TEX41
ZEB2−AS1
LOC101928455
145.4
145.6
145.8
146
146.2
Position on chr2 (Mb)

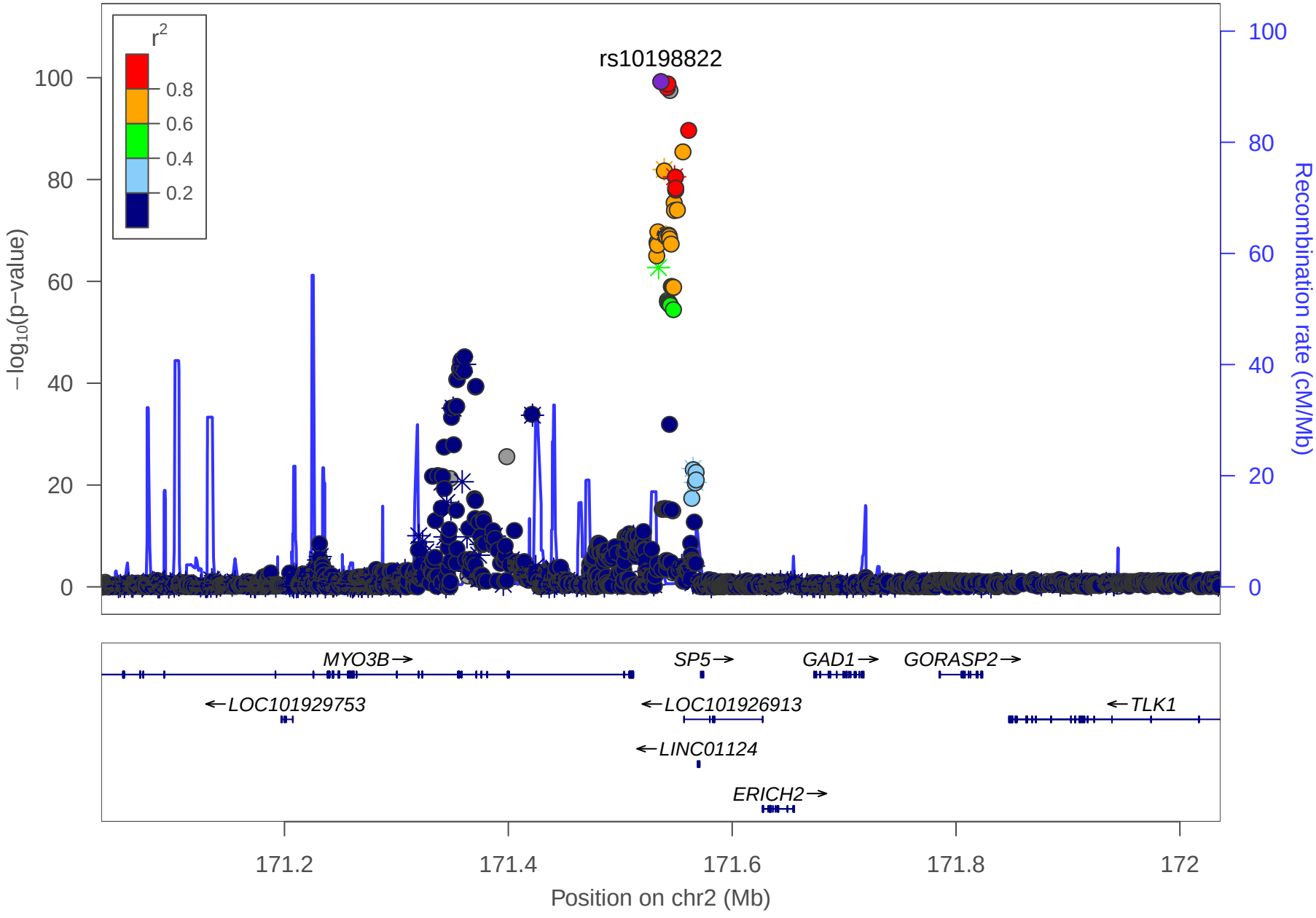
r2
0.8
0.6
0.4
0.2
rs10198822
100
80
60
40
20
0
−log10(p−value)
100
80
60
40
20
0
Recombination rate (cM/Mb)
MYO3B→
SP5→
GAD1→
GORASP2→
←LOC101929753
←LOC101926913
←TLK1
←LINC01124
ERICH2→
171.2
171.4
171.6
171.8
172
Position on chr2 (Mb)

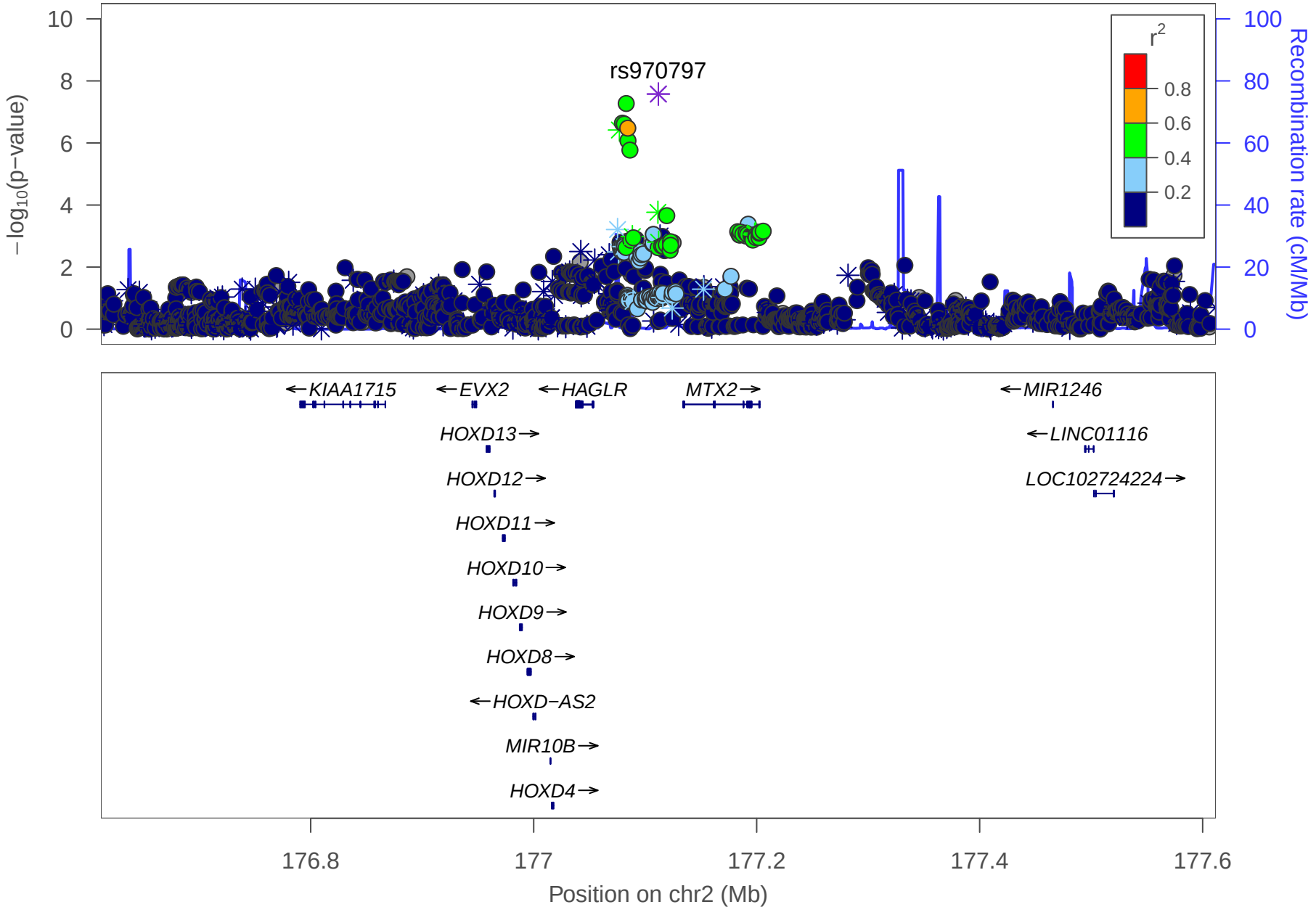
rs970797
r2
0.8
0.6
0.4
0.2
−log10(p−value)
Recombination rate (cM/Mb)
10
8
6
4
2
0
100
80
60
40
20
0
←KIAA1715
←EVX2
←HAGLR
MTX2→
←MIR1246
HOXD13→
←LINC01116
HOXD12→
LOC102724224→
HOXD11→
HOXD10→
HOXD9→
HOXD8→
←HOXD−AS2
MIR10B→
HOXD4→
176.8
177
177.2
177.4
177.6
Position on chr2 (Mb)

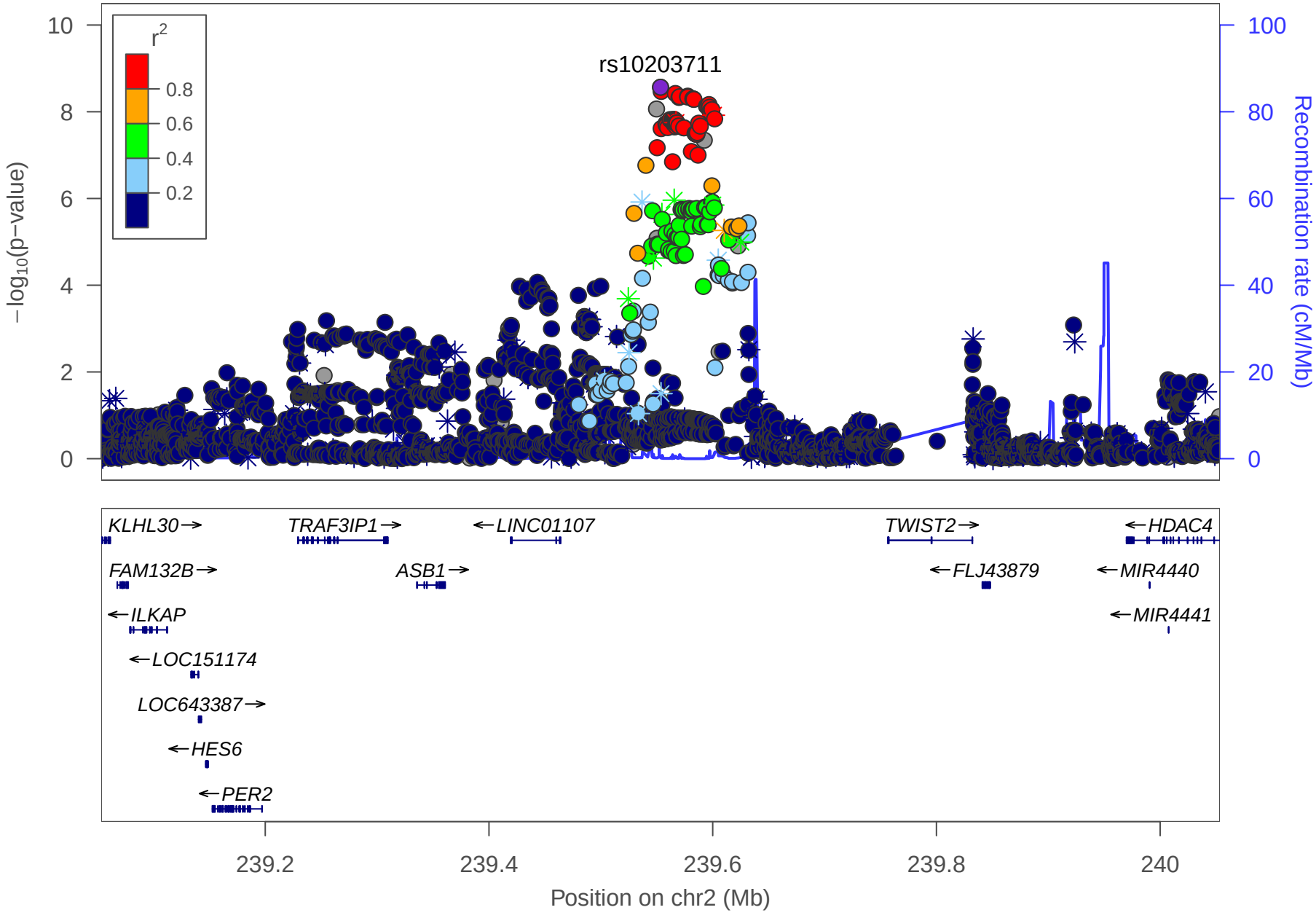
rs10203711
r2
0.8
0.6
0.4
0.2
−log10(p−value)
Recombination rate (cM/Mb)
10
8
6
4
2
0
100
80
60
40
20
0
KLHL30
TRAF3IP1
LINC01107
TWIST2
HDAC4
FAM132B
ASB1
FLJ43879
MIR4440
ILKAP
MIR4441
LOC151174
LOC643387
HES6
PER2
239.2
239.4
239.6
239.8
240
Position on chr2 (Mb)

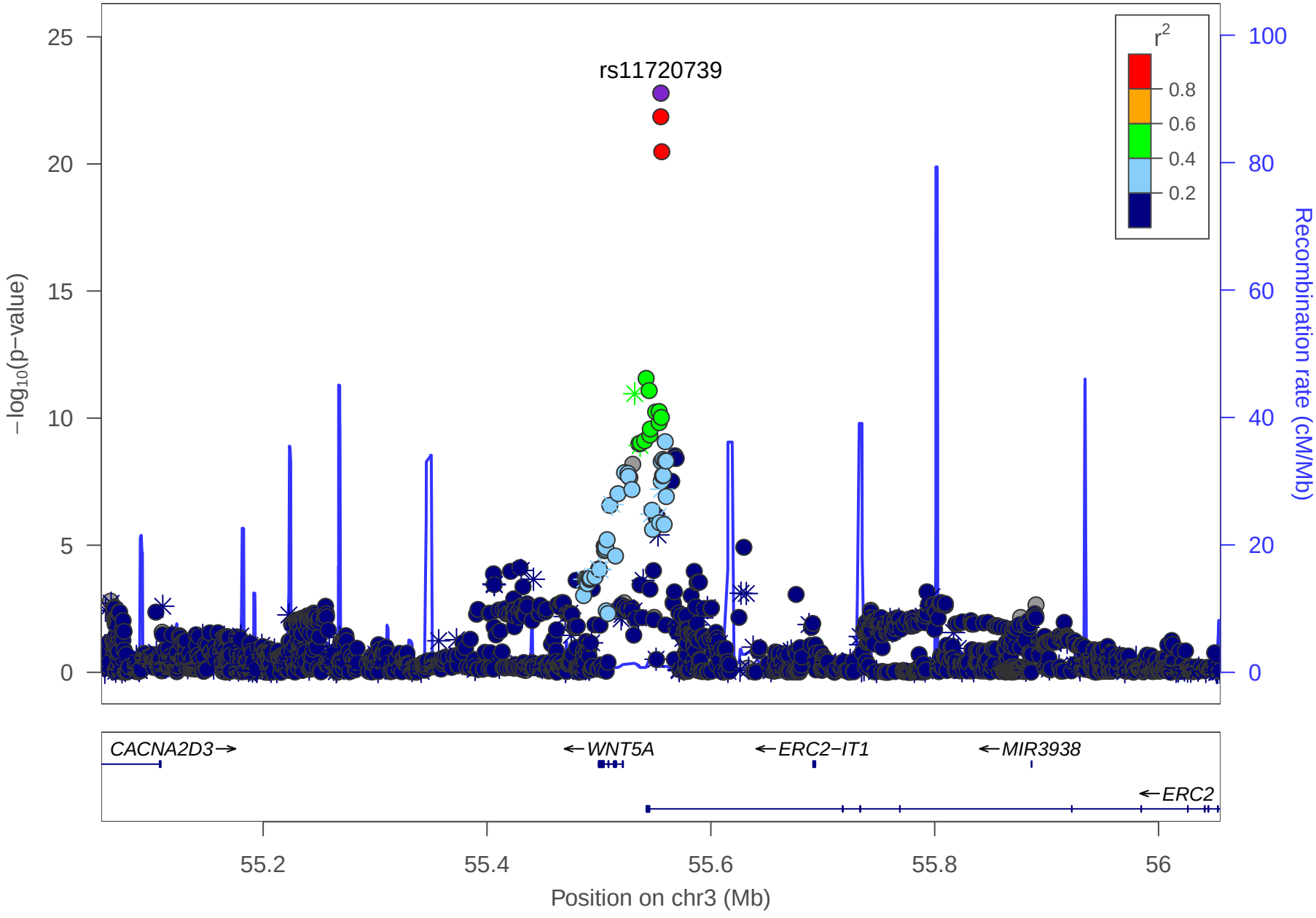
rs11720739
r2
0.8
0.6
0.4
0.2
−log10(p−value)
Recombination rate (cM/Mb)
25
20
15
10
5
0
100
80
60
40
20
0
CACNA2D3→
←WNT5A
←ERC2−IT1
←MIR3938
←ERC2
55.2
55.4
55.6
55.8
56
Position on chr3 (Mb)

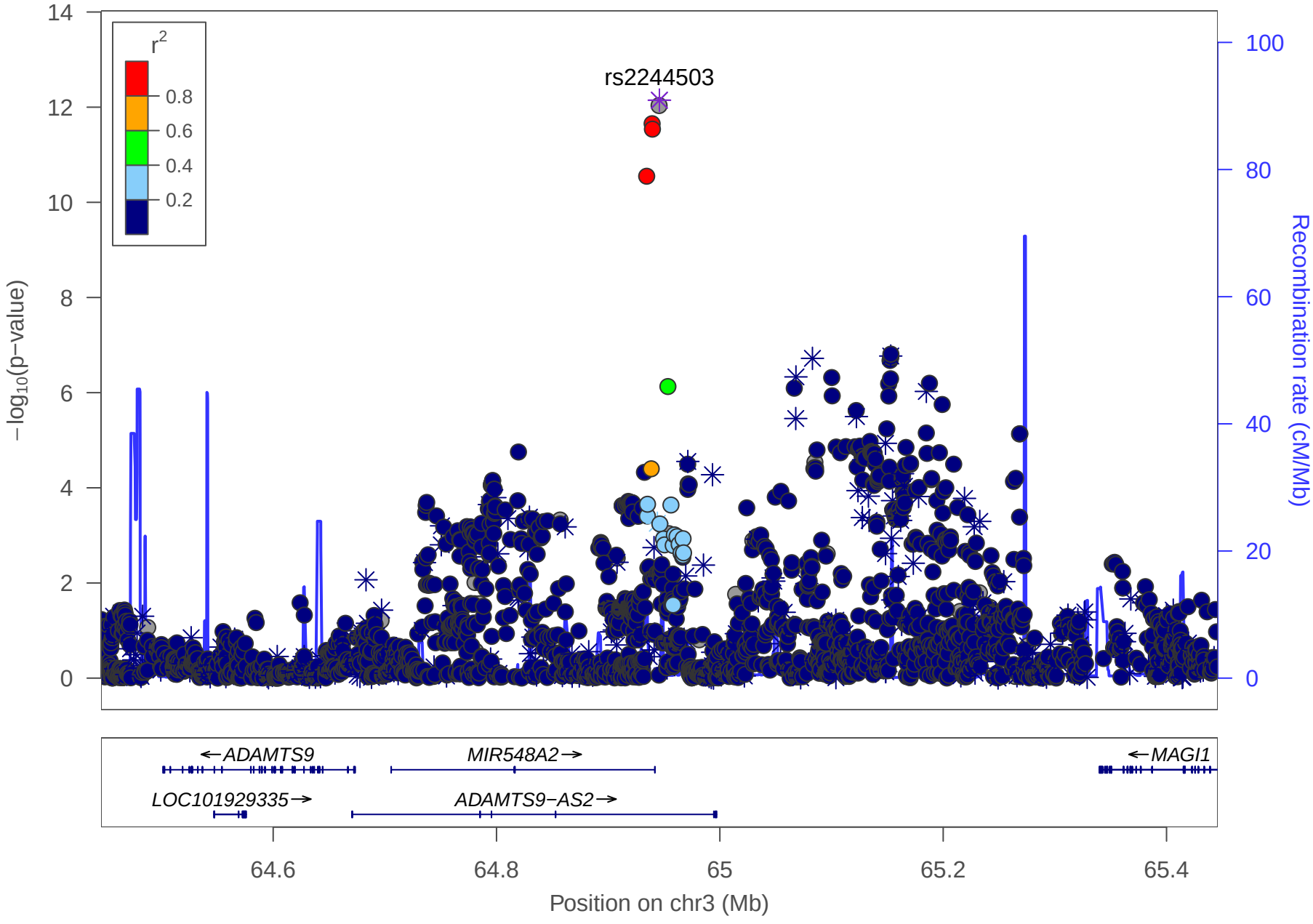
rs2244503
r2
0.8
0.6
0.4
0.2
−log10(p−value)
Recombination rate (cM/Mb)
ADAMTS9
MIR548A2
MAGI1
LOC101929335
ADAMTS9−AS2
Position on chr3 (Mb)

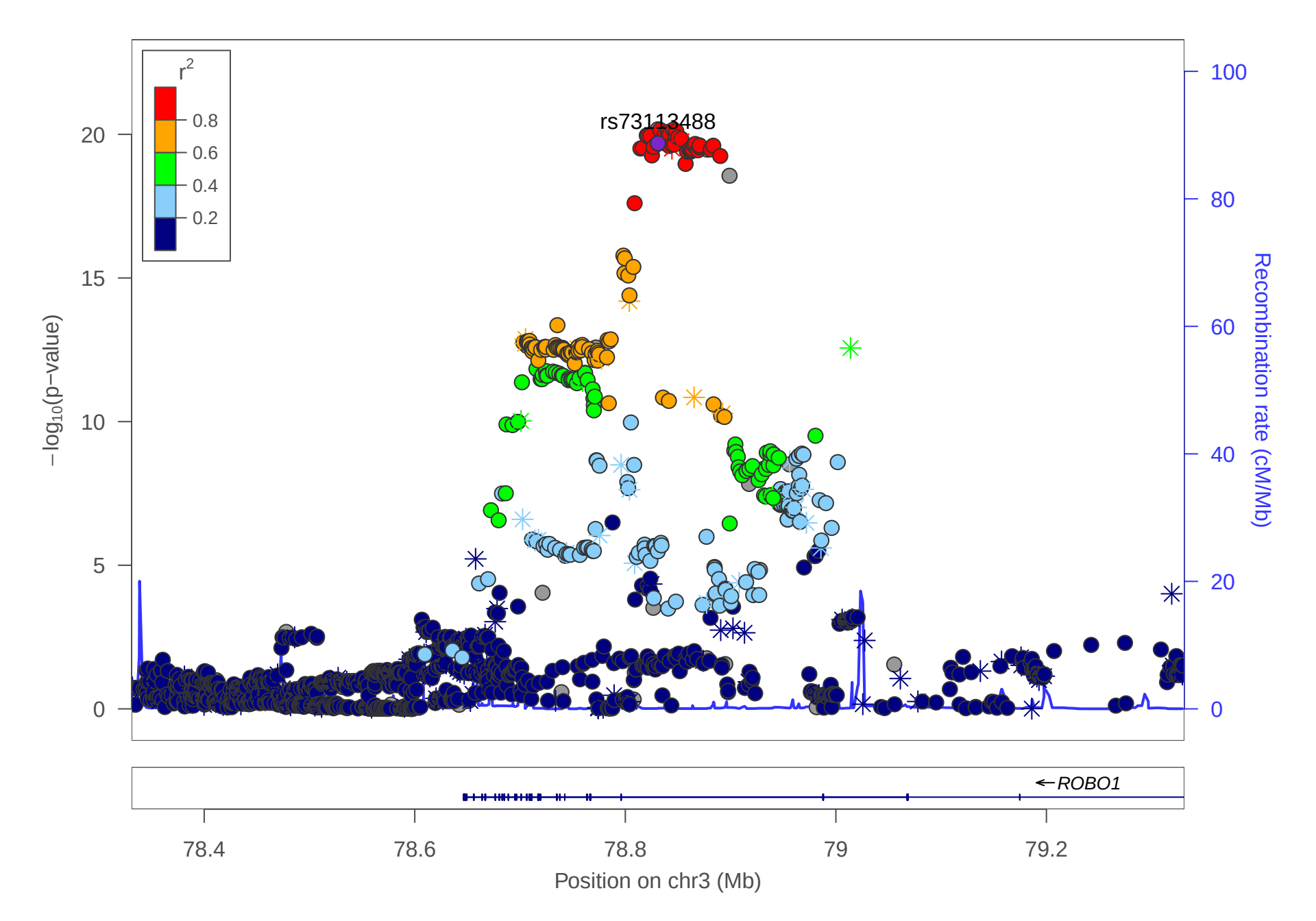
r2
0.8
0.6
0.4
0.2
rs73113488
20
15
10
5
0
−log10(p−value)
100
80
60
40
20
0
Recombination rate (cM/Mb)
←ROBO1
78.4
78.6
78.8
79
79.2
Position on chr3 (Mb)

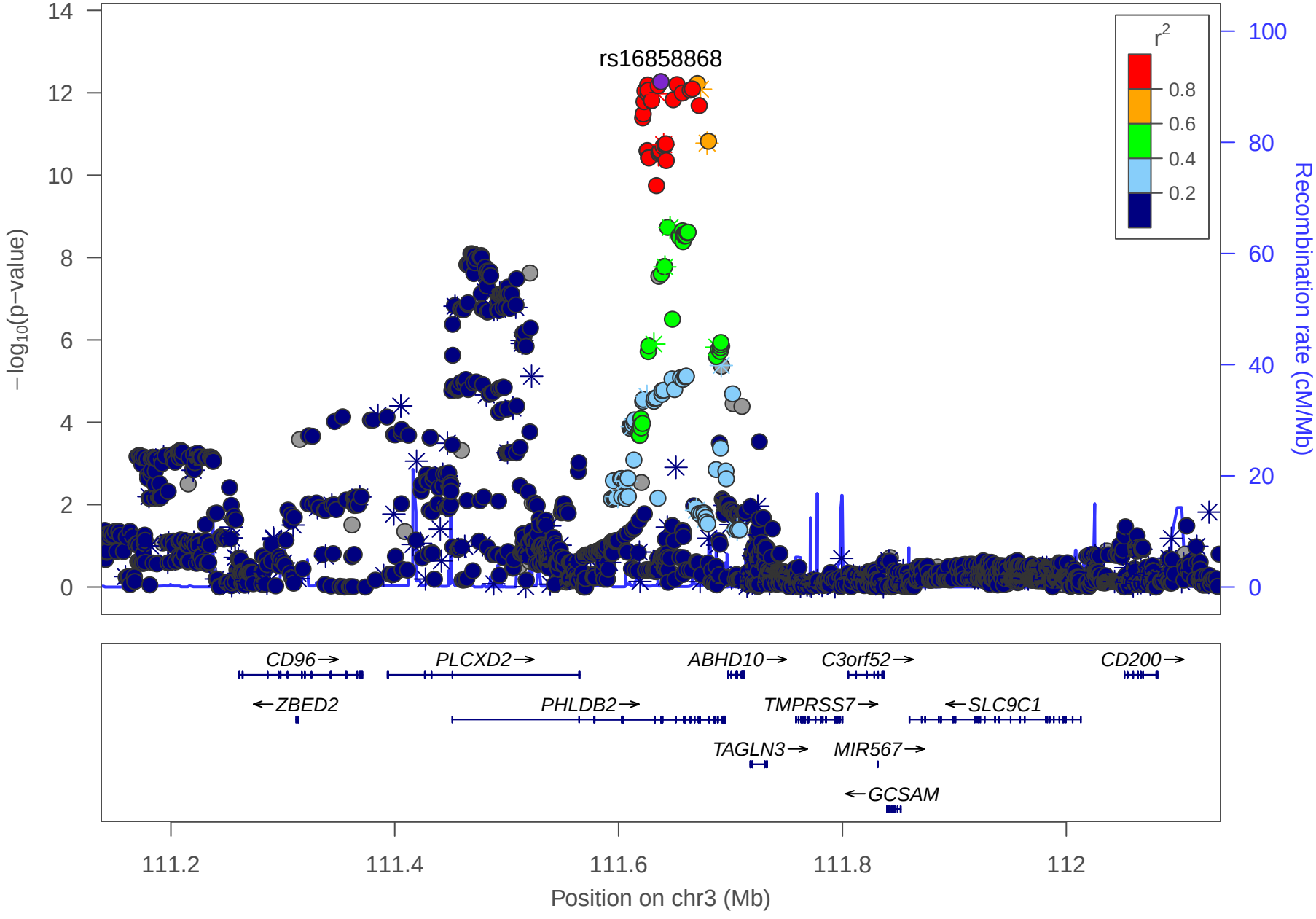
rs16858868
r2
0.8
0.6
0.4
0.2
−log10(p−value)
Recombination rate (cM/Mb)
14
12
10
8
6
4
2
0
100
80
60
40
20
0
CD96→
PLCXD2→
ABHD10→
C3orf52→
CD200→
←ZBED2
PHLDB2→
TMPRSS7→
←SLC9C1
TAGLN3→
MIR567→
←GCSAM
111.2
111.4
111.6
111.8
112
Position on chr3 (Mb)

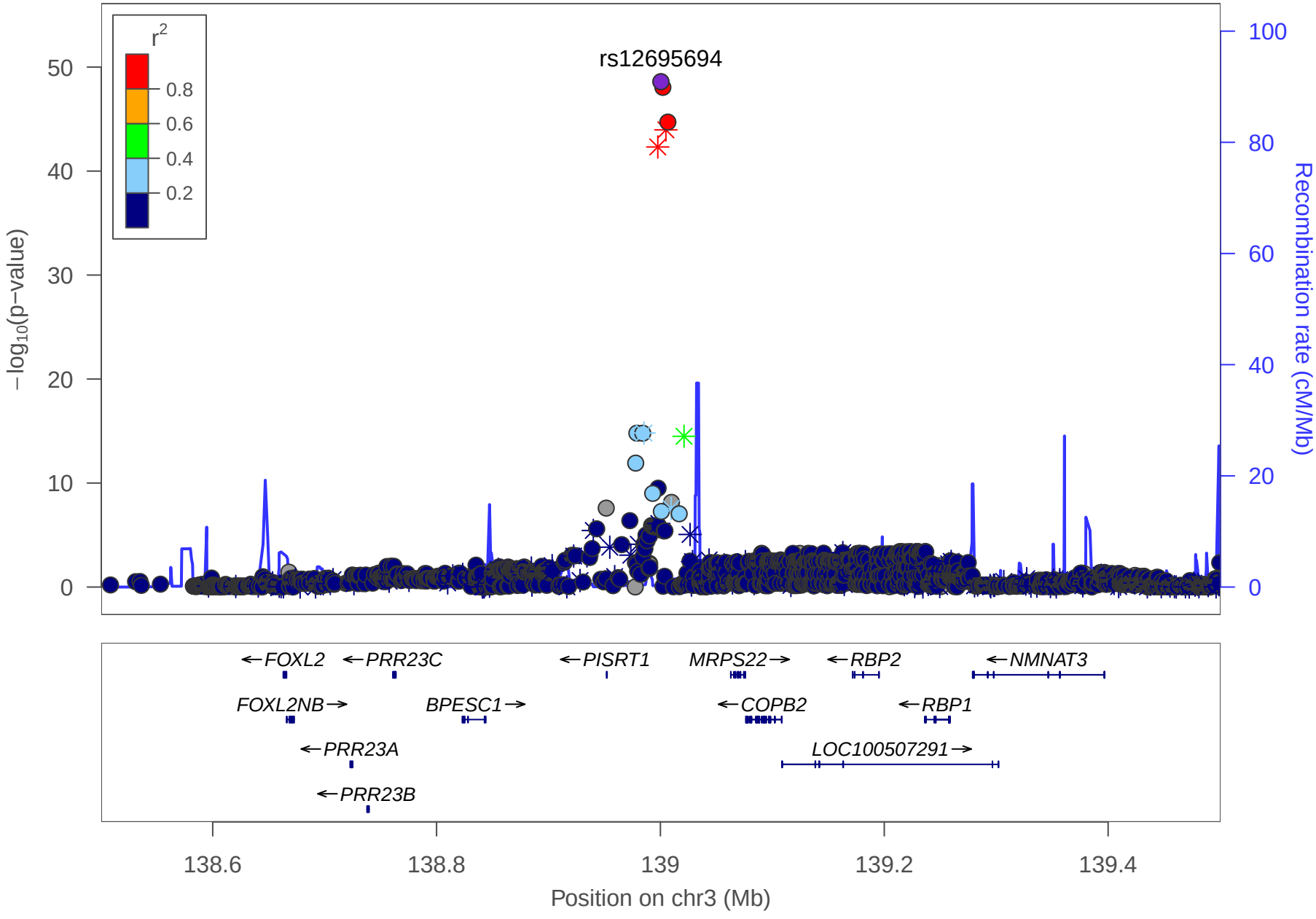
rs12695694
r2
0.8
0.6
0.4
0.2
−log10(p−value)
Recombination rate (cM/Mb)
FOXL2
PRR23C
PISRT1
MRPS22
RBP2
NMNAT3
FOXL2NB
BPESC1
COPB2
RBP1
PRR23A
LOC100507291
PRR23B
Position on chr3 (Mb)

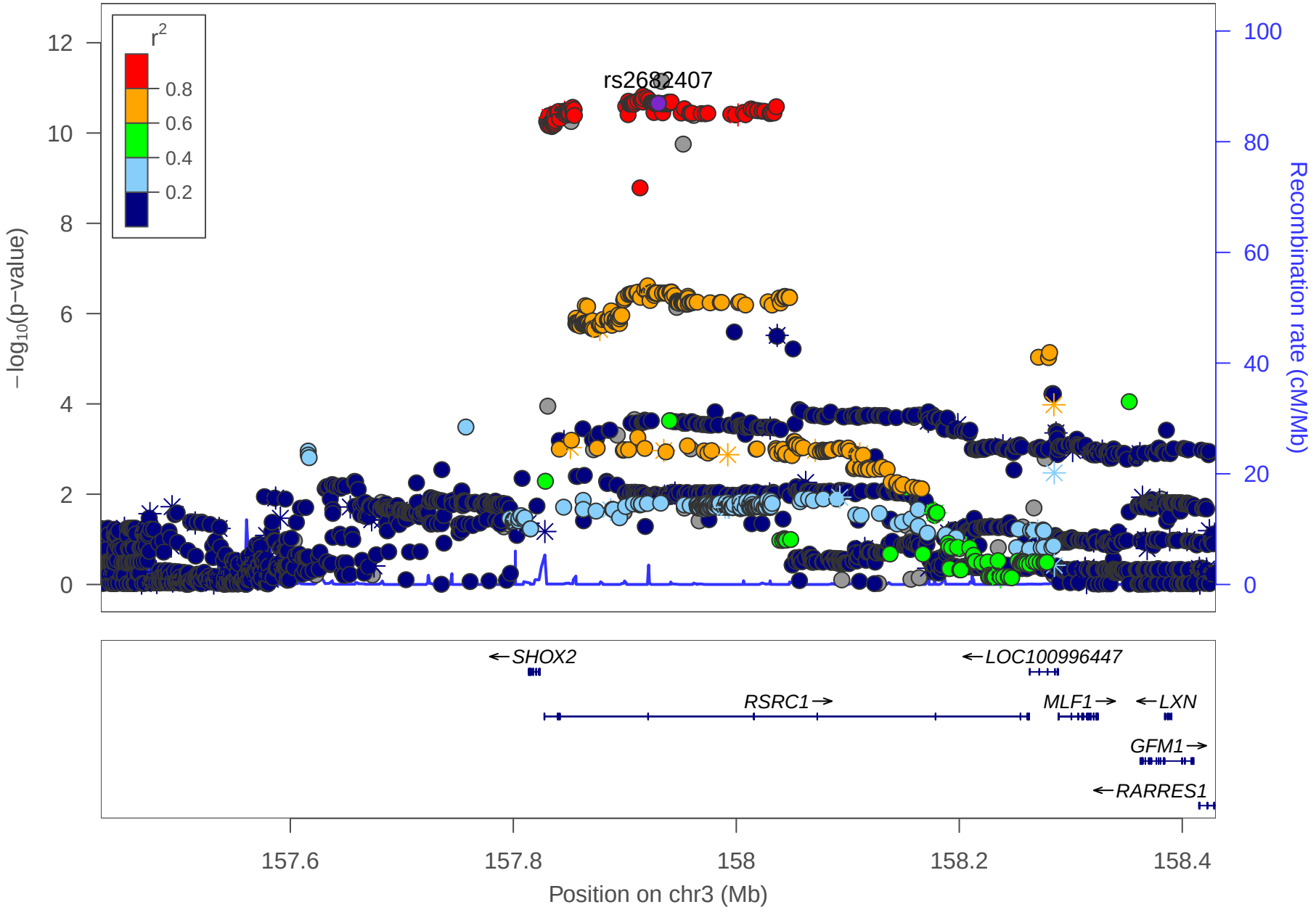
r2
0.8
0.6
0.4
0.2
rs2682407
−log10(p−value)
Recombination rate (cM/Mb)
SHOX2
LOC100996447
RSRC1
MLF1
LXN
GFM1
RARRES1
Position on chr3 (Mb)

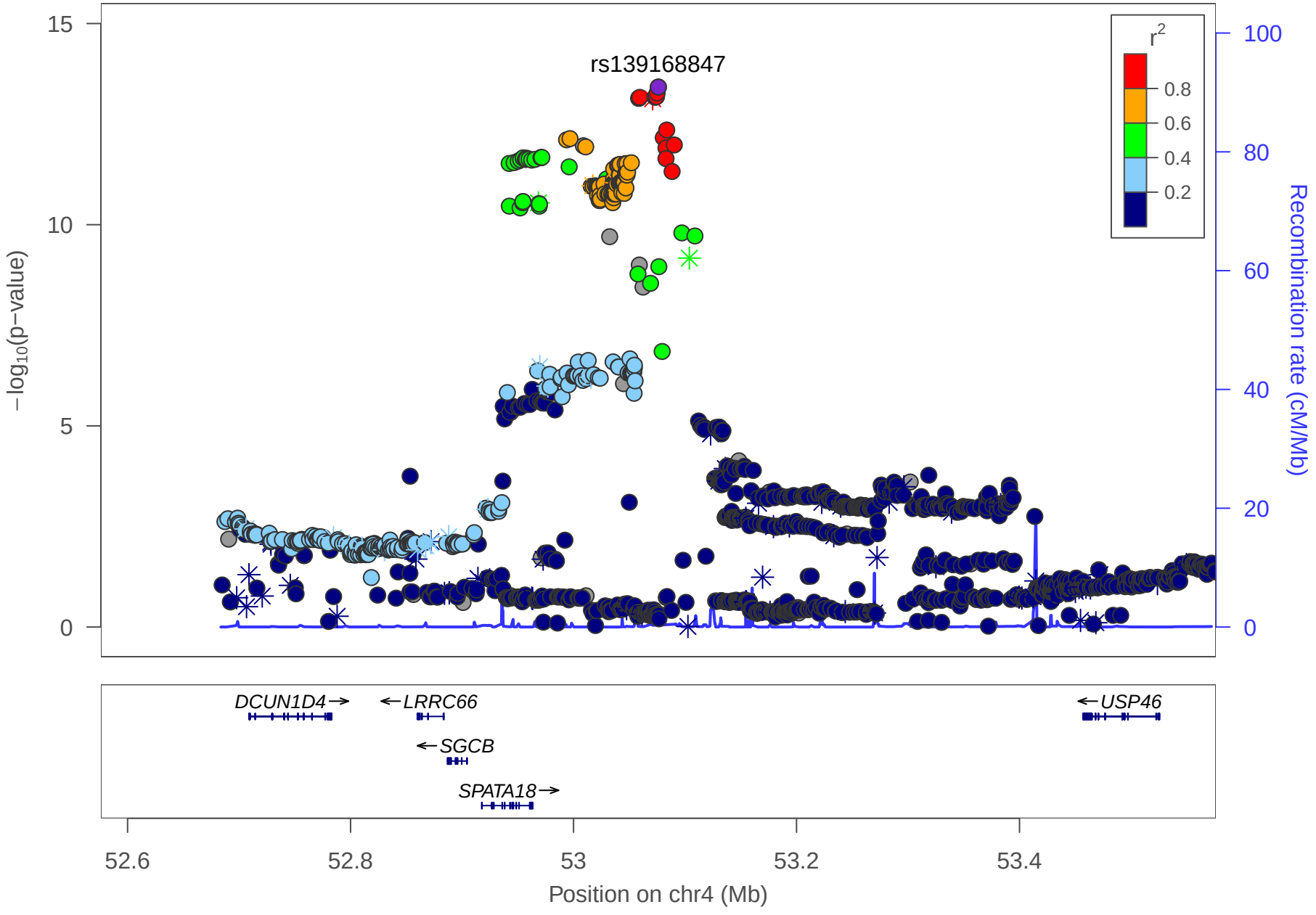
rs139168847
r2
0.8
0.6
0.4
0.2
15
10
5
0
100
80
60
40
20
0
−log10(p−value)
Recombination rate (cM/Mb)
DCUN1D4→
←LRRC66
←USP46
←SGCB
SPATA18→
52.6
52.8
53
53.2
53.4
Position on chr4 (Mb)

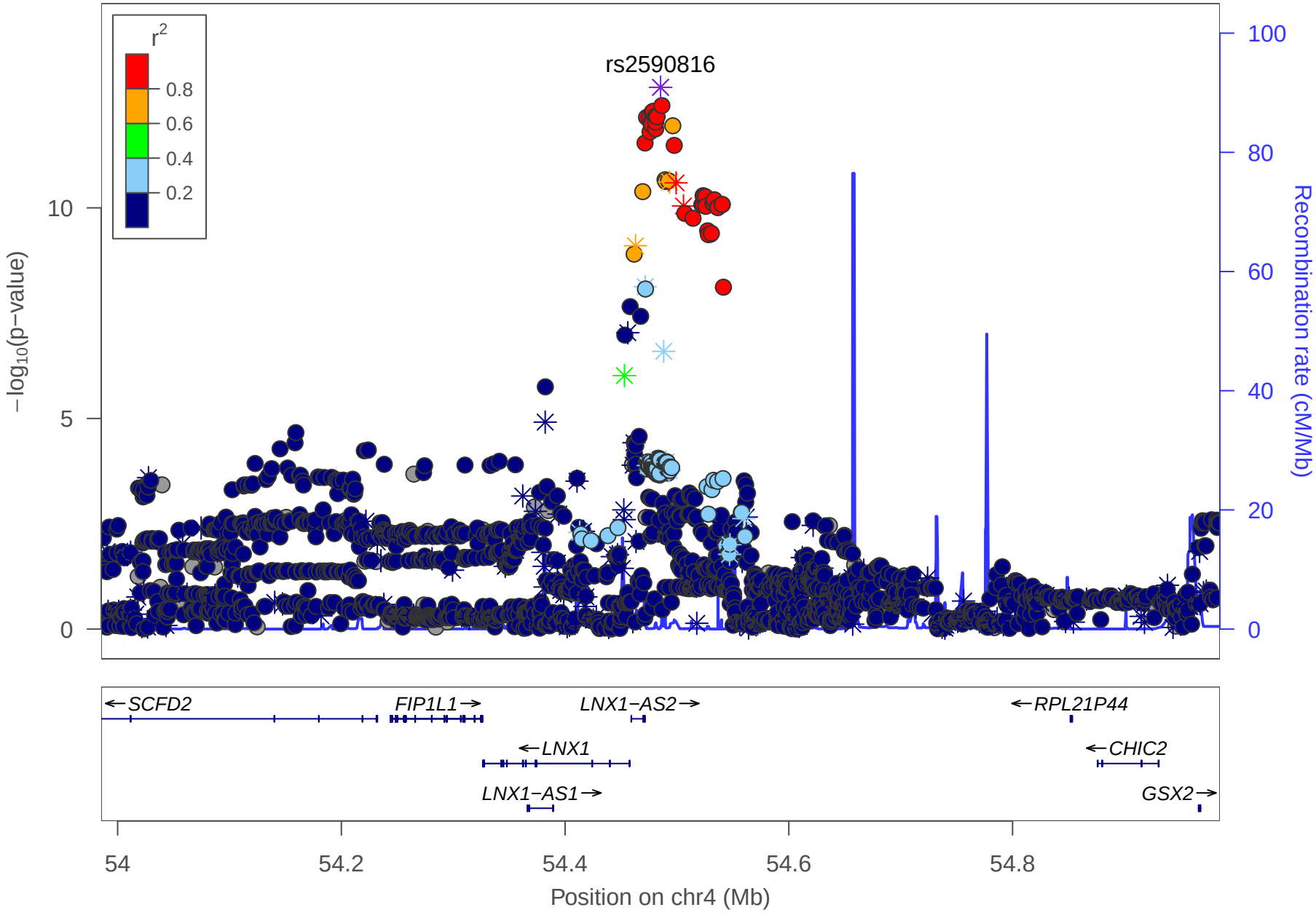
r2
0.8
0.6
0.4
0.2
rs2590816
10
5
0
−log10(p−value)
100
80
60
40
20
0
Recombination rate (cM/Mb)
←SCFD2
FIP1L1→
LNX1−AS2→
←RPL21P44
←LNX1
←CHIC2
LNX1−AS1→
GSX2→
54
54.2
54.4
54.6
54.8
Position on chr4 (Mb)

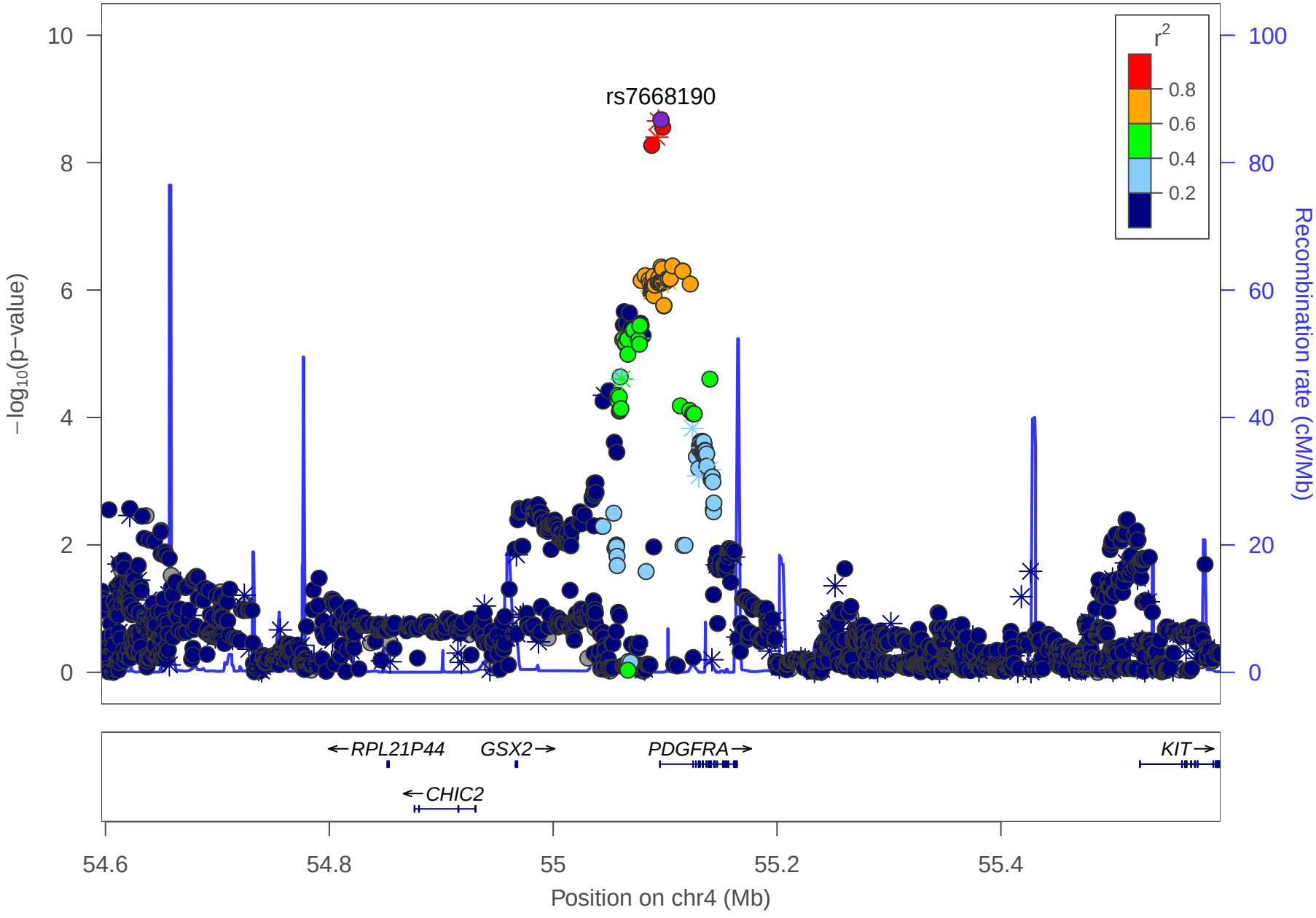
rs7668190
r2
0.8
0.6
0.4
0.2
10
8
6
4
2
0
100
80
60
40
20
0
−log10(p−value)
Recombination rate (cM/Mb)
←RPL21P44
GSX2→
PDGFRA→
KIT→
←CHIC2
54.6
54.8
55
55.2
55.4
Position on chr4 (Mb)

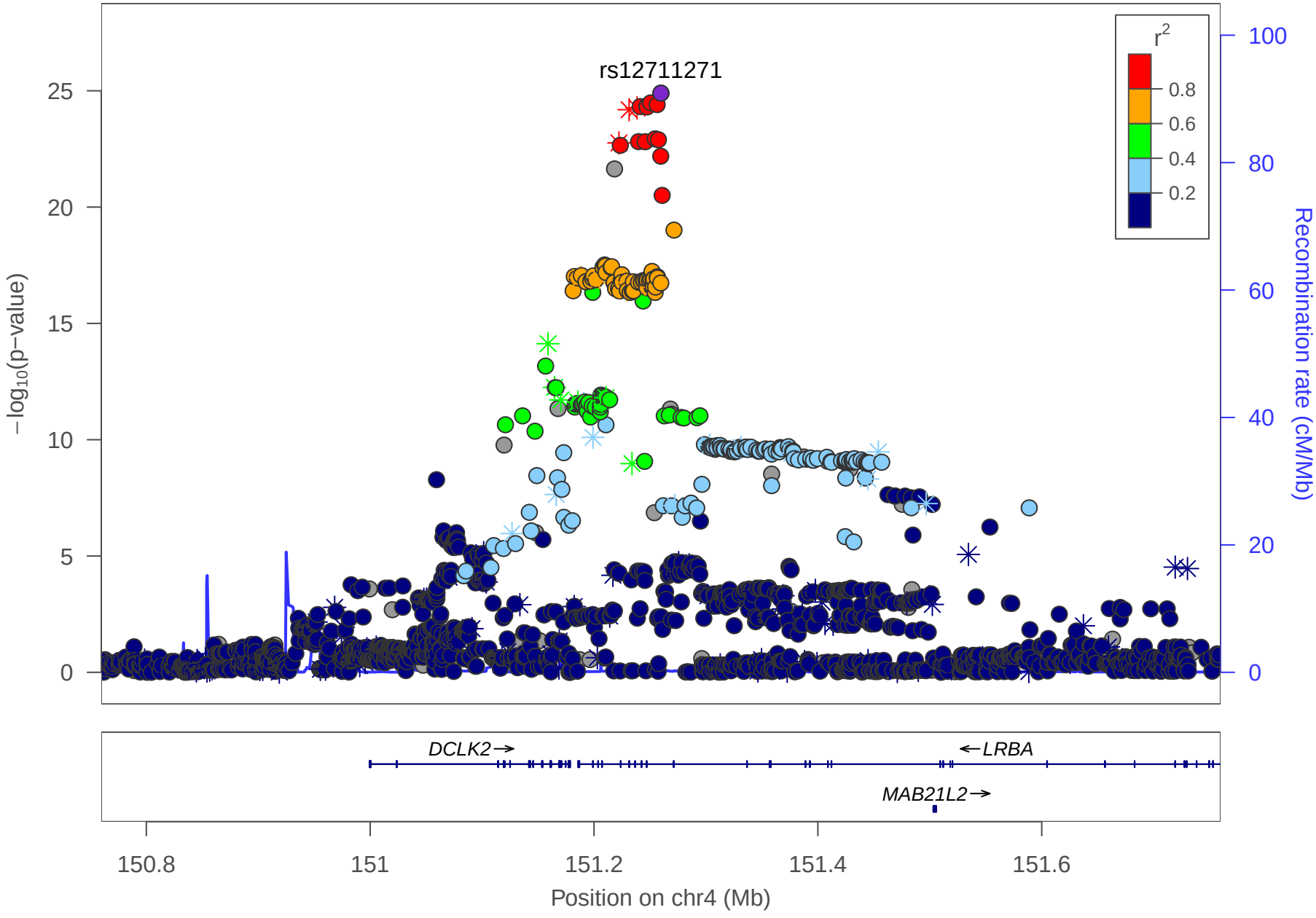
rs12711271
r2
0.8
0.6
0.4
0.2
25
20
15
10
5
0
−log10(p−value)
100
80
60
40
20
0
Recombination rate (cM/Mb)
DCLK2→
←LRBA
MAB21L2→
150.8
151
151.2
151.4
151.6
Position on chr4 (Mb)

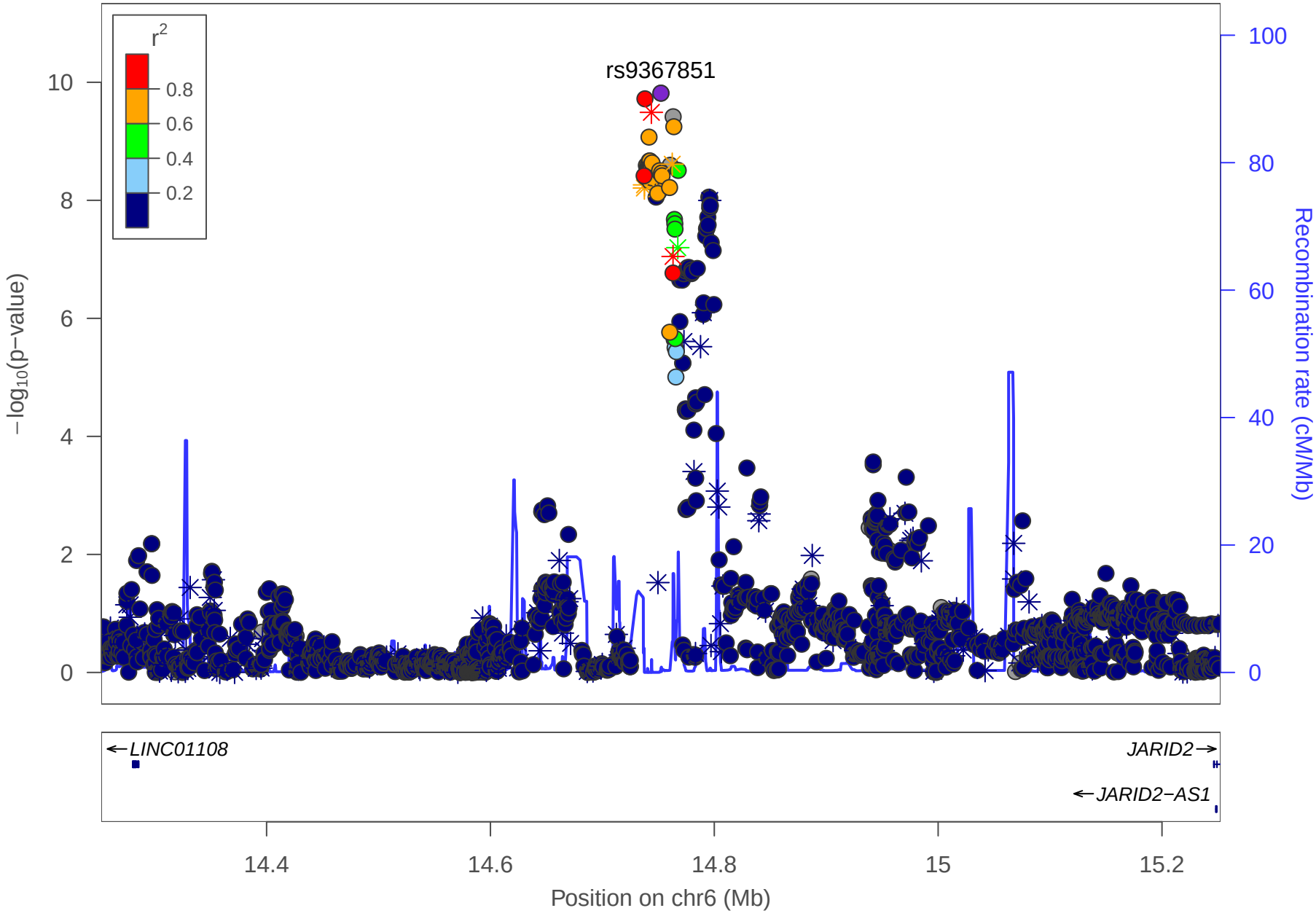
r2
0.8
0.6
0.4
0.2
rs9367851
10
8
6
4
2
0
−log10(p−value)
100
80
60
40
20
0
Recombination rate (cM/Mb)
←LINC01108
JARID2→
←JARID2−AS1
14.4
14.6
14.8
15
15.2
Position on chr6 (Mb)

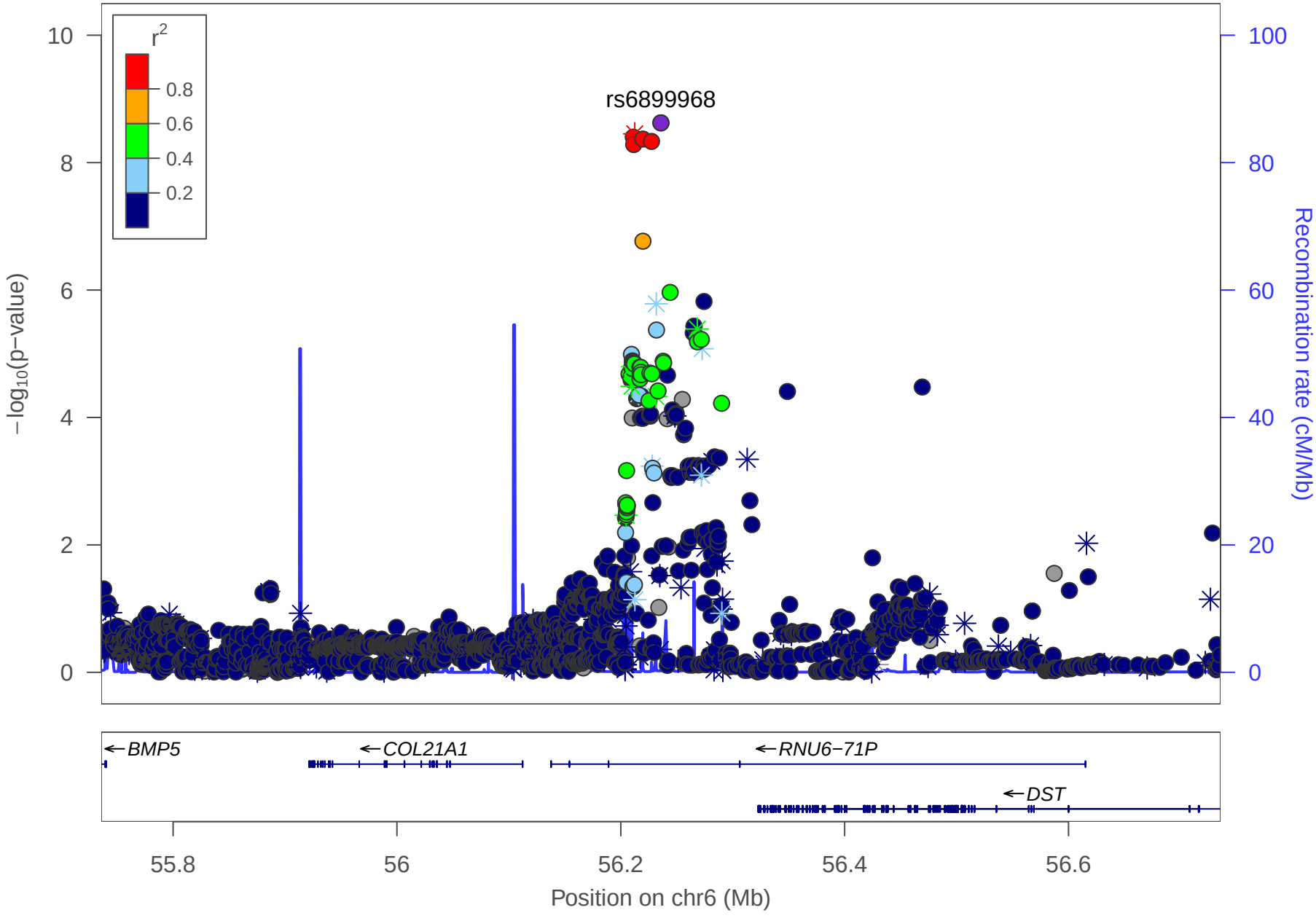
r2
0.8
0.6
0.4
0.2
rs6899968
10
8
6
4
2
0
100
80
60
40
20
0
−log10(p−value)
Recombination rate (cM/Mb)
←BMP5
←COL21A1
←RNU6−71P
←DST
55.8
56
56.2
56.4
56.6
Position on chr6 (Mb)

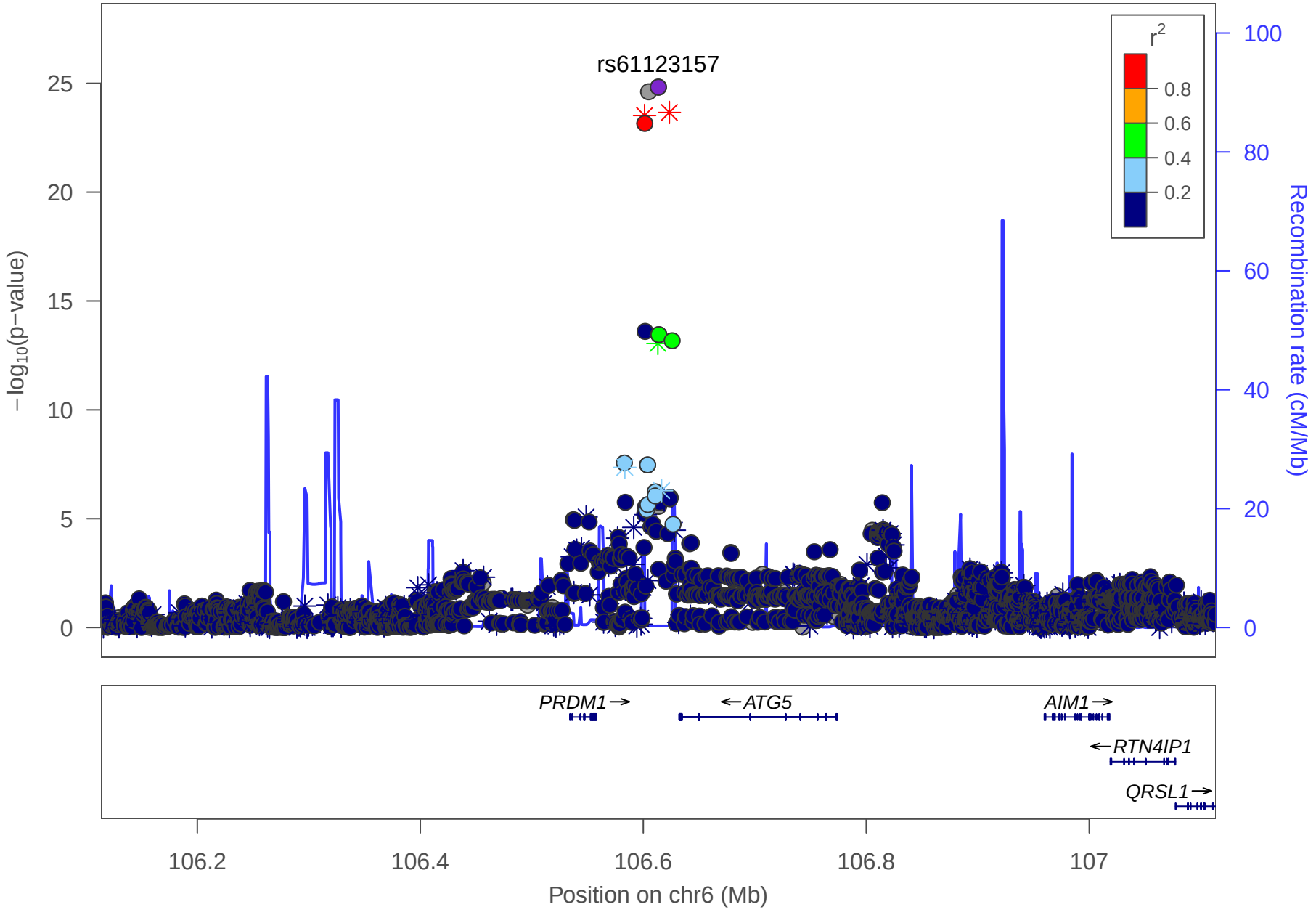
rs61123157
r2
0.8
0.6
0.4
0.2
−log10(p−value)
Recombination rate (cM/Mb)
25
20
15
10
5
0
100
80
60
40
20
0
PRDM1
ATG5
AIM1
RTN4IP1
QRSL1
106.2
106.4
106.6
106.8
107
Position on chr6 (Mb)

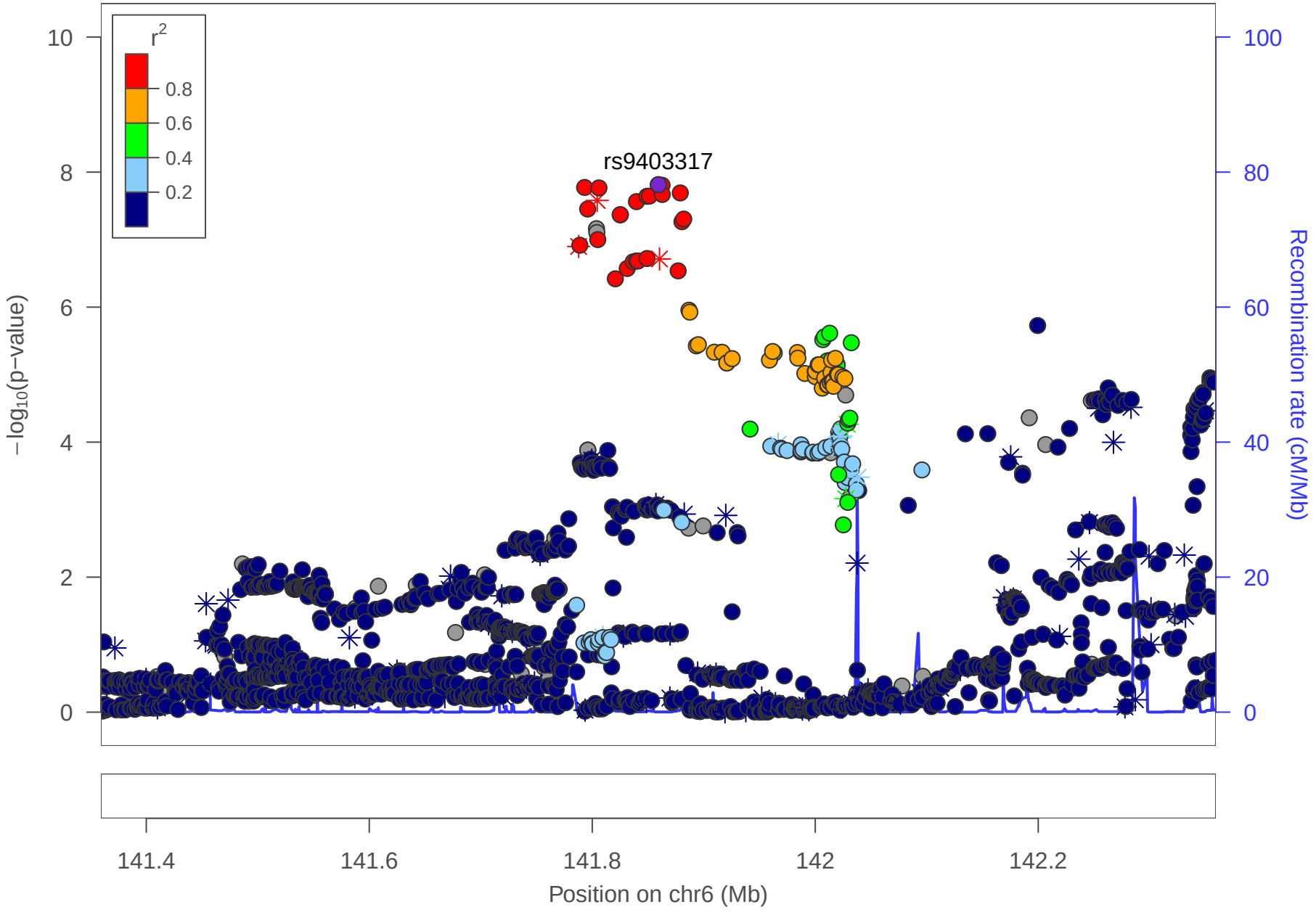
r2
0.8
0.6
0.4
0.2
rs9403317
10
8
6
4
2
0
−log10(p−value)
100
80
60
40
20
0
Recombination rate (cM/Mb)
141.4
141.6
141.8
142
142.2
Position on chr6 (Mb)

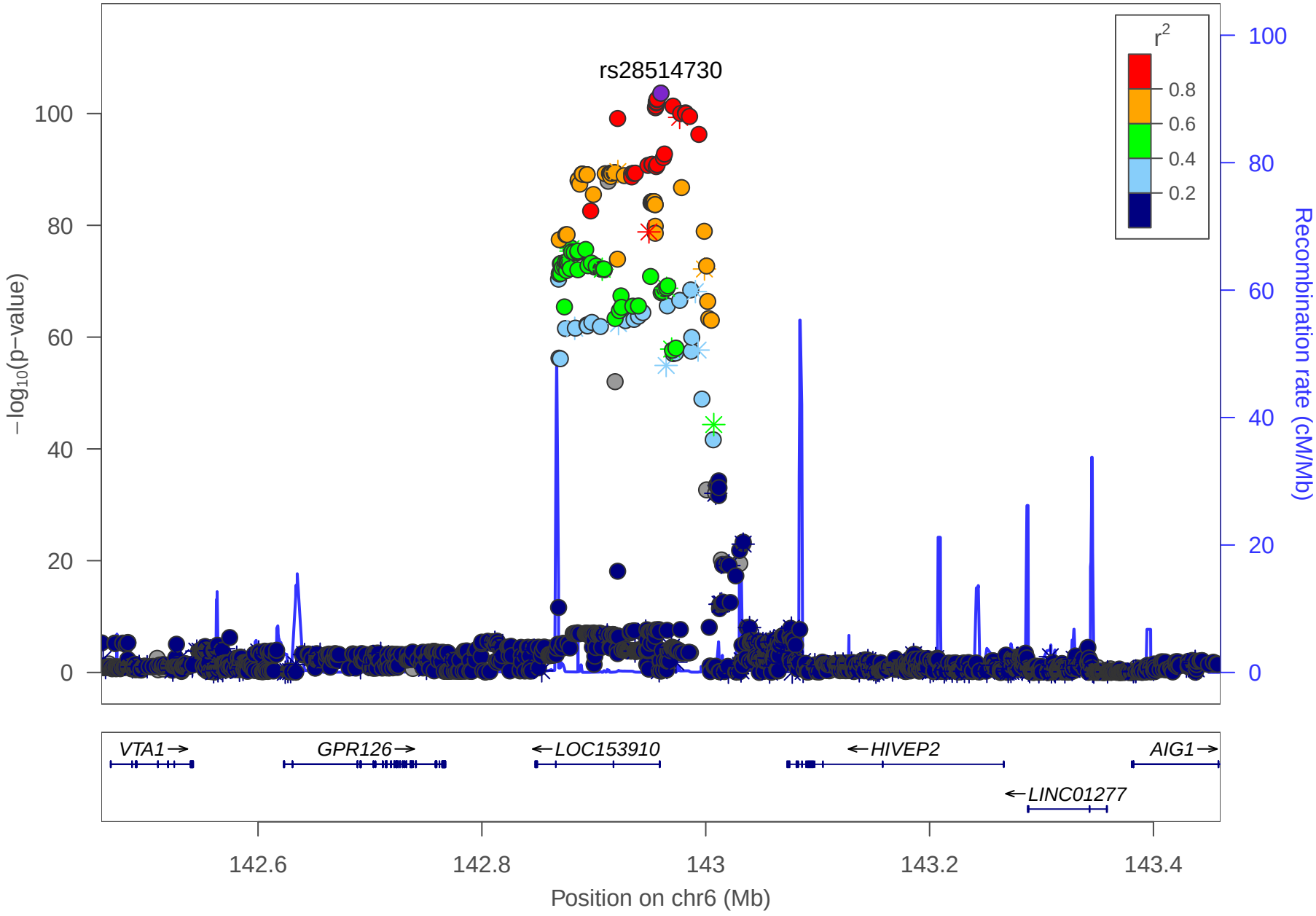
rs28514730
r2
0.8
0.6
0.4
0.2
100
80
60
40
20
0
−log10(p−value)
Recombination rate (cM/Mb)
VTA1
GPR126
LOC153910
HIVEP2
AIG1
LINC01277
142.6
142.8
143
143.2
143.4
Position on chr6 (Mb)

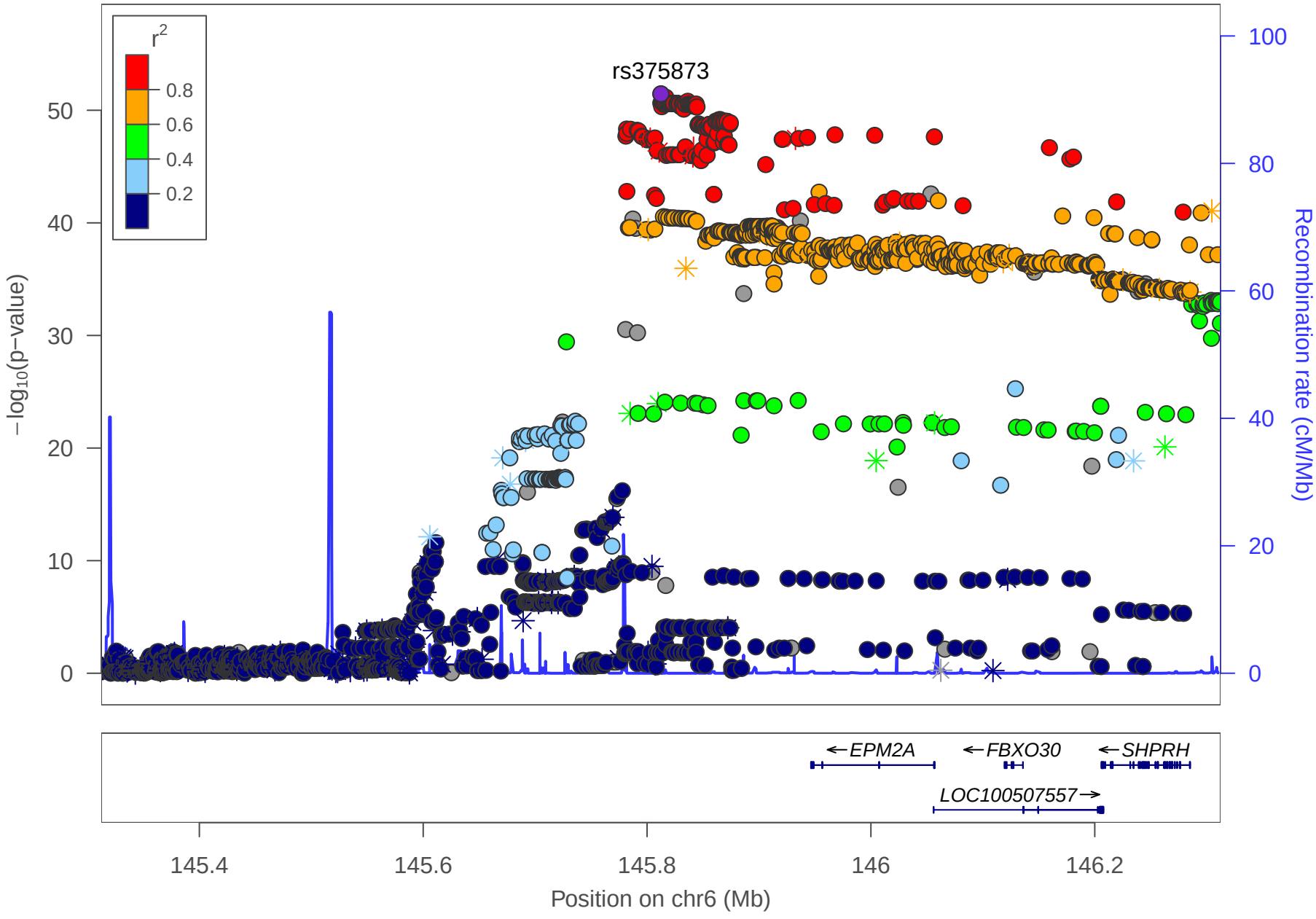
r2
0.8
0.6
0.4
0.2
rs375873
−log10(p−value)
Recombination rate (cM/Mb)
0
10
20
30
40
50
0
20
40
60
80
100
EPM2A
FBXO30
SHPRH
LOC100507557
145.4
145.6
145.8
146
146.2
Position on chr6 (Mb)

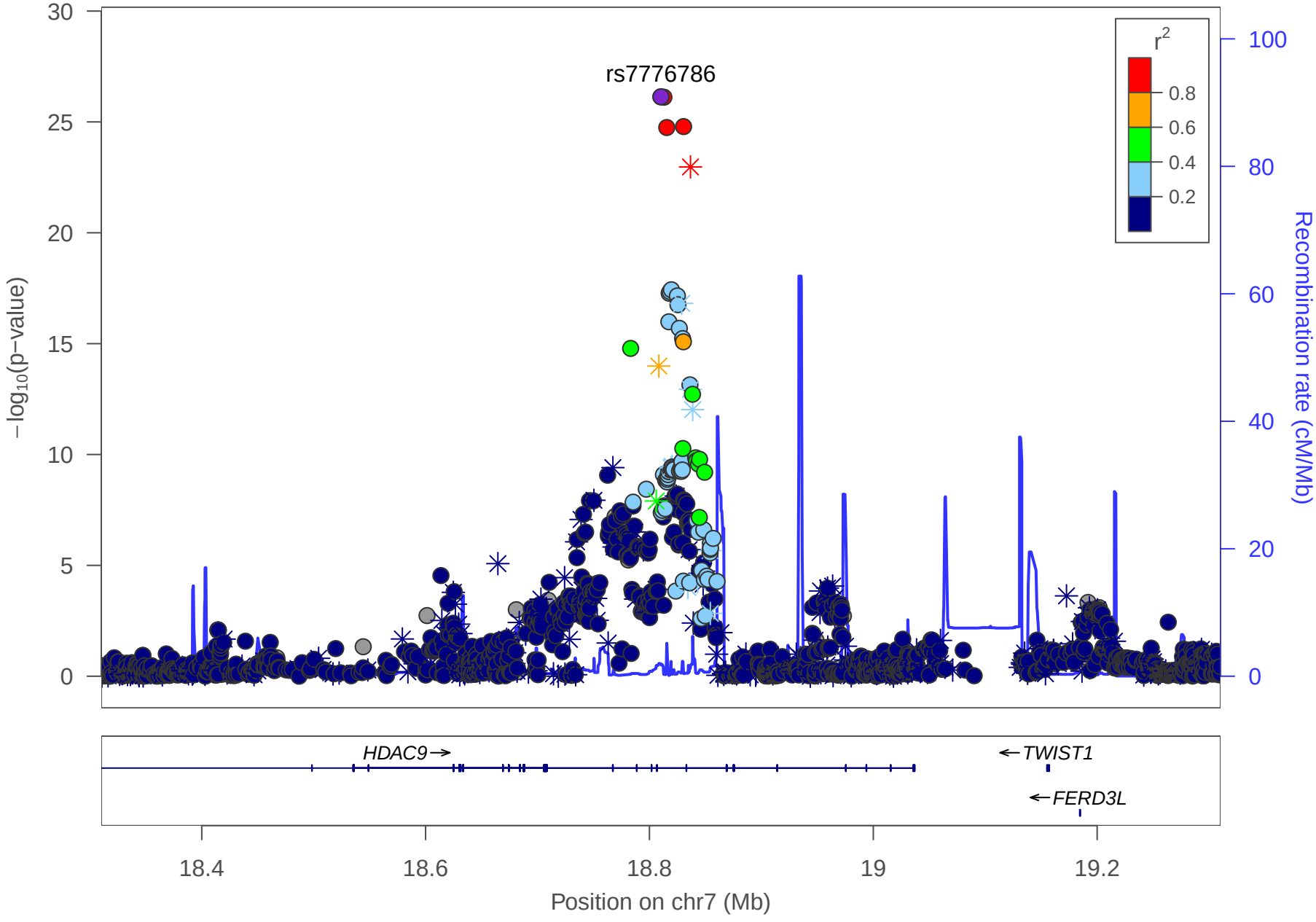
rs7776786
r2
0.8
0.6
0.4
0.2
30
25
20
15
10
5
0
100
80
60
40
20
0
−log10(p−value)
Recombination rate (cM/Mb)
HDAC9
TWIST1
FERD3L
18.4
18.6
18.8
19
19.2
Position on chr7 (Mb)

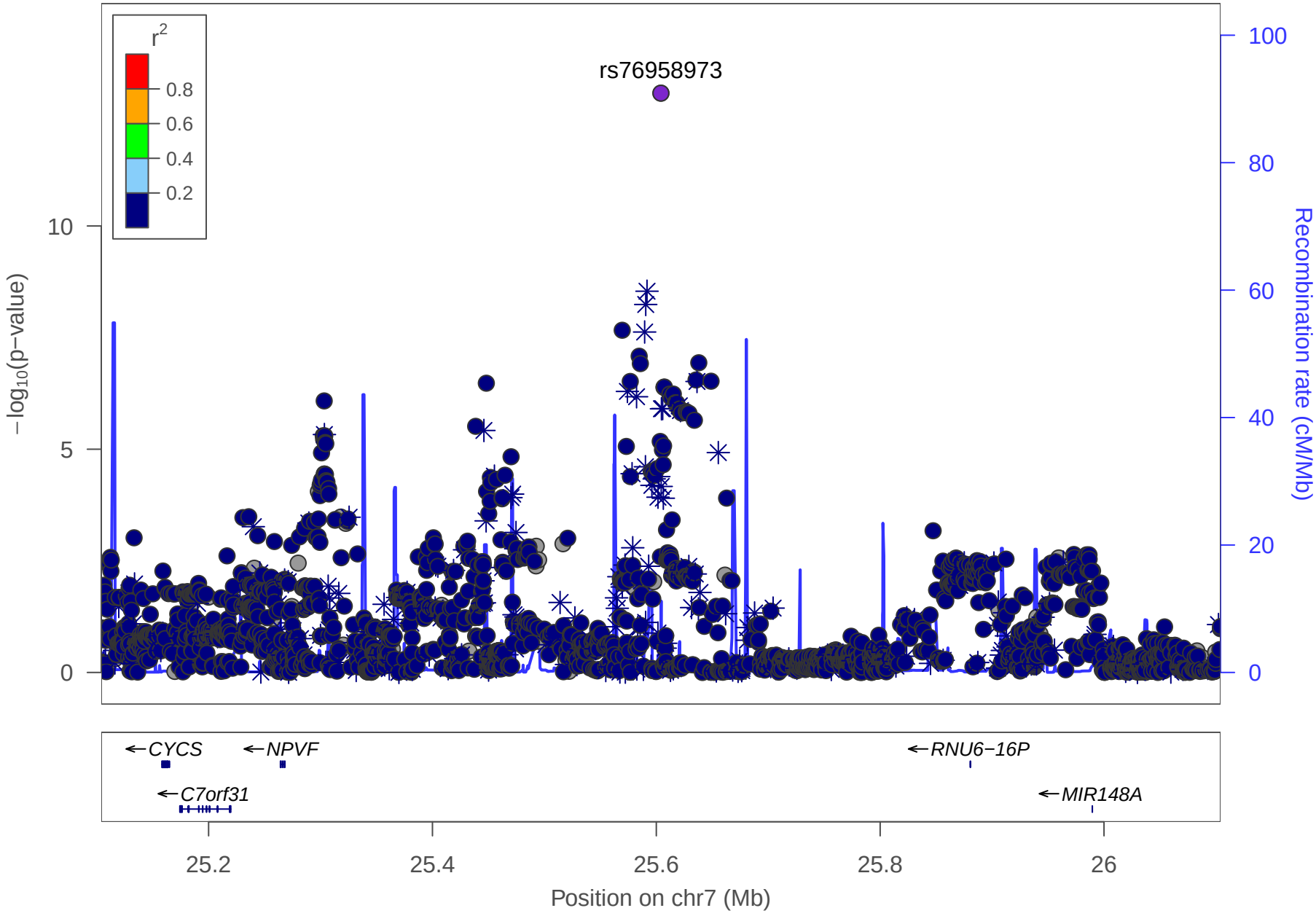
r2
0.8
0.6
0.4
0.2
rs76958973
10
5
0
−log10(p−value)
100
80
60
40
20
0
Recombination rate (cM/Mb)
←CYCS
←NPVF
←RNU6−16P
←C7orf31
←MIR148A
25.2
25.4
25.6
25.8
26
Position on chr7 (Mb)

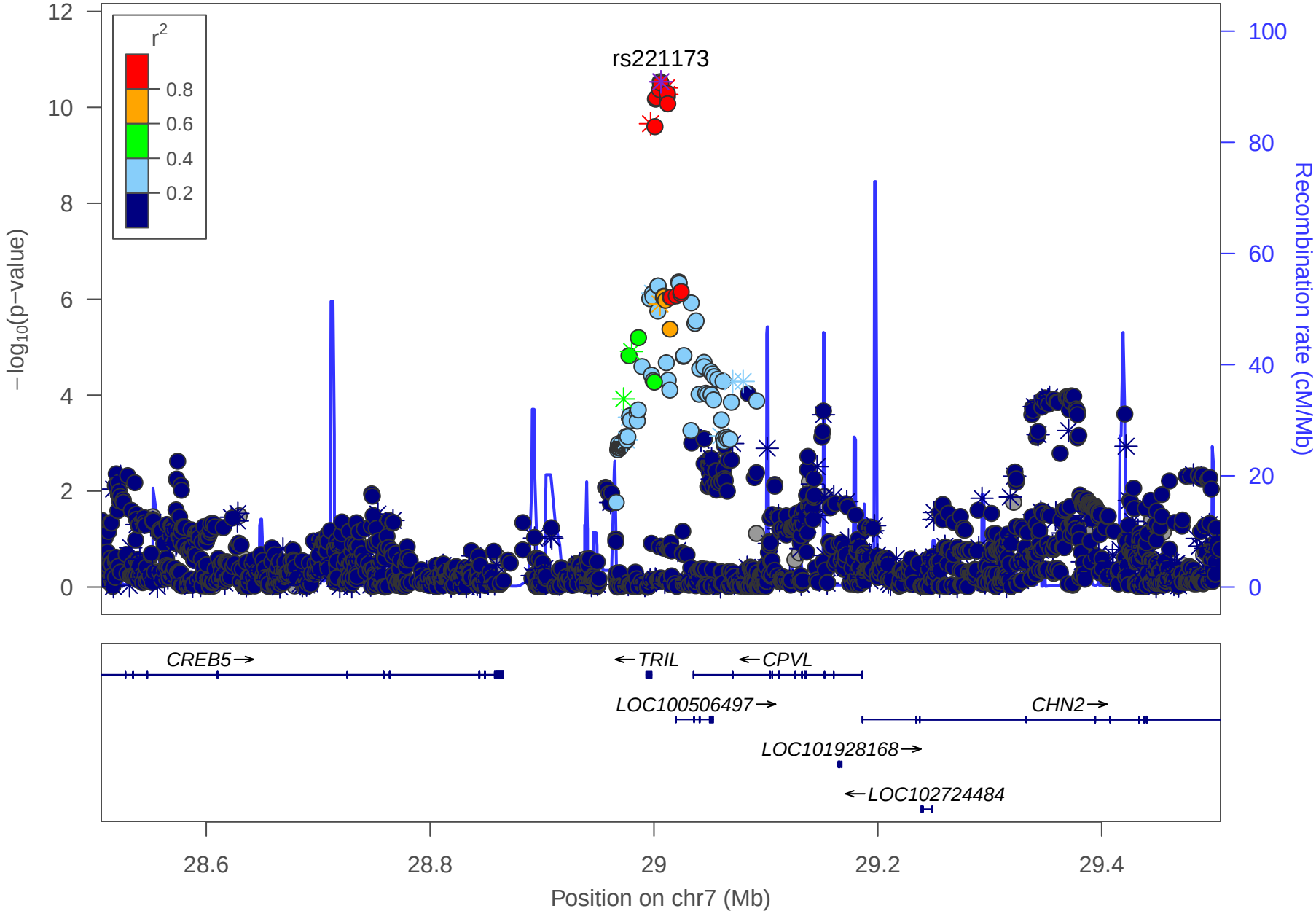
rs221173
r2
0.8
0.6
0.4
0.2
−log10(p−value)
Recombination rate (cM/Mb)
CREB5→
←TRIL
←CPVL
LOC100506497→
CHN2→
LOC101928168→
←LOC102724484
Position on chr7 (Mb)

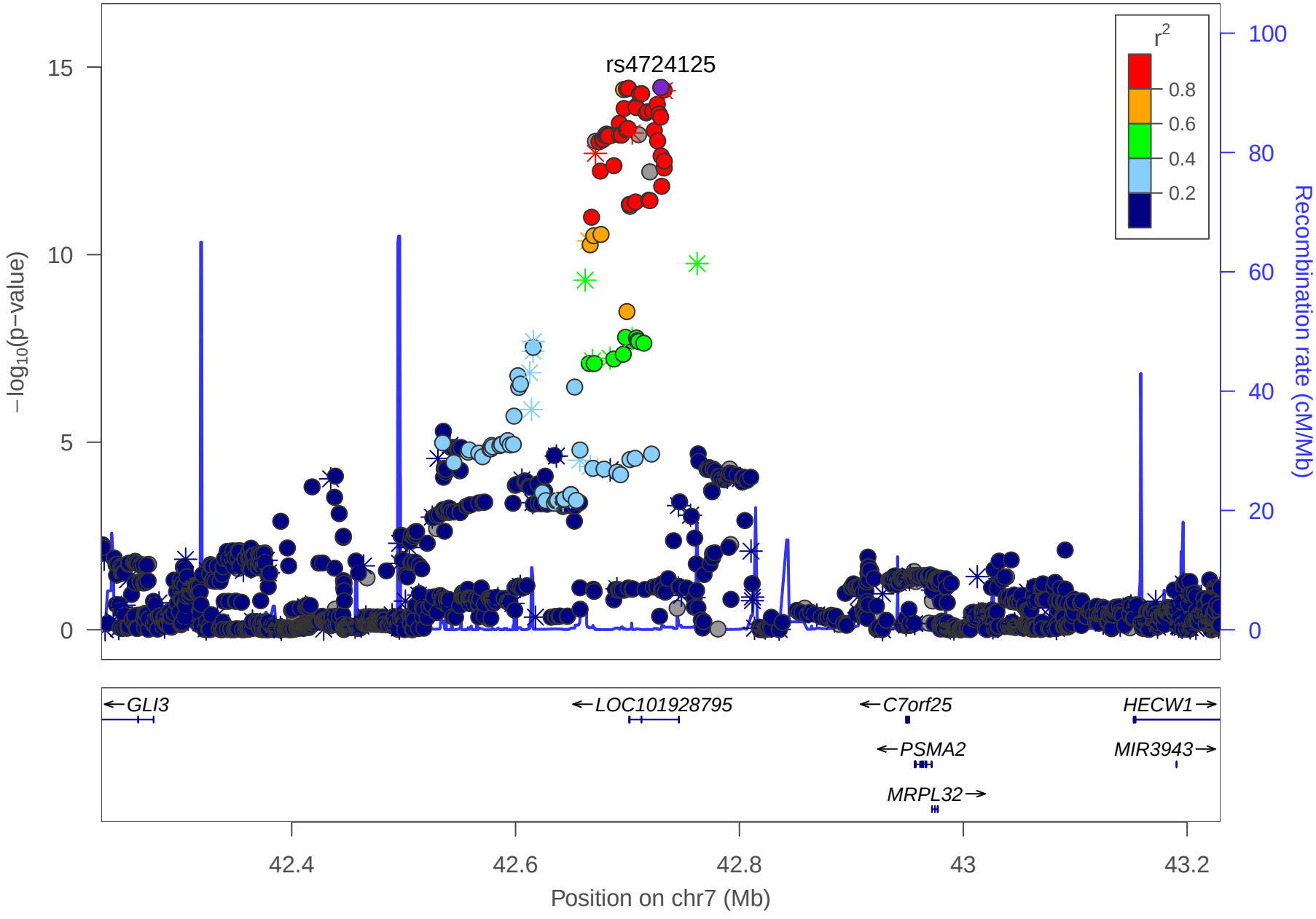
rs4724125
r2
0.8
0.6
0.4
0.2
15
10
5
0
−log10(p−value)
100
80
60
40
20
0
Recombination rate (cM/Mb)
←GLI3
←LOC101928795
←C7orf25
HECW1→
←PSMA2
MIR3943→
MRPL32→
42.4
42.6
42.8
43
43.2
Position on chr7 (Mb)

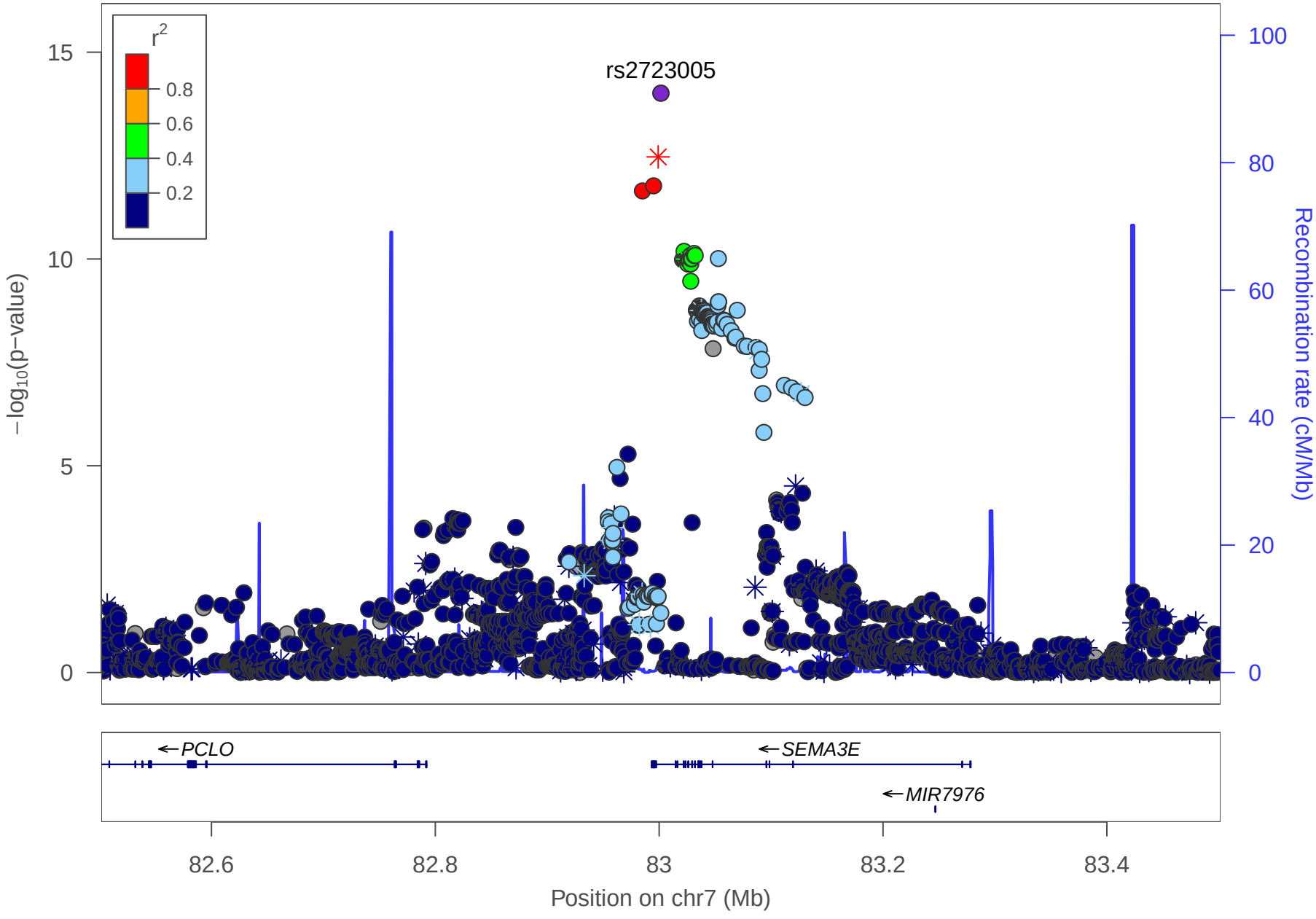
r2
0.8
0.6
0.4
0.2
rs2723005
15
10
5
0
−log10(p−value)
100
80
60
40
20
0
Recombination rate (cM/Mb)
←PCLO
←SEMA3E
←MIR7976
82.6
82.8
83
83.2
83.4
Position on chr7 (Mb)

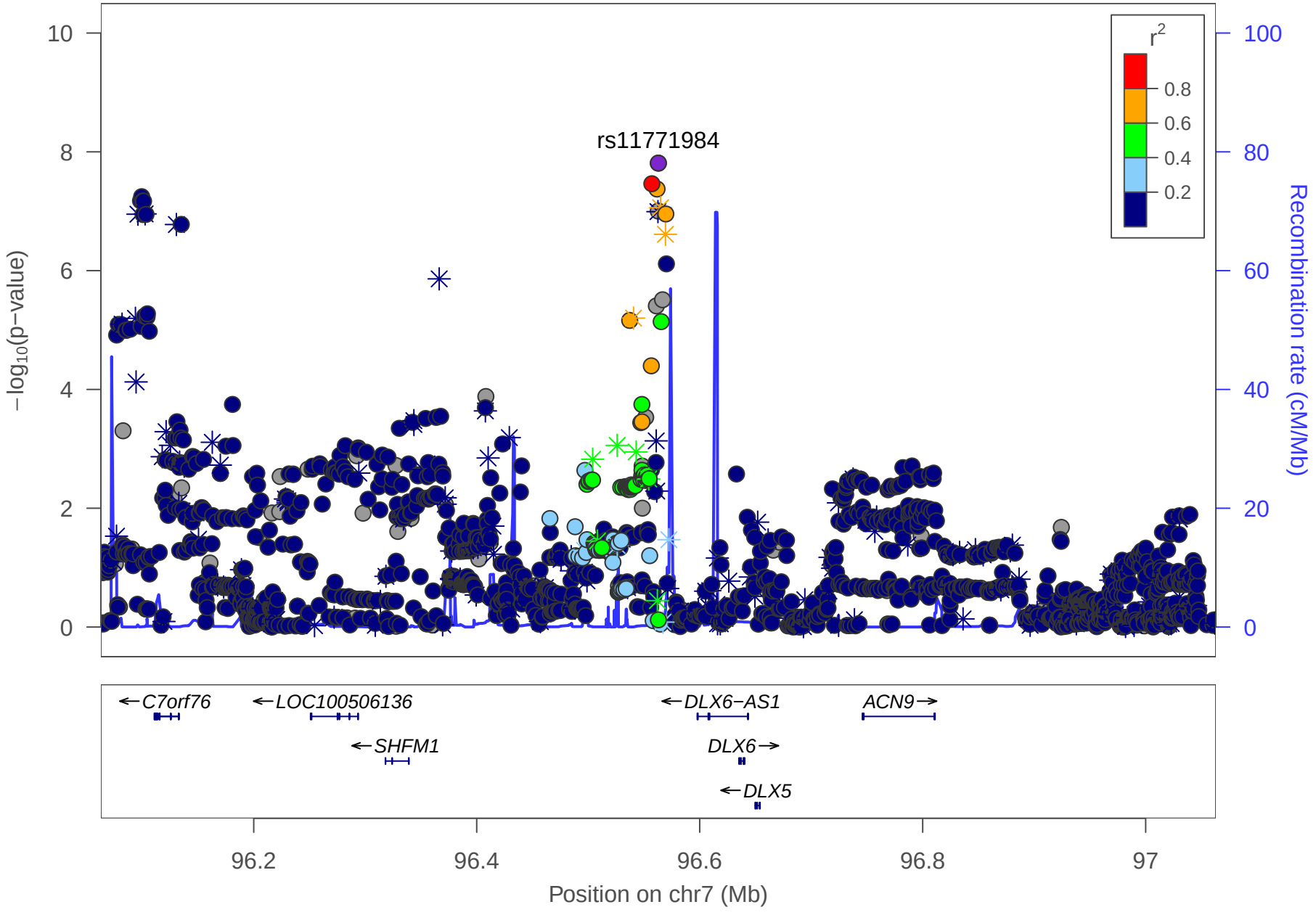
rs11771984
r2
0.8
0.6
0.4
0.2
−log10(p−value)
Recombination rate (cM/Mb)
10
8
6
4
2
0
100
80
60
40
20
0
←C7orf76
←LOC100506136
←SHFM1
←DLX6−AS1
ACN9→
DLX6→
←DLX5
96.2
96.4
96.6
96.8
97
Position on chr7 (Mb)

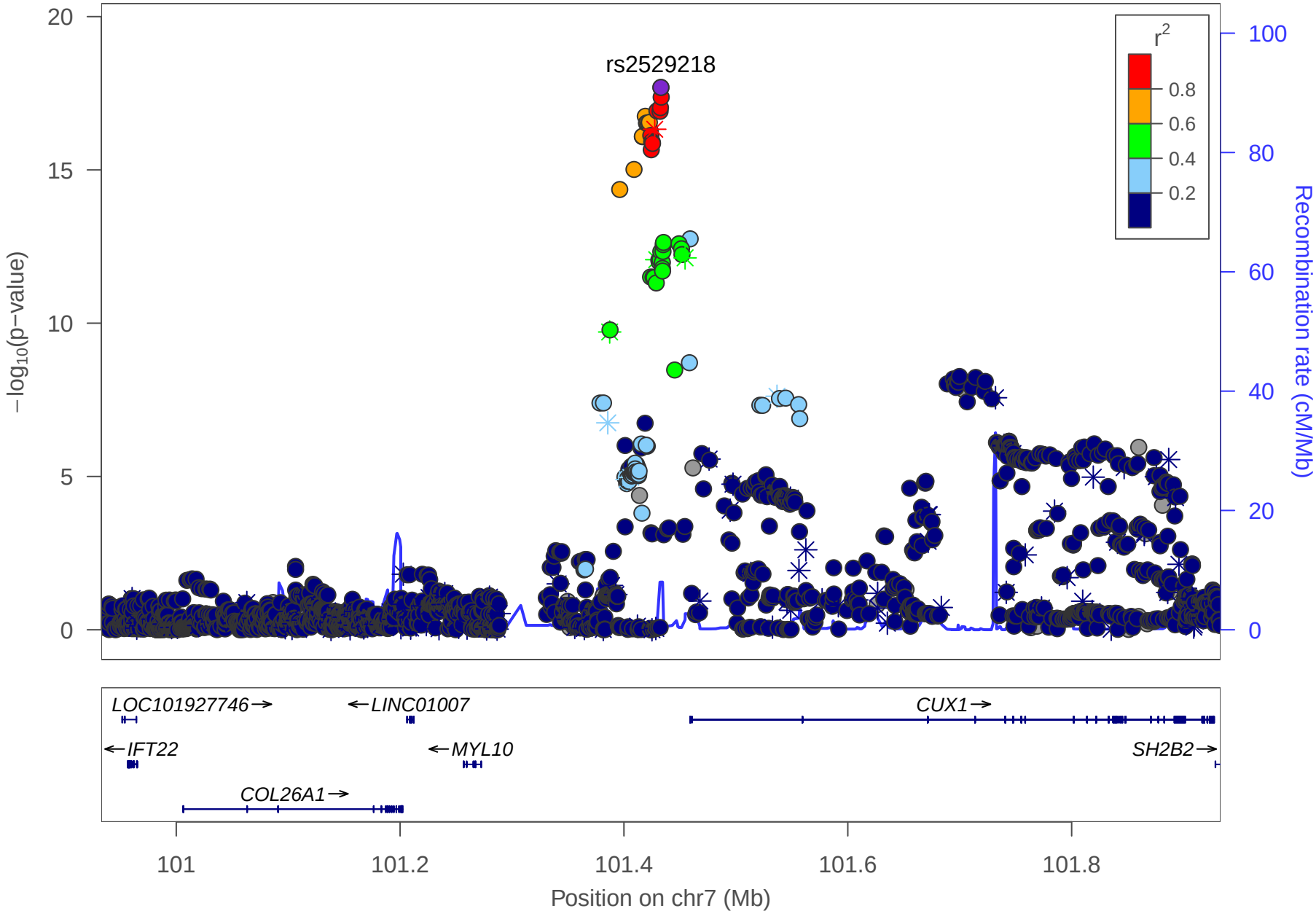
rs2529218
r2
0.8
0.6
0.4
0.2
−log10(p−value)
Recombination rate (cM/Mb)
20
15
10
5
0
100
80
60
40
20
0
LOC101927746
LINC01007
CUX1
IFT22
MYL10
SH2B2
COL26A1
101
101.2
101.4
101.6
101.8
Position on chr7 (Mb)

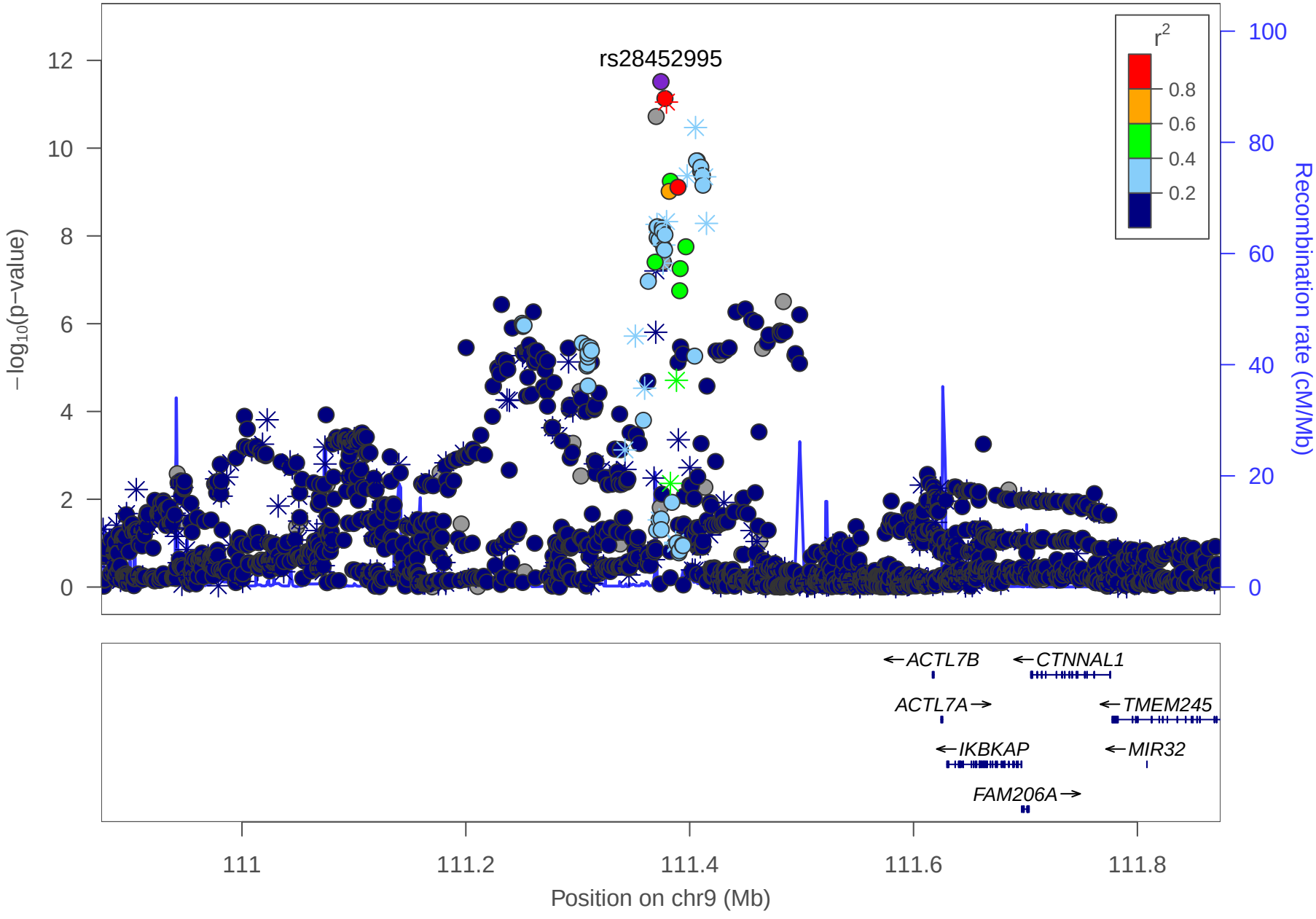
rs28452995
r2
0.8
0.6
0.4
0.2
−log10(p−value)
Recombination rate (cM/Mb)
0
2
4
6
8
10
12
0
20
40
60
80
100
ACTL7B
CTNNAL1
ACTL7A
TMEM245
IKBKAP
MIR32
FAM206A
111
111.2
111.4
111.6
111.8
Position on chr9 (Mb)

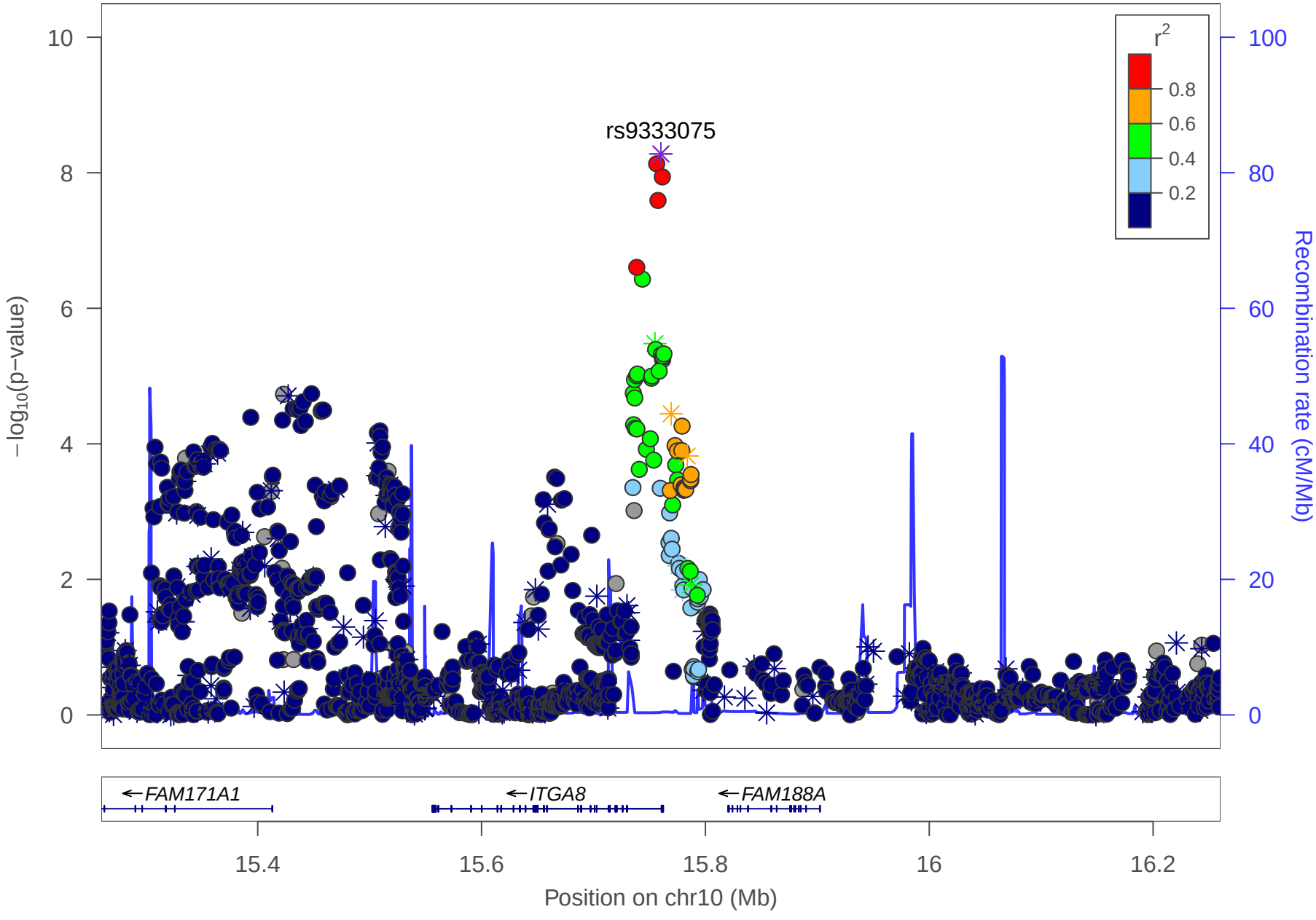
rs9333075
r2
0.8
0.6
0.4
0.2
−log10(p−value)
Recombination rate (cM/Mb)
10
8
6
4
2
0
100
80
60
40
20
0
FAM171A1
ITGA8
FAM188A
15.4
15.6
15.8
16
16.2
Position on chr10 (Mb)

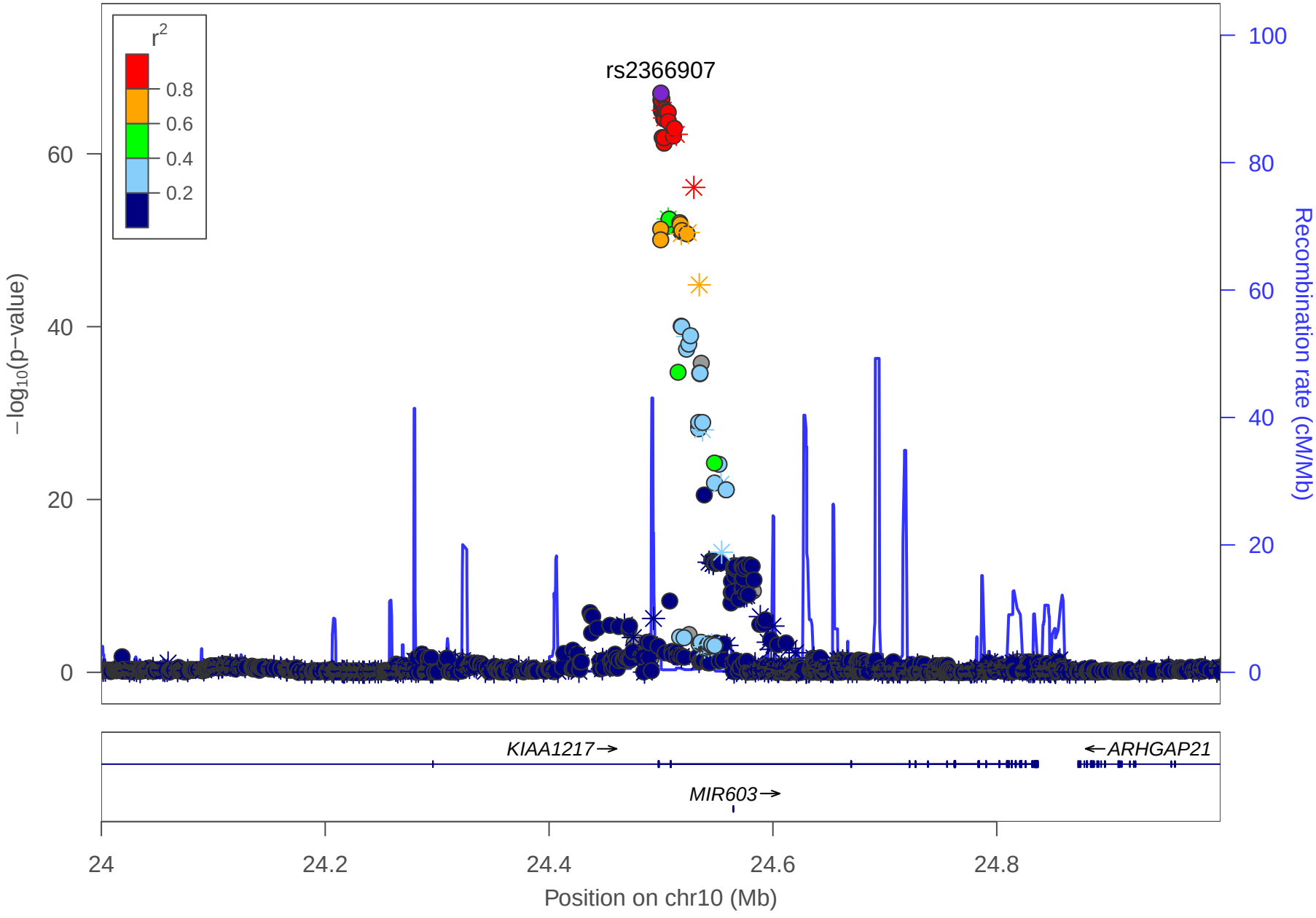
r2
0.8
0.6
0.4
0.2
rs2366907
60
40
20
0
−log10(p−value)
100
80
60
40
20
0
Recombination rate (cM/Mb)
KIAA1217→
←ARHGAP21
MIR603→
24
24.2
24.4
24.6
24.8
Position on chr10 (Mb)

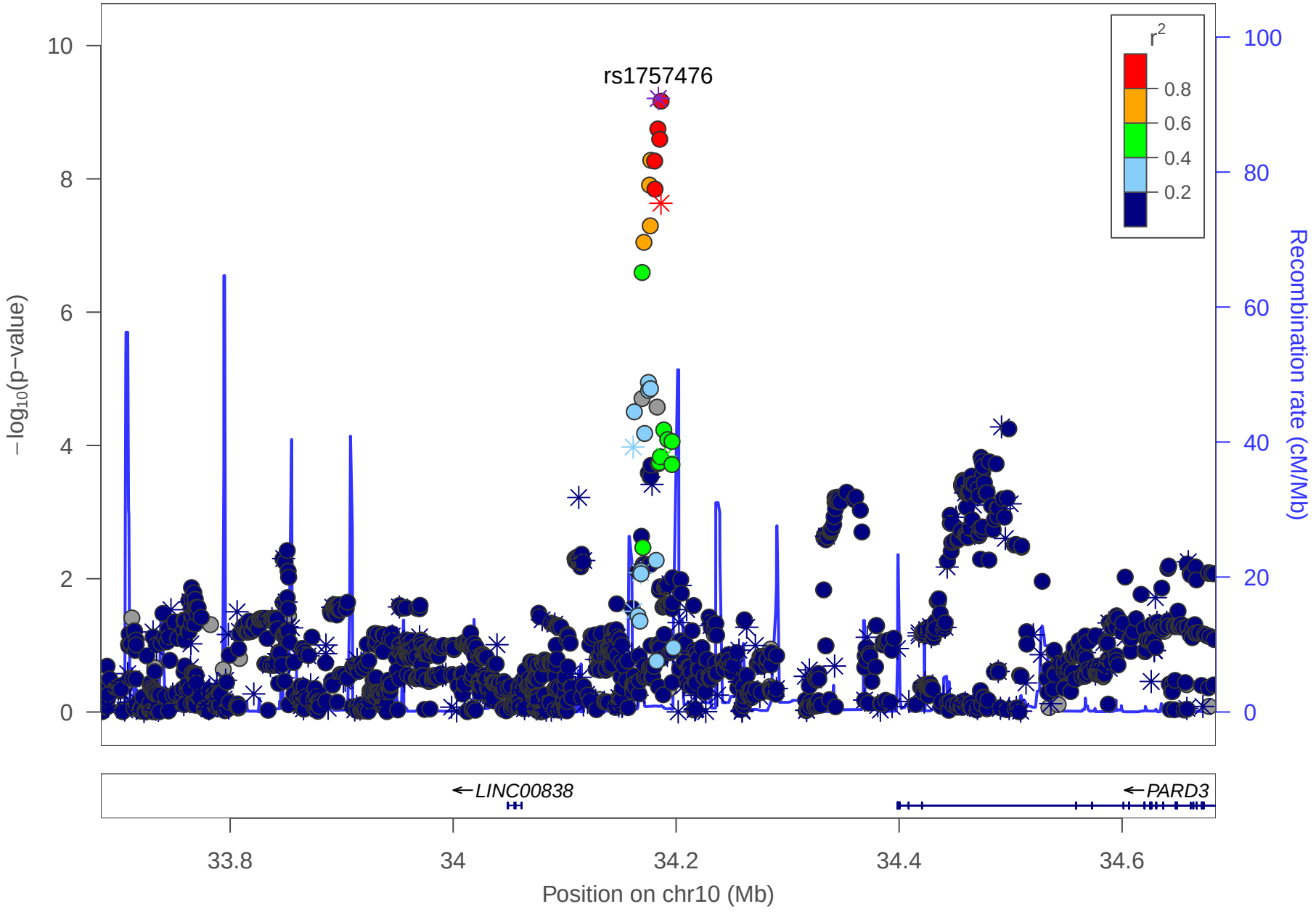
rs1757476
r²
0.8
0.6
0.4
0.2
−log10(p−value)
Recombination rate (cM/Mb)
10
8
6
4
2
0
100
80
60
40
20
0
←LINC00838
←PARD3
33.8
34
34.2
34.4
34.6
Position on chr10 (Mb)

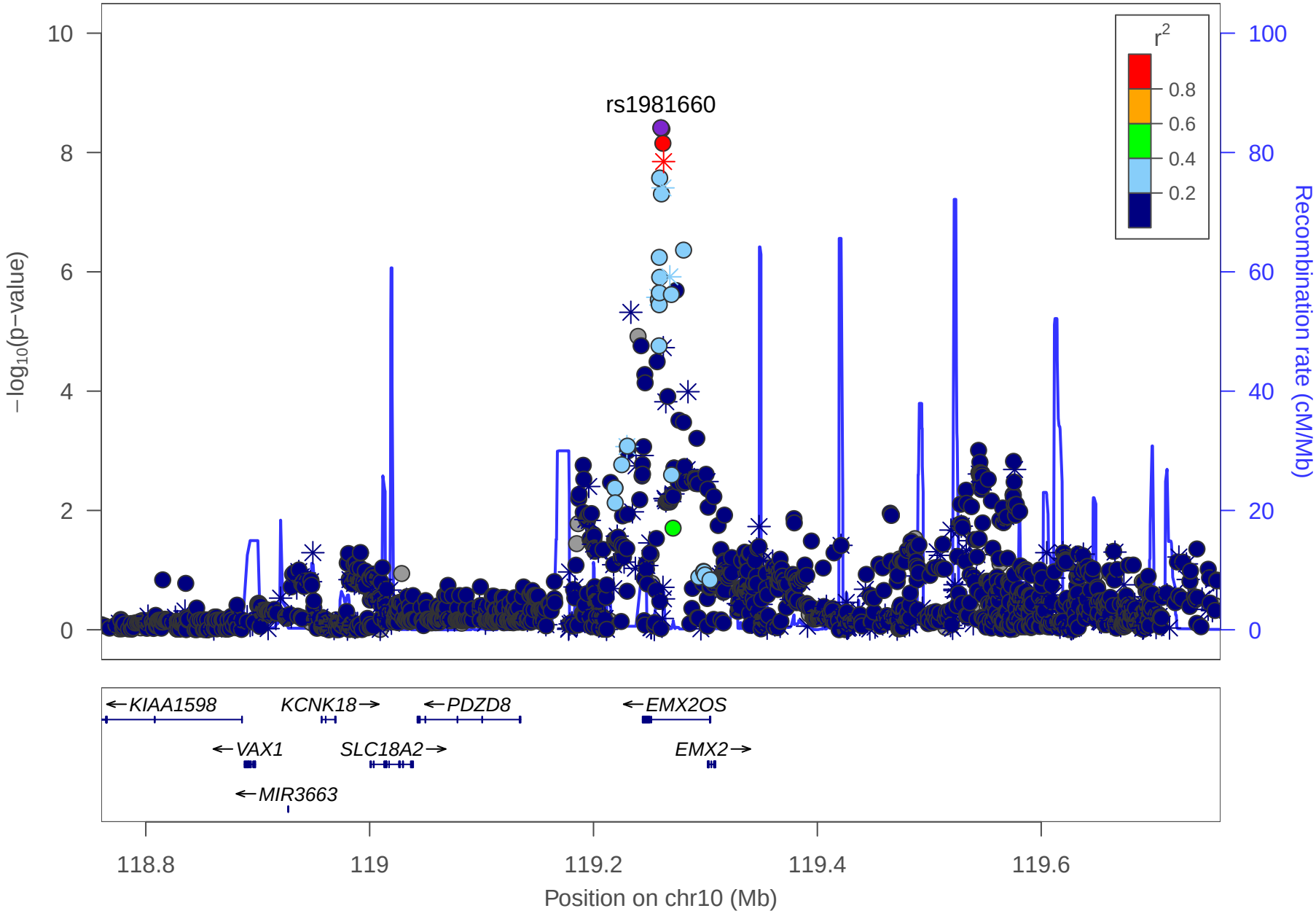
rs1981660
r2
0.8
0.6
0.4
0.2
−log10(p−value)
Recombination rate (cM/Mb)
10
8
6
4
2
0
100
80
60
40
20
0
KIAA1598
KCNK18
PDZD8
EMX2OS
VAX1
SLC18A2
EMX2
MIR3663
118.8
119
119.2
119.4
119.6
Position on chr10 (Mb)

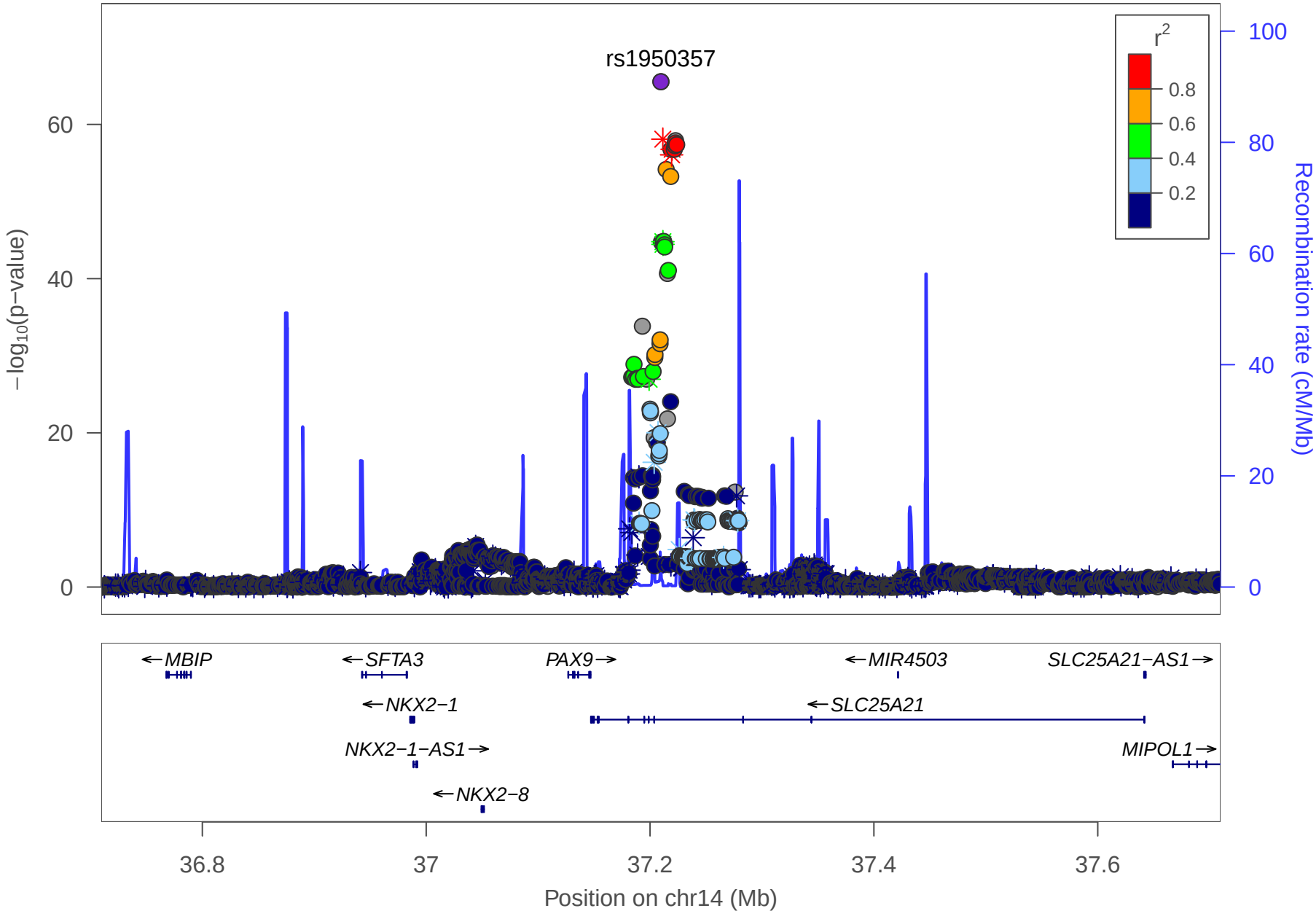
rs1950357
r2
0.8
0.6
0.4
0.2
−log10(p−value)
Recombination rate (cM/Mb)
0
20
40
60
0
20
40
60
80
100
←MBIP
←SFTA3
PAX9→
←MIR4503
SLC25A21−AS1→
←NKX2−1
←SLC25A21
NKX2−1−AS1→
MIPOL1→
←NKX2−8
36.8
37
37.2
37.4
37.6
Position on chr14 (Mb)

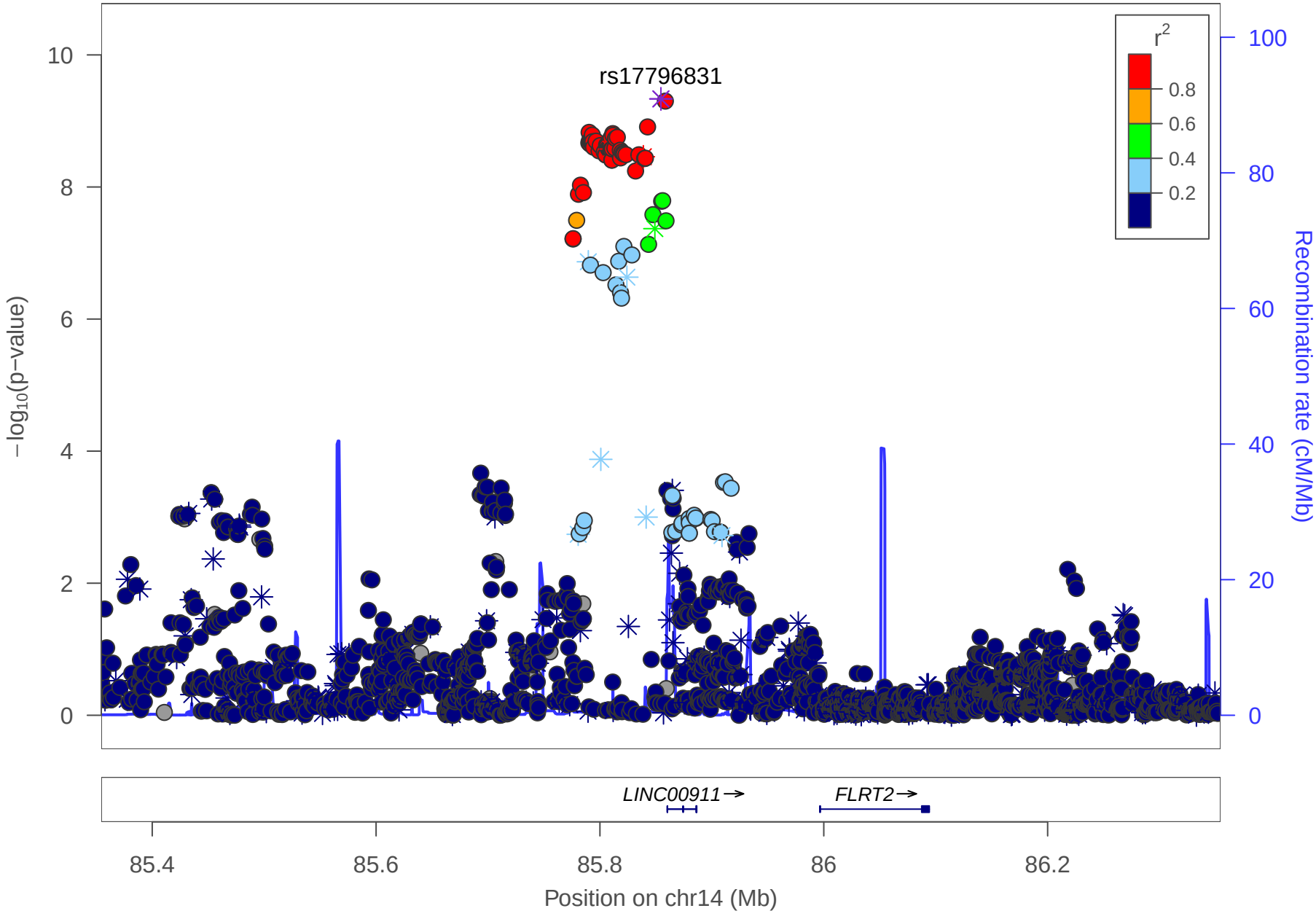
rs17796831
r2
0.8
0.6
0.4
0.2
−log10(p−value)
Recombination rate (cM/Mb)
LINC00911
FLRT2
Position on chr14 (Mb)
85.4
85.6
85.8
86
86.2

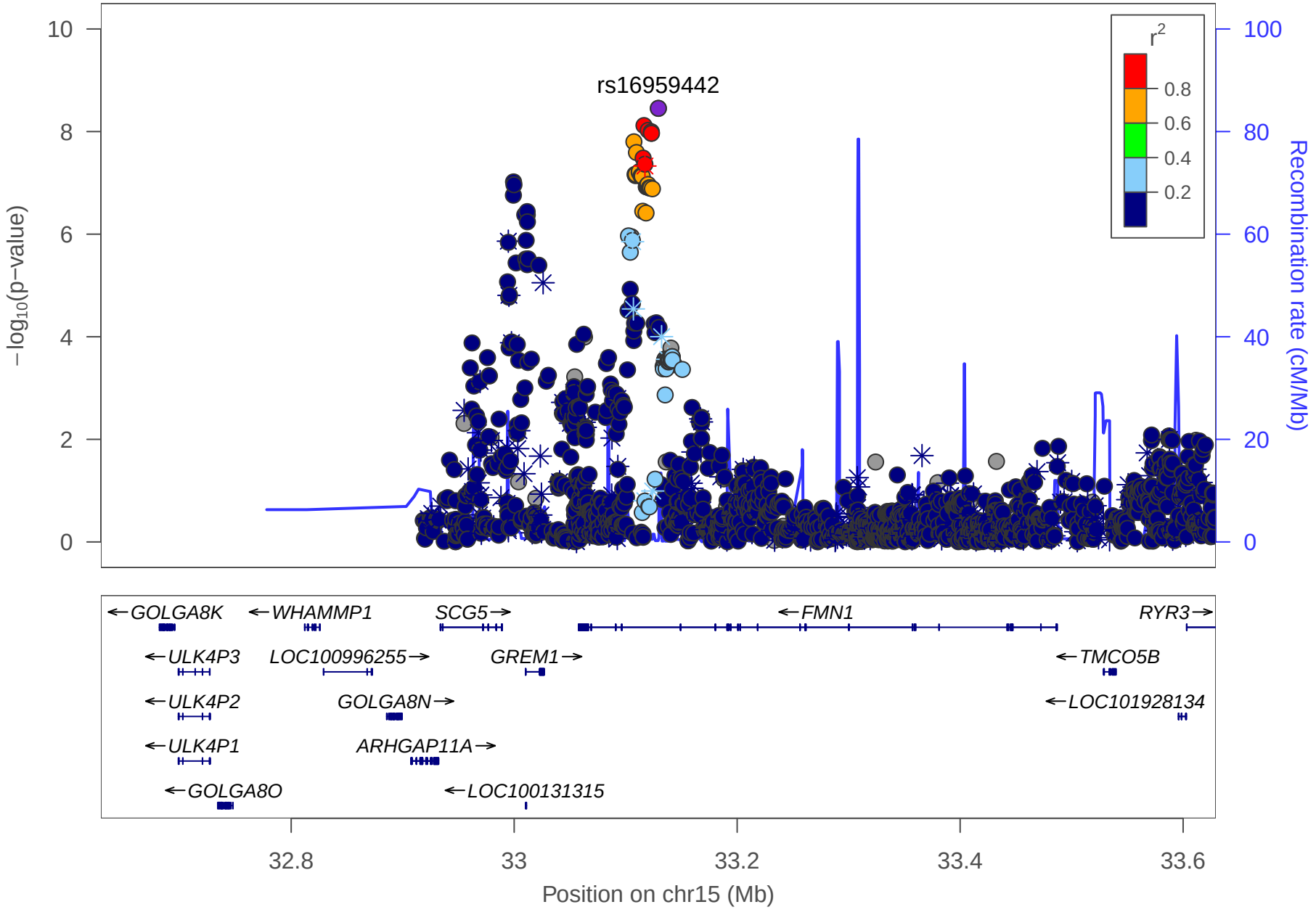
rs16959442
r2
0.8
0.6
0.4
0.2
−log10(p−value)
Recombination rate (cM/Mb)
10
8
6
4
2
0
100
80
60
40
20
0
GOLGA8K
WHAMMP1
SCG5
FMN1
RYR3
ULK4P3
LOC100996255
GREM1
TMCO5B
ULK4P2
GOLGA8N
LOC101928134
ULK4P1
ARHGAP11A
GOLGA8O
LOC100131315
32.8
33
33.2
33.4
33.6
Position on chr15 (Mb)

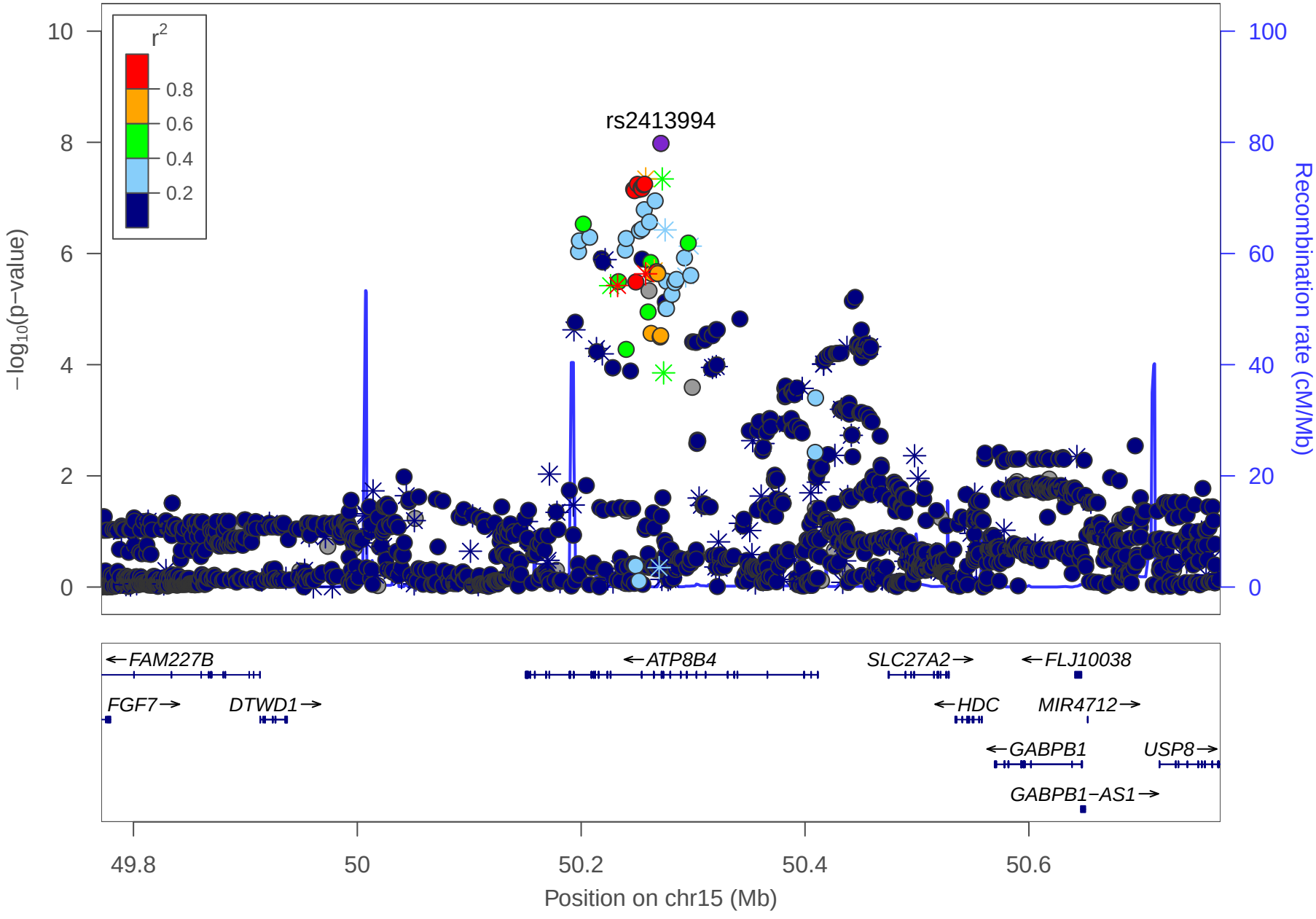
r2
0.8
0.6
0.4
0.2
rs2413994
−log10(p−value)
Recombination rate (cM/Mb)
FAM227B
ATP8B4
SLC27A2
FLJ10038
FGF7
DTWD1
HDC
MIR4712
GABPB1
USP8
GABPB1−AS1
Position on chr15 (Mb)

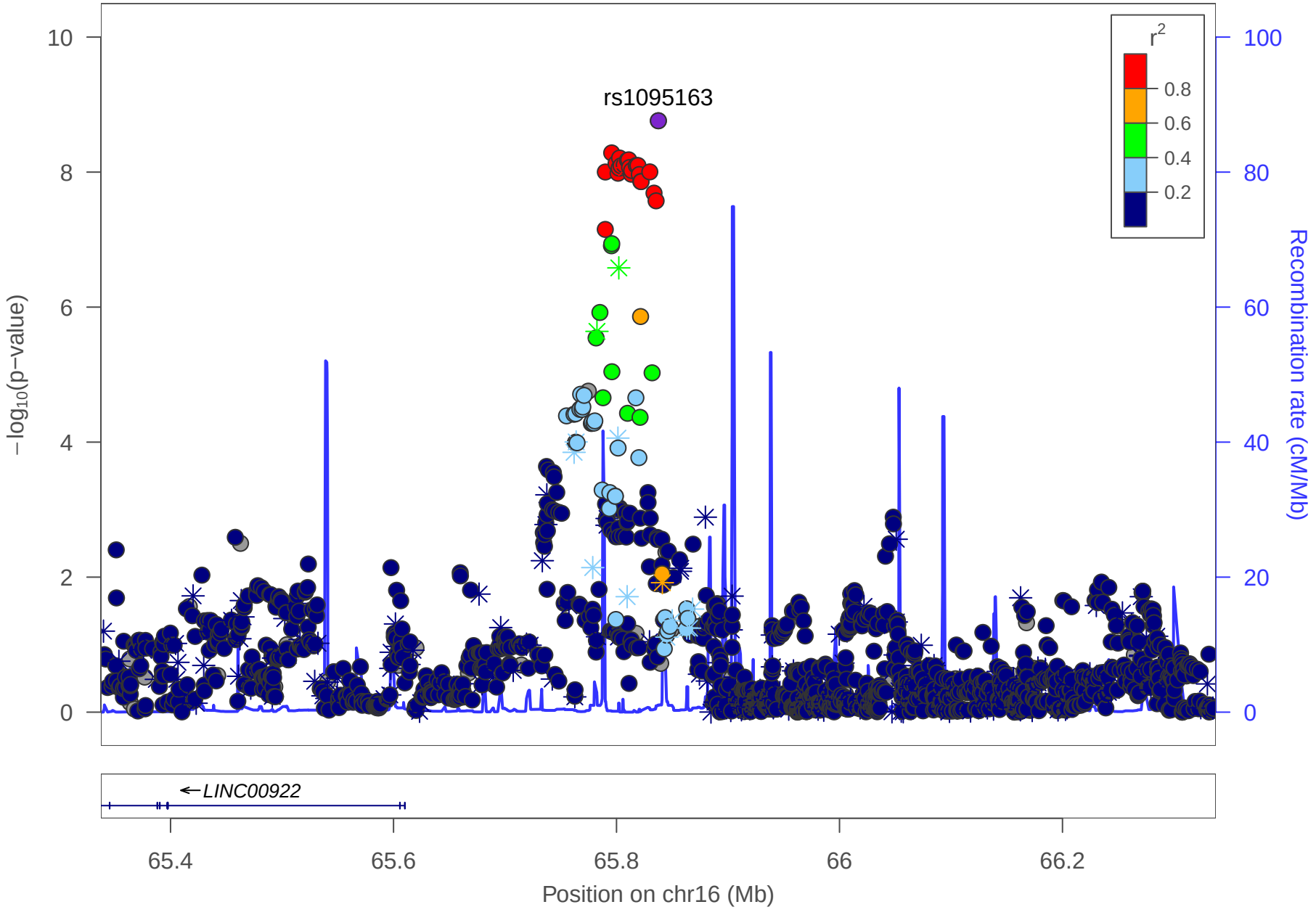
rs1095163
r2
0.8
0.6
0.4
0.2
10
8
6
4
2
0
100
80
60
40
20
0
−log10(p−value)
Recombination rate (cM/Mb)
←LINC00922
65.4
65.6
65.8
66
66.2
Position on chr16 (Mb)

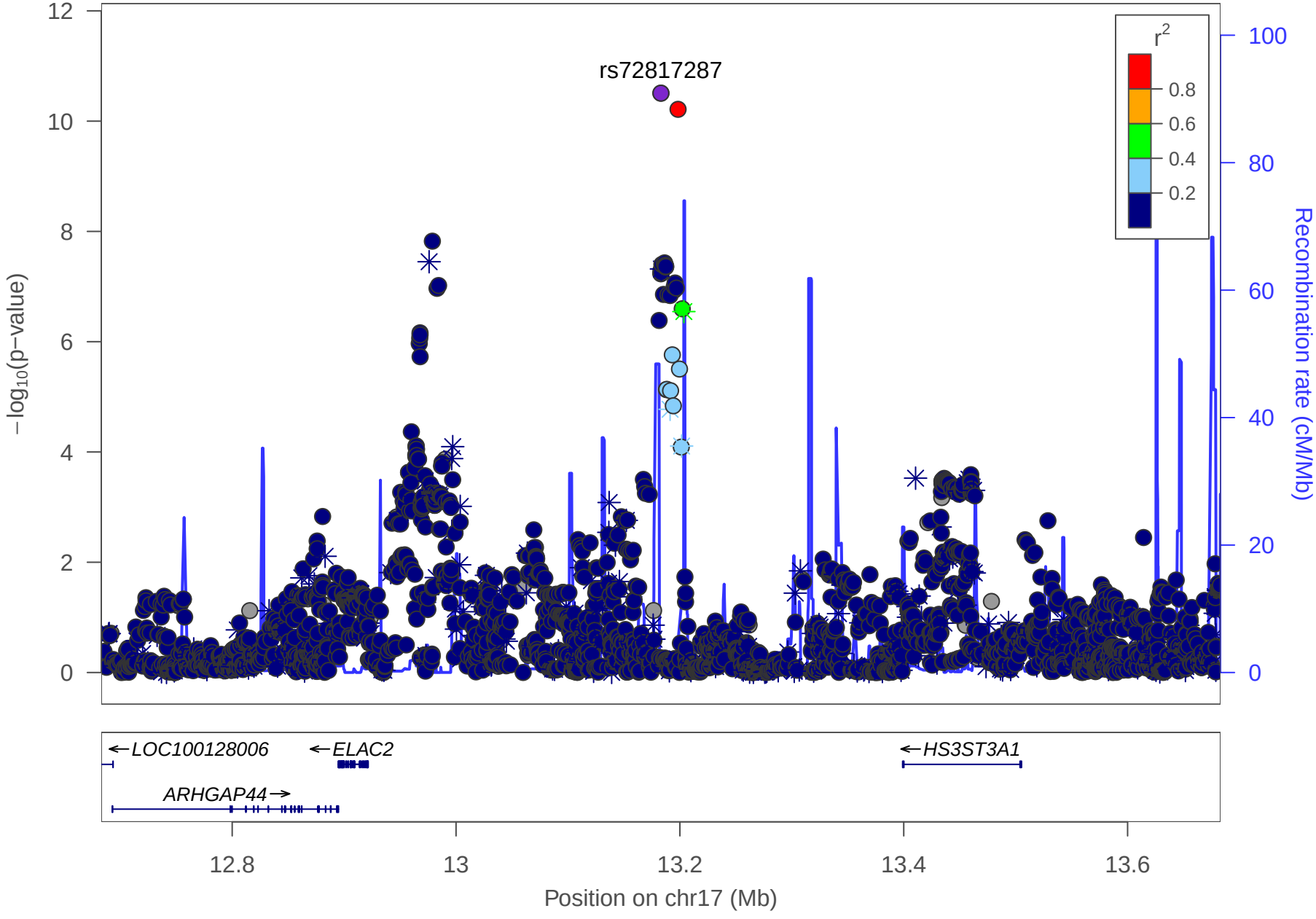
rs72817287
r2
0.8
0.6
0.4
0.2
12
10
8
6
4
2
0
−log10(p−value)
100
80
60
40
20
0
Recombination rate (cM/Mb)
←LOC100128006
←ELAC2
←HS3ST3A1
ARHGAP44→
12.8
13
13.2
13.4
13.6
Position on chr17 (Mb)

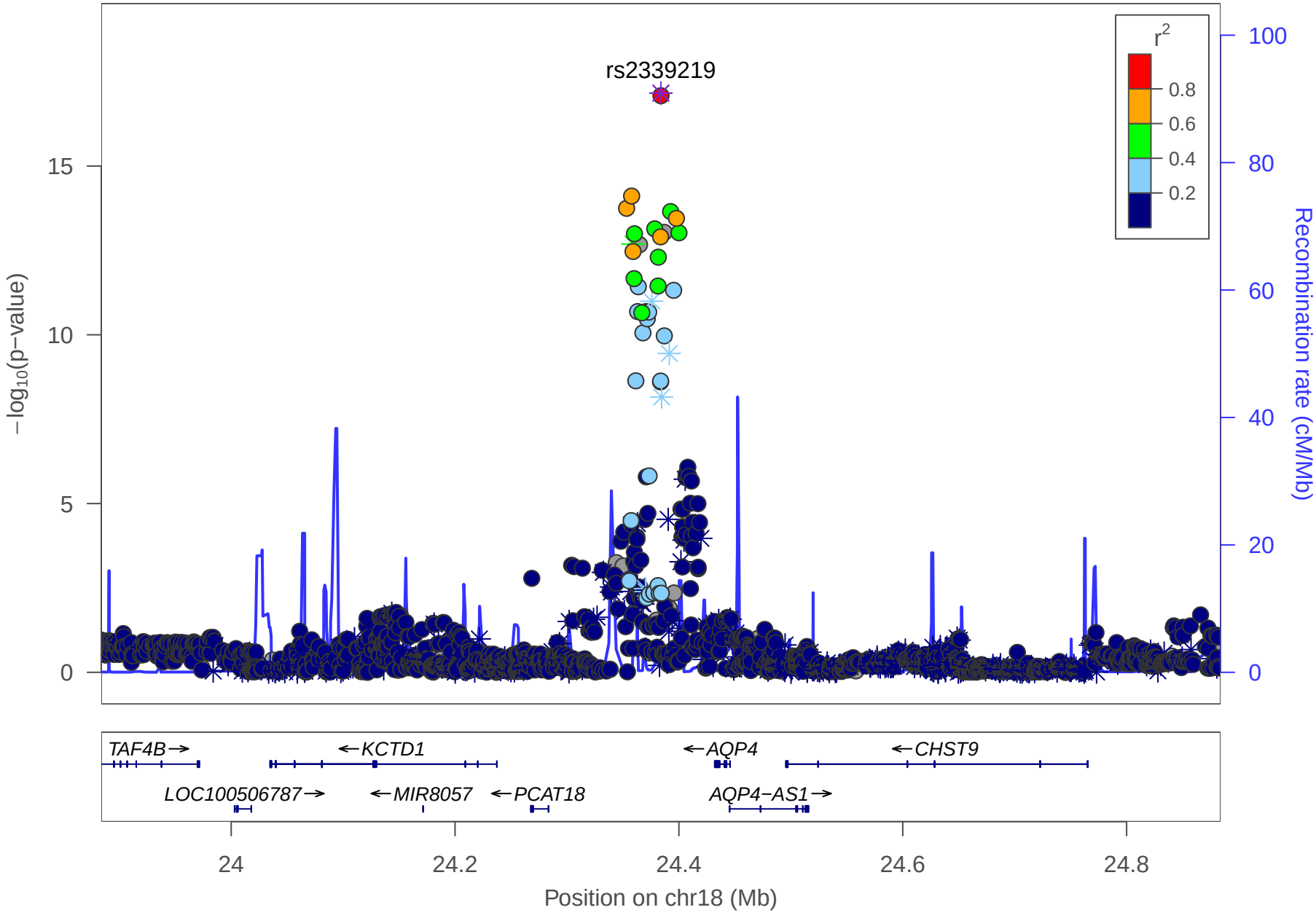
rs2339219
r2
0.8
0.6
0.4
0.2
15
10
5
0
−log10(p−value)
100
80
60
40
20
0
Recombination rate (cM/Mb)
TAF4B
KCTD1
AQP4
CHST9
LOC100506787
MIR8057
PCAT18
AQP4−AS1
24
24.2
24.4
24.6
24.8
Position on chr18 (Mb)

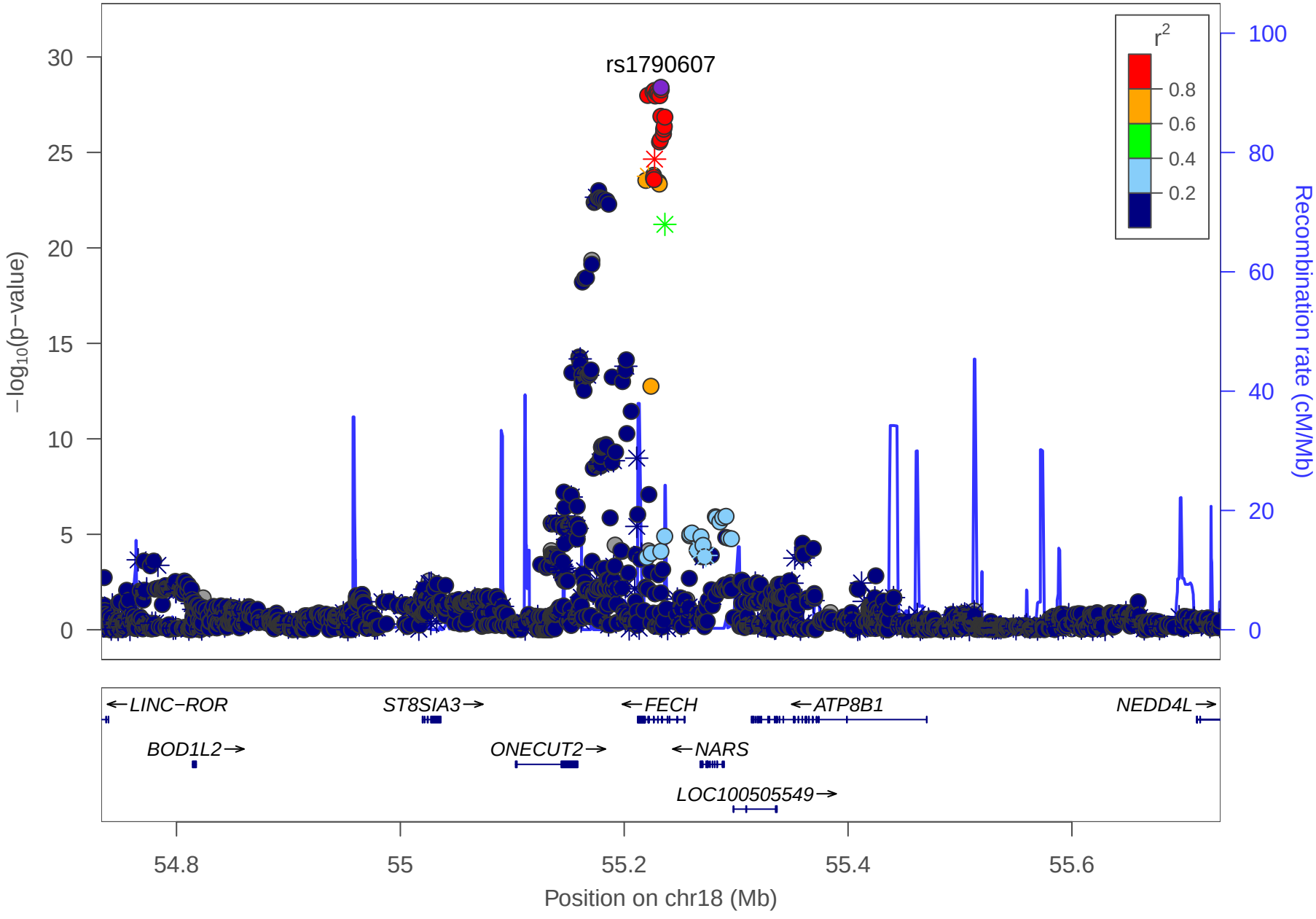
rs1790607
r2
0.8
0.6
0.4
0.2
−log10(p−value)
Recombination rate (cM/Mb)
30
25
20
15
10
5
0
100
80
60
40
20
0
←LINC−ROR
ST8SIA3→
←FECH
←ATP8B1
NEDD4L→
BOD1L2→
ONECUT2→
←NARS
LOC100505549→
54.8
55
55.2
55.4
55.6
Position on chr18 (Mb)

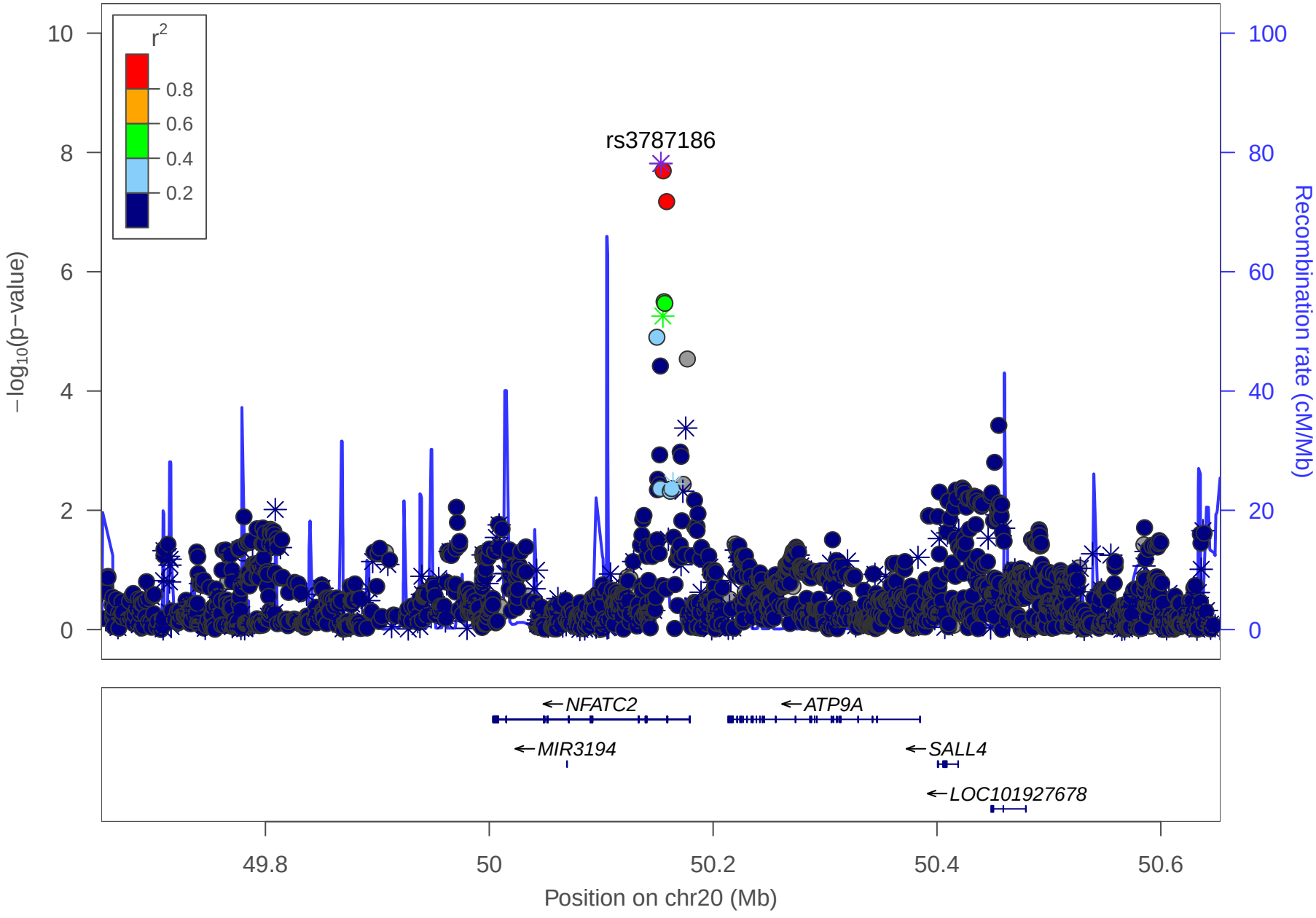
r2
0.8
0.6
0.4
0.2
rs3787186
−log10(p−value)
Recombination rate (cM/Mb)
10
8
6
4
2
0
100
80
60
40
20
0
NFATC2
ATP9A
MIR3194
SALL4
LOC101927678
49.8
50
50.2
50.4
50.6
Position on chr20 (Mb)

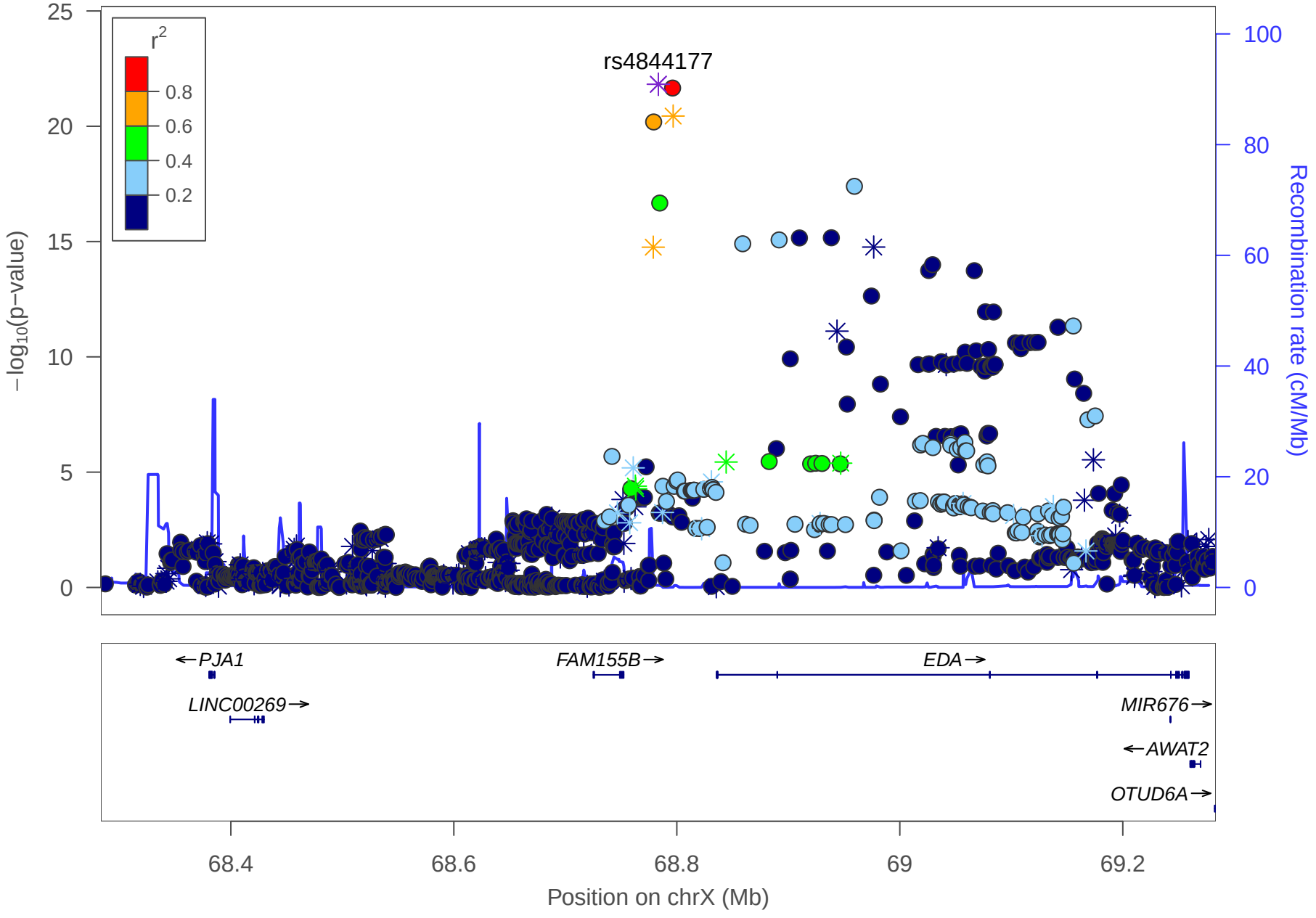
rs4844177
r2
0.8
0.6
0.4
0.2
−log10(p−value)
Recombination rate (cM/Mb)
25
20
15
10
5
0
100
80
60
40
20
0
PJA1
FAM155B
EDA
LINC00269
MIR676
AWAT2
OTUD6A
68.4
68.6
68.8
69
69.2
Position on chrX (Mb)

Figure S2: Regional association plots showing significant associations observed in the meta-analysis across all four cohorts.

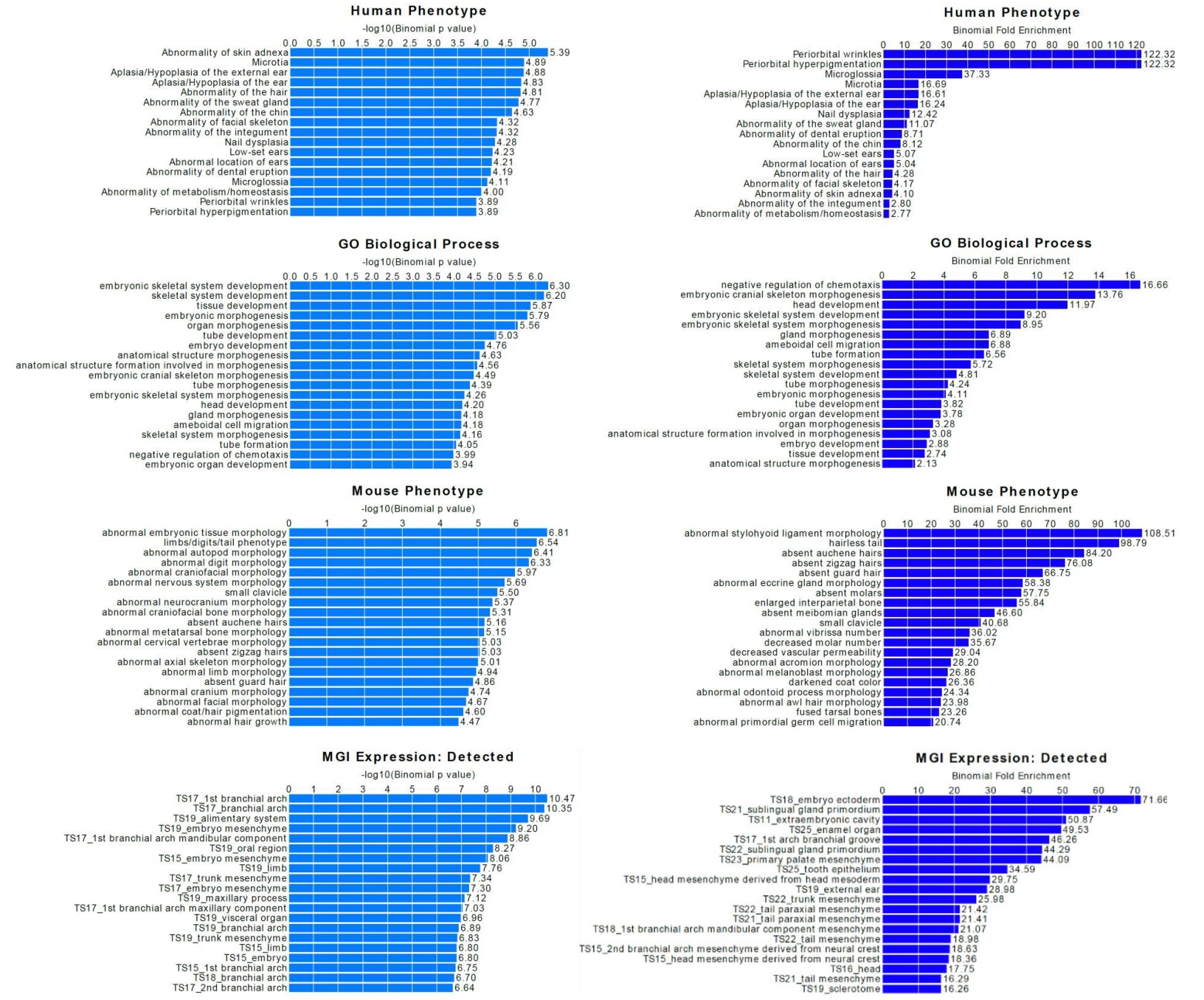

Figure S3: Enrichment for annotation across ontologies for 91 genes (i.e., nearest two genes up to 1000kb from the lead SNP) across 49 loci identified in the meta-analysis across all four cohorts. From top to bottom: human phenotype, Gene Ontology (GO) biological processes, mouse phenotype, and MGI expression ontologies. Left: significant annotations ordered by -log10-transformed p-values (up to 20 shown). Right: significant annotations order by fold enrichment (up to 20 shown).

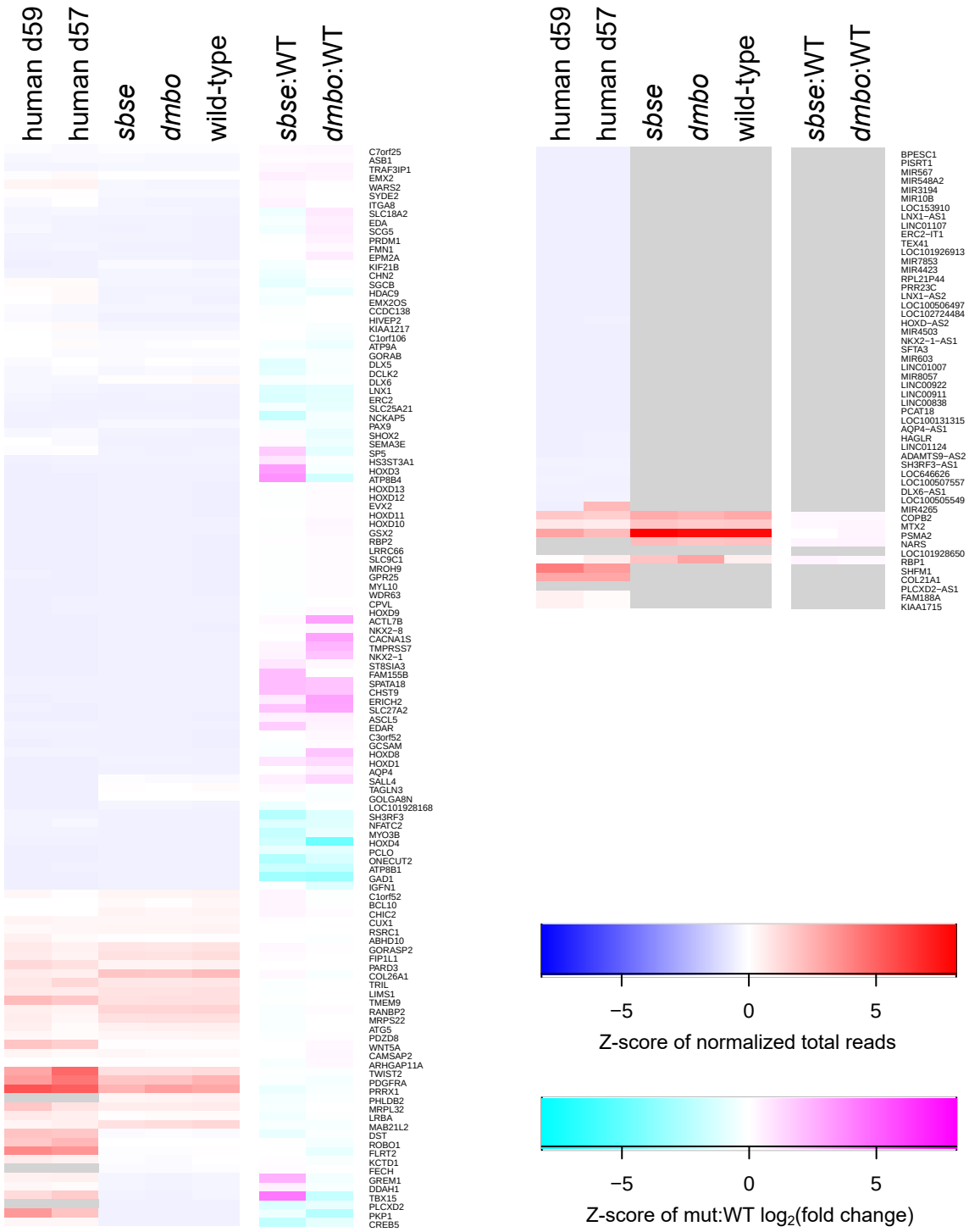

Figure S4: Heatmaps of gene expression in fetal human pinna (at days 59 and 57) and embryonic mouse second branchial arch tissue (in *sbse* mutants, *dmbo* mutants, and wild-type), and fold change of mutant mouse compared to wild-type mouse for 174 genes within 250 kb of the 49 lead SNPs observed in the genetic association meta-analysis across all cohorts. Genes are clustered by expression patterns with the bottom of the heatmap wrapping around to a second column. The shading scale is shown for Z-scores of expression and fold change. Genes for which expression data were not measured are shown in gray.

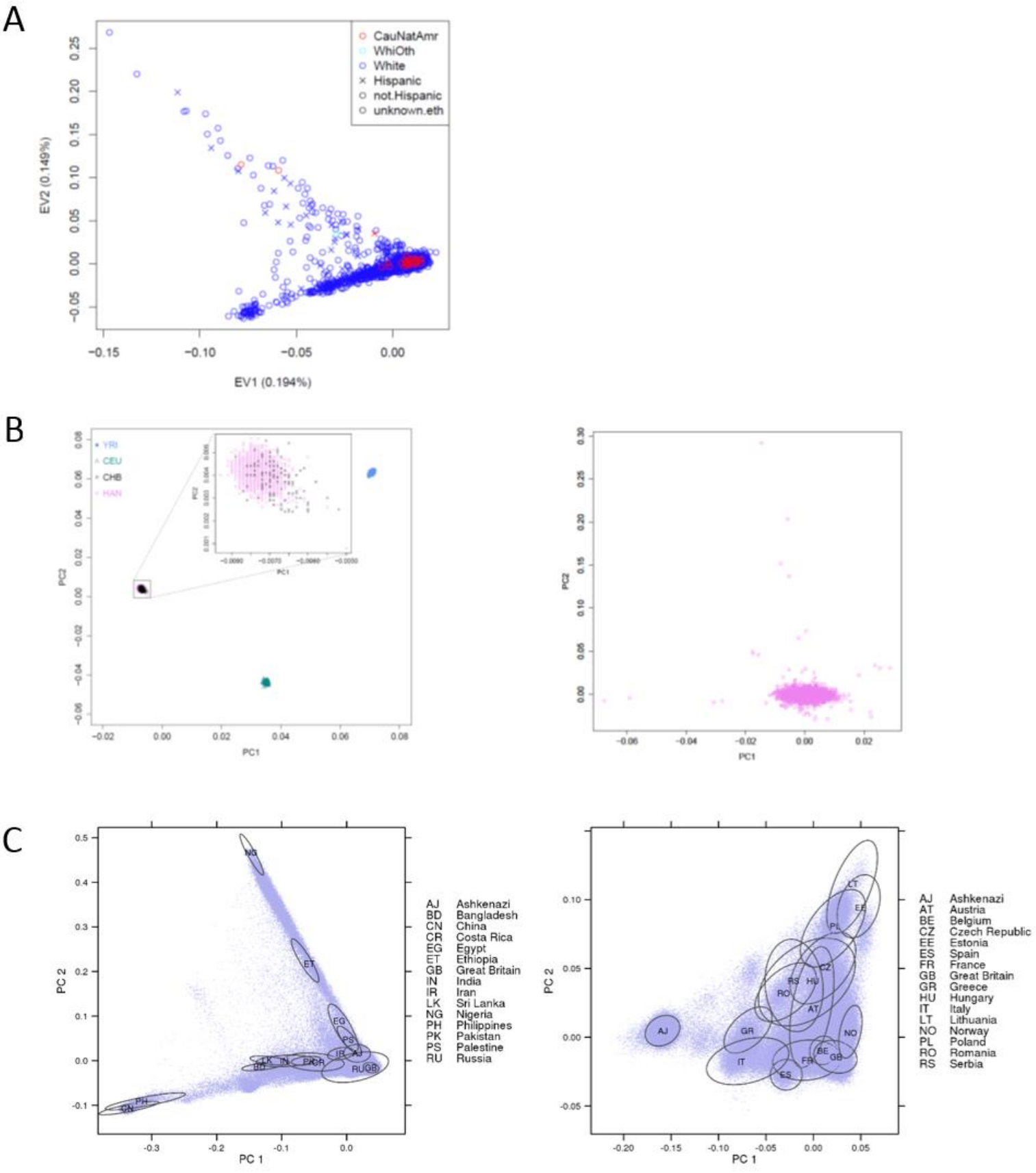

Figure S5: Population structure of cohorts is indicated by principal components of ancestry: (A) European American, (B) Chinese (left, with HapMap controls, right, analysis sample), and (C) 23andMe (left, entire sample, right, European American sample used in the analysis)

Table S1: Characteristics of the cohorts

	European American	Latin American	Chinese	23andMe European ancestry
N	1,791	5062	2,857	64,950
sex (% female)	59.46	52.7	63.67	51.01
age (mean [range])	22.35 [3-40]	24.4 [18 – 43]	56.14 [31-87]	
earlobe attachment (%)				
free	82.52	11.7	3.12	73.75
partially attached	9.94	75.6	31.92	
attached	7.54	12.7	64.96	26.25
ancestry	European	Admixed	East Asian	European
genotyping platform	Illumina HumanOmni Express+Exome	Illumina HumanOmni Express	Illumina HumanOmni Zhonghua-8	Illumina HumanHap550, HumanOmni Express, or custom array
# genotyped SNPs passing QC	653,629	671,772	795,597	1,044,759
# imputed SNPs	10,156,807	9,143,600	7,383,741	15,573,758
regression analysis	linear	linear	linear	logistic
covariates	Age, sex	age, sex, height, BMI	age, sex, BMI	age, sex, genotyping platform
principal components of ancestry included	3	5	0 [a]	5
genomic inflation factor	0.994	1.02	1.037	1.254 [b]

[a] Principal components analysis indicated negligible population structure, therefore no adjustments were made for principal components of ancestry in the Chinese sample.

[b] Genomic inflation for a subset of 1000 individuals with attached vs. 1000 with unattached earlobes was 1.002.

Table S3: Genetic data quality control filtering criteria

Filter	SNPs omitted	SNPs cumulatively retained
European American		
None (all SNPs)		968,515
Technical filters	8,470	960,045
Missing call rate ≥ 2%	9,675	950,370
>1 discordant calls in 69 duplicates [a]	26	950,344
>1 Mendelian error across 8 HapMap trios	122	950,222
HWE p-value < 10^{-4}	2,038	948,184
Allele frequency difference ≥ 0.2 between sexes [b]	274	947,910
Heterozygosity difference ≥ 0.3 between sexes [b]	41	947,869
Positional duplicates	19,597	928,272
Monomorphic (MAF = 0)	108,485	819,787
MAF < 0.01	164,959	654,828
non-autosomal or X	1,199	653,629
Latin American		
None (all SNPs)		730,525
Chromosome 0 (SNPs without assigned location)	1230	729,295
Missing call rate ≥ 5%	3550	725,745
MAF < 0.01 (includes monomorphic)	53973	671,772
Chinese cohort		
None (all SNPs)		887,270
Technical filters	278	886,992
Missing call rate ≥ 2%	18,628	868,364
Minor Allele Frequency < 0.01	67,873	800,491
HWE p-value < 10-3	2,588	797,903
Positional duplicates	2,306	795,597

[a] one duplicate was removed from QC filters due to a chromosomal anomaly

[b] filter applied to SNPs on autosomes and XY pseudo-autosomal region

Table S4: Summary of imputation methods and quality control filters

	European American	Latin American	Chinese	23andMe
Reference data source	1000 Genomes Project Phase 3	1000 Genomes Project Phase 1	1000 Genomes Project Phase 3	1000 Genomes Project Phase 1
Pre-phasing	SHAPEIT2	SHAPEIT2	SHAPEIT2	custom tool based on BEAGLE
Imputation	IMPUTE2	IMPUTE2	IMPUTE2	Minimac2
Other quality control procedures	masked variant analysis	masked variant analysis0	-	-
Imputation filters				
genotype probability (per SNP per person)	> 0.9	> 0.8	> 0.9	-
INFO score (per SNP)	> 0.5	> 0.4	> 0.6	-
MAF	> 0.01	> 0.01	> 0.02	-
Missing rate	-	-	< 0.05	-
HWE	-	-	≥ 10e-6	-
concordance (concord_type0) for masked variant analysis	-	> 0.7	-	-
info_type0-concord_type0 (chip genotype quality measure)	-	> 0.1	-	-